ENHANCED MODULAR MULTILEVEL CONVERTER-BASED STATCOM WITH HYBRID ENERGY STORAGE

A Dissertation

Presented in Partial Fulfillment of the Requirements for the

Degree of Doctor of Philosophy

with a

Major in Electrical Engineering

in the

College of Graduate Studies

University of Idaho

by

Carlet M. Enang

Major Professor: Brian K. Johnson, Ph.D.

Committee Members: Herbert L. Hess, Ph.D.; Yacine Chakhchoukh, Ph.D.;

Daniel Conte de Leon, Ph.D.

Department Administrator: Joseph D. Law, Ph.D.

May 2020

Authorization to Submit Dissertation

This Dissertation of Carlet M. Enang, submitted for the degree of Doctor of Philosophy with a major in Electrical Engineering and titled "Enhanced Modular Multilevel Converter-Based STATCOM with Hybrid Energy Storage," has been reviewed in final form. Permission, as indicated by the signatures and dates below, is now granted to submit final copies to the College of Graduate Studies for approval.

Major Professor: _____ Date: _____
Brian K. Johnson, Ph.D.

Committee Members: _____ Date: _____
Herbert L. Hess, Ph.D.

_____ Date: _____
Yacine Chakhchoukh, Ph.D.

_____ Date: _____
Daniel Conte de Leon, Ph.D.

Department Administrator: _____ Date: _____
Joseph D. Law, Ph.D.

Abstract

With the advent of power electronic converter-based generation technology in the power utility industry, there is an increasing need for sources of dynamically controllable real and reactive power to maintain stability of electric power systems. Static Synchronous Compensators (STATCOMs) improve the stability of electric power systems by dynamically controlling reactive power supply to the system. However, they cannot provide dynamic real power control. In this dissertation, a device capable of both dynamic real power and reactive power control is presented. The device consists of a modular multilevel converter (MMC) -based STATCOM combined with a hybrid energy storage system that combines a battery energy storage system with a supercapacitor energy storage system. Matlab/Simulink is utilized to examine the stability of the response of an electric transmission system under fault conditions without compensation, with a STATCOM alone and with the enhanced energy storage system. Simulation plots show that the system stability improves significantly when the hybrid energy storage system is combined with the STATCOM for dynamic real and reactive power compensation.

Acknowledgments

I would like to thank enormously my advisor, Dr. Brian K. Johnson, for his endless advice, guidance and inspiration throughout my research work. I am also appreciative to the committee members Dr. Herbert L Hess, Dr. Yacine Chakhchoukh, and Dr. Daniel Conte de Leon for creating time to review and make recommendations on my dissertation.

I am thankful to Pacific Gas and Electric Company for the financial assistance and to my co-workers for their technical support and encouragement throughout the research process.

I am especially appreciative to my entire family for always being there for me and enduring those long night vigils. Above all, the biggest appreciations go to the almighty God for successfully walking me through the long journey of the doctoral program.

Dedications

To Mum and Dad,

Rudolf Enang and Lucy Enang

In loving memories

Table of Contents

Authorization to Submit Dissertation ii
Abstract iii
Acknowledgments iv
Dedications v
Table of Contents vi
List of Figures x
List of Tables xv
Chapter 1: Introduction 1
1.1 Problem Statement 3
1.2 Research Objectives and Main Contributions 5
1.3 State of the Art 5
1.4 Dissertation Outline 7
Chapter 2: Overview of FACTS Devices 10
2.1 Series Controllers 11
2.2 Shunt controllers 12
2.3 Combined Series-Series Controllers 13
2.4 Combined Series-Shunt Controllers 14
2.5 Benefits of SVC and STATCOM in Electric Utility Applications 15
2.5.1 Basic Description of an SVC 15
2.5.2 Basic description of a STATCOM 19
2.5.3 The MMC-based STATCOM at a Glance 24
2.5.4 Performance Characteristics of STATCOM and SVC 29
2.6 Summary 32
Chapter 3: Power Converter Technology 34
3.1 Definition of Power Converters 34
3.2 Voltage Sourced Converters Overview 36
3.3 Control Schemes For STATCOMs 38
3.3.1 PWM Switching Scheme for two level VSC 39
3.3.2 Real and Reactive Power Control of STATCOM 41
3.3.3 Dynamic Model of Real and Reactive Power Controller 44
3.4 Modular Multilevel Converter History and Benefits 46

3.5 Multilevel Inverter Topologies 46
3.6 Equivalent Circuit of Half Bridge VSC 48
3.7 Sinusoidal Approximation of Multilevel Converter 49
Chapter 4: MMC-based STATCOM with Hybrid Energy Storage 52
4.1 Introduction of the E-STATCOM/BE3SC 52
4.2 Overview of the E-STATCOM/BE3SC Design 55
4.3 Mathematical Representation of E-STATCOM/BE3SC Control 57
4.4 Principles of Operations of MMC with Separate DC Sources 60
4.5 Total Harmonic Distortion (THD) Calculation 61
4.5.1 THD Calculation 61
4.6 Summary 64
Chapter 5: Hybrid Energy Storage System (HESS) 66
5.1 Hybrid Energy Storage Systems 66
5.1.1 Supercapacitor Description 66
5.1.2 Battery Description 69
5.1.3 Combining Batteries with Supercapacitors 70
5.2 The Ragone Plot 70
5.3 Sizing Energy Storage System for the E-STATCOM/BE3SC 71
5.3.1 Energy Stored in a Supercapacitor 73
5.3.2 Supercapacitor Model 74
5.3.3 Battery Model 74
5.4 Battery and Supercapacitor Power and Energy Equations 76
5.5 Supercapacitor Charge and Discharge Characteristics 77
5.6 Battery Characteristics 80
5.6.1 Battery Discharge Curve 80
5.6.2 Battery Temperature Characteristics 82
5.6.3 Battery State of Charge (SOC) and State of Health (SOH) 84
5.6.4 Battery Life 84
5.6.5 State of Health 87
5.6.6 Sizing the Energy Storage System 89
5.7 Summary 91
Chapter 6: Bidirectional dc-dc Converter Control in 92
Battery-Supercapacitor Hybrid Energy Storage System 92
6.1 Introduction 92

6.2 Basic Design 94
6.3 Power flow Modes 95
6.3.1 Charge Supercapacitor and Battery Mode 95
6.3.2 Discharge Battery and Supercapacitor Mode 96
6.3.3 Charge/discharge mode 96
6.3.4 Normal mode 96
6.4 Bidirectional dc-dc converter control 97
6.4.1 Control strategy 99
6.5 Sizing the hybrid energy storage system 101
6.6 Simulation results 106
6.7 Summary 109
Chapter 7: Enhanced STATCOM Model Implemented in Matlab/Simulink 111
7.1 Introduction 111
7.2 The 500 kV Grid Model 111
7.3 MMC STATCOM 115
7.3.1 MMC STATCOM Parameters 118
7.3.2 STATCOM Gain Parameters 119
7.4 Hybrid Energy Storage system sizing 121
7.5 Bidirectional dc-dc Step-up Converter 122
7.6 Summary 123
Chapter 8: Evaluation and Analysis of Simulation Results 124
8.1 Dynamic response to Moderate Step Change in Reactive Power Command 125
8.2 Submodule Capacitor Voltage Comparison 126
8.3 Impact of Increasing Number of Submodules on AC Voltage Waveform 127
8.4 Verification of Converter Ouput Current Against Reactive Power Command 128
8.5 Response During Recovery From a Close-In Three-Phase Fault 129
8.6 Control of Hybrid Energy Storage System Charge/Discharge Operations 134
8.6.1 Control of charge/discharge operations when no power transfer is required 134
8.6.2 Control of charge/discharge operations at $Pcommand \neq 0$ 137
8.7 System Voltage Magnitude Response to Changes in Solar Generation Output 138
8.8 System Frequency Response to Changes in Solar Generation Output 139
8.9 E-STATCOM/BE3SC connected to mitigate high voltages 143
8.10 E-STATCOM/BE3SC used to mitigate low frequency issues due to Loss of PV 145
8.11 Summary of Simulation Results 148

8.12 Assumptions, Challenges and Validation 150
Chapter 9: Summary, Conclusions and Future Work 152
9.1 Summary 152
9.2 Conclusions 154
9.3 Future Work 155
References 157
Appendix A 165
Appendix B 166

List of Figures

Figure 1.1: MMC with four power modules and generated ac voltage 2

Figure 2.1: Series control of FACTS device [1]…….11

Figure 2.2: Phasor diagram of series control device [1] 12

Figure 2.3: Shunt (Parallel) control of FACTS device [1] 13

Figure 2.4: Phasor diagram of shunt control device [1] 13

Figure 2.5: Series - shunt control of FACTS device [1] 14

Figure 2.6: Phasor diagram of the series - shunt control of FACTS device [1] 14

Figure 2.7: Basic representation of an SVC [14] 18

Figure 2.8: Simplified diagram of a STATCOM 19

Figure 2.9: Simplified Principal Arrangement of STATCOM 20

Figure 2.10: Basic operation of the STATCOM 21

Figure 2.11: Waveforms of a two-level, three-level and four-level STATCOM [20] 26

Figure 2.12: High and low voltage operating ranges of STATCOM versus SVC [20][21]. 28

Figure 2.13: V/I characteristics of STATCOM versus SVC [20][21] 28

Figure 2.14:V-I characteristics of a STATCOM [22] 30

Figure 2.15: V-I characteristics of an SVC [23][24] 30

Figure 2.16: STATCOM and simple utility system equivalent circuit 31

Figure 3.1: Schematic diagram of the single-phase, full-bridge, two-level VSC……...37

Figure 3.2: Evolution of switch converters for HVDC and FACTS [3] 38

Figure 3.3: Carrier-based PWM switching technique [31] 40

Figure 3.4: VSC real and reactive power Controller 41

Figure 3.5: Voltage-mode control of real and reactive power for VSC 42

Figure 3.6: Current-mode control of real and reactive power for VSC [31] 43

Figure 3.7:Multilevel Inverter Topologies 48

Figure 3.8: Equivalent circuit of multilevel voltage-sources converter 49

Figure 3.9: Example multilevel sinusoidal approximation [47] 50

Figure 4.1: Basic diagram of an E-STATCOM/BE3SC……53

Figure 4.2: Single-phase, two-submodule topology of E-STATCOM/BE3SC..... 54

Figure 4.3: MMC with separate dc sources 60

Figure 4.4: Plot of THD of sinewave [52]..... 63

Figure 5.1: Schematic of an electrochemical double-layer capacitor……68

Figure 5.2: Ragone plot showing performance of a range of electrochemical devices [57]..71

Figure 5.3: Basic diagram of an E-STATCOM/BE3SC with 4 MMC submodules per phase 72

Figure 5.4: Equivalent circuit of supercapacitor ladder [65]..... 74

Figure 5.5: Equivalent circuit of Lithium Ion Battery used in the Research [66] 74

Figure 5.6: Supercapacitor SOC for a 10,000 F supercapacitor 78

Figure 5.7: Supercapacitor discharge voltage for a 10,000 F 79

Figure 5.8: Supercapacitor discharge current for a 10,000 F 79

Figure 5.9: Battery discharge characteristics for a Lithium Ion battery [67] 82

Figure 5.10: Performance of Lithium ion batteries at different operating temperatures [57] 83

Figure 5.11:Battery calendar: Increasing internal resistance with time and temperature [57] 85

Figure 5.12: Depth of discharge versus cycle life for Lithium ion battery [57] 86

Figure 5.13: Impact of battery aging due to charge-discharge operations [74][75] 87

Figure 6.1: Basic design and power flow modes……95

Figure 6.2: Bidirectional dc-dc converter for hybrid energy storage system (HESS)..... 99

Figure 6.3: Control strategy 100

Figure 6.4: Control block diagram..... 101

Figure 6.5: DC link voltage for supercapacitor connected alone 107

Figure 6.6: DC link voltage for battery connected alone..... 107

Figure 6.7: DC link voltage of hybrid energy storage system (HESS) 108

Figure 6.8: Battery charging 108

Figure 6.9: Supercapacitor discharging 108

Figure 6.10: Negative discharge current of HESS..... 109

Figure 7.1**:** 500 kV system studied……...113

Figure 7.2: Single-phase, three-submodule MMC STATCOM topology with hybrid energy storage connected to two submodules 116

Figure 7.3: Converter output voltage per phase..... 117

Figure 7.4: Schematic representation of full-bridge dc-dc converter transformer 118

Figure 8.1: Dynamic response for moderate step change in $Qref$ in MMC STATCOM operation……...126

Figure 8.2: Capacitor voltage of three submodules with E-STATCOM/BE3SC..... 127

Figure 8.3: Capacitor voltage of three submodules with MMC STATCOM alone 127

Figure 8.4: Converter output voltage per phase with 22-submodules 128

Figure 8.5: Converter output voltage per phase with 11-submodules 128

Figure 8.6: Converter output peak current with 22-submodule E-STATCOM/BE3SC..... 129

Figure 8.7: Voltage measured at SUB L for a three-phase fault on the 500 kV line..... 130

Figure 8.8: Fault current measured at SUB L for a three-phase fault on the 500 kV line... 130

Figure 8.9: Voltage measured at SUB L for a three-phase fault on the 500 kV line..... 131

Figure 8.10: Fault current measured at SUB L for a three-phase fault on the 500 kV line. 132

Figure 8.11: Voltage measured at SUB L for a three-phase fault on the 500 kV line..... 133

Figure 8.12: Fault current measured at SUB L for a three-phase fault on the 500 kV line. 133

Figure 8.13: Battery state of charge providing charge balance between battery and supercapacitor 135

Figure 8.14: Battery discharge current providing charge balance between battery and supercapacitor 135

Figure 8.15: Battery voltage providing charge balance between battery and supercapacitor 136

Figure 8.16: Supercapacitor state of charge providing charge balance between battery and supercapacitor 136

Figure 8.17: AC power command = 0 136

Figure 8.18: Supercapacitor state of charge discharging to the grid 138

Figure 8.19: Supercapacitor current when discharging to the grid..... 138

Figure 8.20: Supercapacitor voltage when discharging to the grid 138

Figure 8.21: RMS voltage response for all generation (3,170MW) with E-STATCOM/BE3SC 139

Figure 8.22: Low frequency variations at SUB G, for reduced PV at SUB G, without compensation 140

Figure 8.23: Low frequency variations at SUBS L, G, D, and M 141

Figure 8.24: Frequency increase at SUB G with reduced PV, ... 142

Figure 8.25: System frequency response for full generation restored at SUB G 143

Figure 8.26: High voltages without E-STATCOM/BE3SC 144

Figure 8.27: E-STATCOM/BE3SC used to regulate system voltage..... 145

Figure 8.28: Low voltages at SUB G and SUB L due to reduced PV generation at SUB G 147

Figure 8.29: E-STATCOM/BE3SC installed at SUB G to mitigate low voltages 147

List of Tables

Table 2.1: Comparison of MMC STATCOM and SVC 23

Table 4.1: Amplitudes of harmonics of distorted sine wave……..63

Table 6.1: Supercapacitor specifications……..105

Table 6.2: Battery specifications 106

Table 6.3: Bidirectional dc-dc converter specifications 106

Table 7.1: Operating voltage ranges of the 500 kV system……..114

Table 7.2: MMC STATCOM Parameters 119

Table 7.3: Battery specifications 121

Table 7.4: Supercapacitor specifications 122

Table 7.5: Bidirectional dc-dc converter specifications 122

Table 7.6: High frequency transformer specifications 123

Table 8.1: Bus voltages comparison without compensation, with MMC STATCOM……148

Table 8.2: Frequency response without compensation and with E-STATCOM/BE3SC.... 149

Table 8.3: Comparison of 11-submodule MMC STATCOM and 22-submodule MMC STATCOM 149

Table 8.4: Low level capacitor out voltage level for the MMC STATCOM and E-STATCOM/BE3SC 150

Chapter 1: Introduction

In ac power systems, there is an increasing need to efficiently control reactive power that is consumed in every component of the power system, from the generating centers to the load centers. Flexible AC Transmission System (FACTS) devices such as Static VAR Compensators (SVCs) and Static Synchronous Compensators (STATCOMs), have seen significant applications in accomplishing dynamic reactive power control [1]. Other FACTS devices such as Thyristor Controlled Series Capacitors (TCSC) and Unified Power Flow Controllers (UPFC) have seen some application. There is an extensive number of papers published proposing additional applications.

With the advent of improved semiconductor technology and modern voltage sourced converter (VSC) topologies, STATCOMs build on the proven benefits of speed, modularity and small footprint with improved response time and lower harmonics over the other FACTS devices. STATCOMs continuously provide variable reactive power in response to voltage variations, supporting the stability of the grid. They generate or absorb reactive power by electronically processing voltage or current waveforms in the VSC, using relatively small ac capacitors and inductors as filters, without the need for larger ac capacitor and reactor elements for generating and absorbing reactive power [2].

Modular multilevel converter (MMC) - based VSC applications have attracted a lot of interest for increasing ratings for high voltage and high-power applications with reduced switching losses and reduced harmonics. Both the size of voltage steps and related voltage gradient are minimized if the ac voltage generated by the converter can be selected in small

increments. Having smaller voltage increments at each switching instance reduces losses and reduces voltage harmonics, and indirectly reduces current harmonic distortion. This is accomplished by increasing the number of submodules connected in series [3].

Figure 1.1 shows the power modules in a four-module MMC and the generated ac voltage waveform. Transmission level MMCs have several hundred modules, but a case with four modules is shown for simplicity.

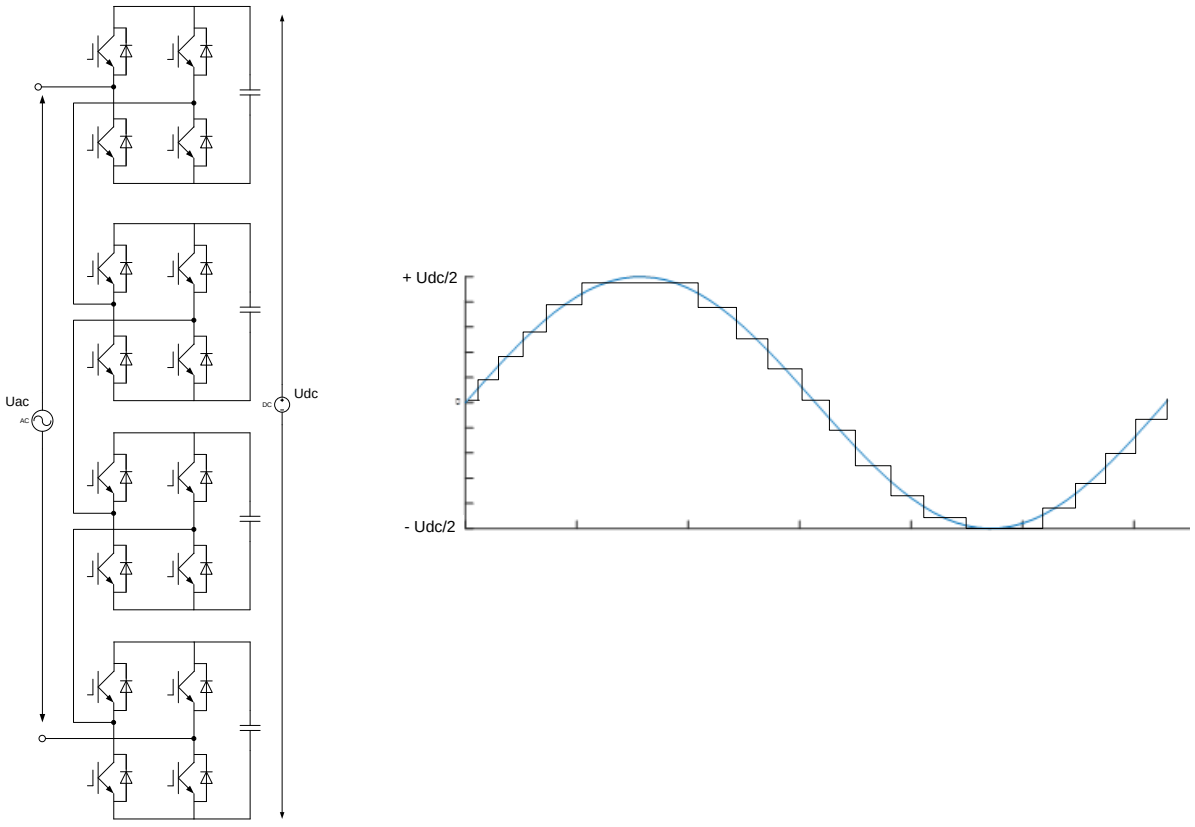

(a) MMC power modules (b) Generated ac Voltage

Figure 1.1: MMC with four power modules and generated ac voltage

Combining an MMC STATCOM with an energy storage system (ESS) could provide capability to dynamically inject both real and reactive power to the medium or high voltage grid for better power quality and stability [4]. Energy storage could also provide improved flexibility for integration of renewables to the electric grid.

This dissertation proposes a device that will dynamically control both real and reactive power injections, improve the performance of the electric transmission system during normal and abnormal conditions and help meet a state's utility mandates for clean energy storage.

The proposed device, Enhanced STATCOM (E-STATCOM) with hybrid energy storage system combines battery energy storage with a supercapacitor (BE3SC). This design will be discussed in later sections of the dissertation. Choosing appropriate ratings for the energy storage devices is important for accomplishing accurate results.

Matlab/Simulink is utilized to simulate the stability of the response of an electric transmission system under fault and line outage conditions for the following cases: without compensation, with a STATCOM alone, and with the enhanced STATCOM with energy storage. Simulation results show that the system stability improves significantly when the STATCOM is combined with the hybrid energy storage system for power compensation.

1.1 Problem Statement

As power flows from generation to load centers, reactive power is consumed through the conductors and equipment linking the centers. This can result in low voltages and stability issues in the electric system, especially during disturbances under high loadings. The severity of the issues depends on the operating state of the system. During peak demand periods, a fault on the electric system should result in more serious stability issues than during off-peak demand periods. There are mechanically switched devices such as shunt capacitors and shunt reactors that can be switched ON and OFF to control slow voltage fluctuations as needed. Synchronous condensers are synchronous machines where field current is continuously varied slowly to control voltage fluctuations. This slow response poses a burden to system

operators and may result in cascaded outages if the devices are not switched accurately and in a timely manner. There are also automatic controls and transformer tap changing to help regulate voltages, but they are slow and limited in operations per day or hour.

Stand-alone STATCOMs have also been utilized to provide dynamic reactive compensation. However, stand-alone reactive compensation does not always suffice to mitigate a stability issue or to recover from a serious fault condition other than in localized cases. In most cases, real power injection is also needed to recover from a serious disturbance or to make the system stable to avoid cascaded outages [5]. Operating the system by monitoring and manually switching reactive power devices is not fast enough and it is not an effective technique in today's modern electric system operations.

With the advent of power electronic converter-based generation technology in the power utility industry, there is an increasing need for dynamically controllable real and reactive power to maintain stability of electric power systems [5]. Static STATCOMs and SVCs have been vital in dynamic reactive compensation, but they cannot provide dynamic real power support. This research will propose a device capable of both dynamic real and reactive power control.

The device consists of a modular multilevel converter based STATCOM combined with a hybrid energy storage system that combines battery energy storage with a supercapacitor energy storage system. The proposed device will provide capability to control both active and reactive power flows as well as provide more flexibility and versatility in operating the power system [5].

1.2 Research Objectives and Main Contributions

The objective of this research is to develop a device that will efficiently enhance stability of the electric power system without the need to build new infrastructures such as transmission lines and substations. This device should be capable of dynamically controlling real and reactive power flows with the power system at medium or high voltage, for better power quality, stability, maintenance, and operational flexibility.

This potential new application will be useful in electric utility power applications where compensation is needed in bulk electric power transmission and would provide system operators the leverage to schedule routine maintenance activities without risking system exposure to voltage or stability issues during certain disturbances or contingencies. Utilizing modular multilevel converters in the design will increase the rating of the device and make it suitable for high voltage applications, increase reliability, modularity, and future expandability of the system.

In addition to providing a source for real power, adding energy storage to the design will help mitigate the “intermittency” issues that have plagued the solar and wind generation technology for several years. The energy storage system would help prolong the night time usage of stored solar energy.

1.3 State of the Art

Previous work explored the use of MMC-based STATCOMs to improve reactive compensation in power systems and they are now commercially available. To meet today’s growing operational needs, there is a need to integrate an energy storage device that will play

the imperative role of enhancing the control and operation of the power system [6]. In [7], various energy storage systems and their integration with FACTS devices were presented.

In [8], a new cascaded multilevel inverter to integrate and manage grid level energy storage systems was developed. This design reduced the number of separate dc sources seen in most cascaded multilevel inverters but still made them unattractive for solar, wind and other renewable energy generation integration.

In [4], some work was performed to enhance the performance of the STATCOM by adding supercapacitor energy storage to the dc-link of the conventional 2-level STATCOM. This topology provides quick compensation for both real and reactive power changes, but it is only suitable for short lasting stressed conditions in power systems.

Previous work explored integrating battery energy storage with diode-clamped multilevel inverters [9]. If the inverter runs under pulse width modulation (PWM), the diode reverse recovery of the clamp diodes becomes a major design challenge. As a result, this topology is not suitable for high voltage applications as the output voltage is limited.

In [10], studies were performed on static synchronous compensators combined with battery energy storage system (STATCOM/BESS), to regulate four-quadrant active and reactive power, which is an ideal scheme to solve problems of wind farm integration. The control strategy could coordinate charge or discharge of batteries with reactive power compensation of STATCOM.

A model of STATCOM with hybrid battery energy storage (STATCOM/HESS) was designed by using two bidirectional dc-dc converters [11]. This design utilized a combination of conventional STATCOM with battery energy storage and supercapacitors for fast enhancement of voltage stability. In the case studies, the voltage compensation capabilities

were demonstrated by varying loads with various STATCOM design topologies. Further studies are needed with an MMC-based STATCOM design to determine the impact of high voltage power system disturbances and line outages to the system stability.

Previous work in [12] and [13] described the MMC as a new generation STATCOM. However, these designs were limited to reactive power compensation only.

My research will extend the current state of the art by utilizing an MMC-based STATCOM with enhanced energy storage. The design will be compact and modular, versatile and expandable, meet modern standards of state-of-the-art technology and it will be cost effective.

1.4 Dissertation Outline

The primary goal of this dissertation is to introduce a device capable of dynamically controlling both real and reactive power to meet dynamic needs in a power system.

This dissertation is divided into seven chapters. Chapter 1 provides an introduction of the class of power system problems to address, research objectives, main contributions and a review of the state of the art. Chapter 2 provides a general overview of FACTS devices including series and shunt controllers, with emphasis on Static VAR Compensators and Static Synchronous Compensators. Their characteristics and controls are also discussed. In addition, the MMC-based STATCOM is analyzed.

Chapter 3 presents an overview of power converter technology with emphasis on voltage sourced converters with MMC topologies. The VSC is the main building block of the STATCOM. The control scheme of the STATCOM and PWM techniques are also discussed. Modular multilevel converter benefits and topologies such as cascaded, diode-

clamped and flying capacitor designs are covered. The cascaded MMC topology has several distinct benefits over the other options and is a widely utilized converter technology.

Chapter 4 covers the enhanced MMC STATCOM with a hybrid battery and supercapacitor energy storage system. A mathematical representation of the STATCOM control and principles of operation are discussed.

In Chapter 5, the energy storage system is covered. The benefits of combining supercapacitors and batteries are described. A Ragone plot illustrates performances of the energy storage devices in regard to their specific energy and power densities. Sizing of supercapacitors and batteries will also be covered to meet performance expectations of the enhanced STATCOM. The battery and supercapacitor characteristics will be illustrated in relation to discharge rate, temperature, state of charge and impact on battery life.

Chapter 6 will cover the bidirectional dc-dc converter to control the supercapacitor hybrid energy storage system. In this chapter, the basic design and control strategy of the bidirectional converter, power flow modes, charge and discharge operations of the energy storage system will be discussed.

Chapter 7 will discuss implementation of the enhanced STATCOM model in Matlab/Simulink. The MMC STATCOM parameters and gains are calculated. In addition, the sizing of the hybrid energy storage system is calculated based on the system needs, to mitigate stability issues such as low and high frequencies due to generation and load imbalance. Mitigation of these frequency issues could require very large storage levels, unless this was on a small isolated grid.

Chapter 8 presents an evaluation and analysis of simulation results. A 500 kV transmission system is analyzed for dynamic stability response of STATCOM after a three-

phase fault and after a line outage. Dynamic response is analyzed without compensation, with STATCOM alone and with the enhanced MMC STATCOM connected to an energy storage system. Simulation studies are performed for 22 power modules and 11 power modules of the MMC STATCOMs. This chapter also covers the research assumptions, challenges and validation. Chapter 9 presents a brief summary of the research, conclusions and future work.

Chapter 2: Overview of FACTS Devices

Flexible Alternatiing Current Transmission Systems (FACTS) simplify to a combination of power electronics components with traditional power system components. They are intended to improve power system reliability, power transfer capability, transient and dynamic stability as well as voltage regulation. With the advent of improved semiconductor technologies, these FACTS devices have improved in their speed and flexibility [1].

The semiconductor switching technology has evolved from mercury valves in the 1950s, thyristor valves in the 1970s to Integrated Gate Bipolar Transistors (IGBTs) in the early 2000s for VSC topologies. The current FACTS technology is prevalently based on the IGBT as the switching device in voltage sourced converters due to the proven speed and reliability.

FACTS devices can provide series and shunt compensation when connected to the power system. Series compensation on transmission lines modifies the line impedance and the transfer capability of the line. Shunt compensation injects or absorbs reactive power to regulate the voltage at the point of connection.

FACTS devices are classified into four main classes of controllers [1]:

- Series
- Shunt
- Combined series-series
- Combined series-shunt

2.1 Series Controllers

Controllers connected in series with the line are meant to inject voltage in series with the line. If the injected voltage is in phase quadrature with the line current, then the controller only supplies or consumes variable reactive power. To handle real power, other hybrid devices may be involved, which will be discussed later. These reactive power-only devices could be variable impedance devices, which include Thyristor-Controlled Series Capacitors (TCSC), Thyristor-Controlled Series Reactors (TCSR), Thyristor-Switched Series Capacitor (TSSC) and Thyristor-Switched Series Reactor (TSSR). The Static Series Synchronous Compensator (SSSC) is a series voltage source controlled to look like a variable capacitor or inductor. Figure 2.1 represents series compensation on a system where the power transfer capability (P) is controlled by varying the controlled series impedance X_{series} added to the transmission line, where X_{series} can be either capacitive or inductive. Figure 2.2 shows the phasor diagram of the series control system. The phasor labelled *I*, is perpendicular to the phasor difference between *V1* and *V2*, both phasors being dashed lines in this figure.

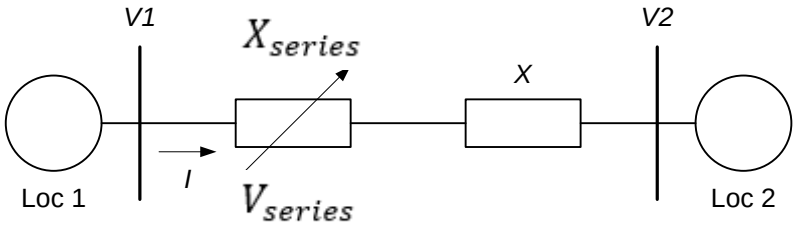

Figure 2.1: Series control of FACTS device [1]

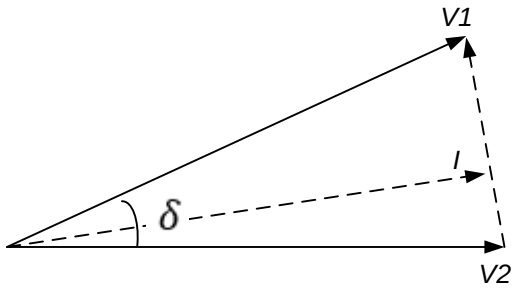

Figure 2.2: Phasor diagram of series control device [1]

If X_{series} is capacitive, the power flow from Loc 1 to Loc 2 is given by:

$$P_{12} = \frac{V_1 V_2 \sin(\delta)}{X - X_{series}} \tag{2.1}$$

The power control capability from Loc 1 to Loc 2 (P_{12}) is proportional to the voltage magnitude V_1 at Loc 1, the voltage magnitude V_2 at Loc 2, the sine of the phase angle between V_1 and V_2, and inversely proportional to the reactance between them. The line resistance is assumed insignificant for this relation and is left out of the equation. Increasing the effective capacitive reactance X_{series} increases the power flow on the line. On the other hand, an inductive injective for X_{series} increases the effective reactance between the two terminals and lowers power transfer.

2.2 Shunt controllers

Shunt controllers connected in shunt with the line are meant to inject current into the system at the point of connection. If the injected line current is in quadrature with the line voltage, variable reactive power supply or consumption could be achieved. Examples of shunt controllers include STATCOMs and SVCs. The common SVCs are made up of Thyristor-Controlled Reactors (TCRs), Thyristor-Switched Reactors (TSRs), Thyristor-Switched Capacitors (TSCs) and Mechanically Switches Capacitors (MSC). Figure 2.3 represents a shunt control system where reactive power is injected into the system and

increases the voltage V_M by injecting capacitive current at the midpoint of the transmission line. The voltage at the midpoint where the shunt compensator is connected increases. There is an inductive impedance between Loc 1 and V_1 that is not shown in the figure. The phasor diagram in Figure 2.4 shows that the injected current from Q is perpendicular to the voltage at the point of connection.

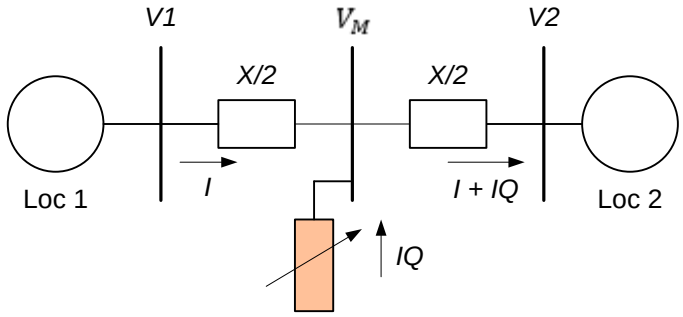

Figure 2.3: Shunt (parallel) control of FACTS device [1]

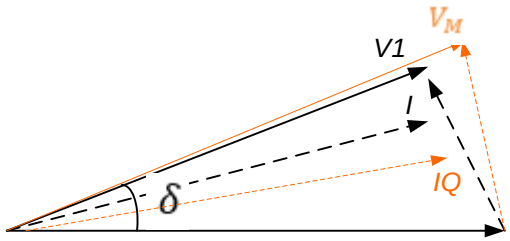

Figure 2.4: Phasor diagram of shunt control device [1]

Power flow from Loc 1 to Loc 2 with a shunt compensator is given by:

$$P_{12} = \frac{V_1 V_M \sin(\delta/2)}{X/2} \tag{2.2}$$

2.3 Combined Series-Series Controllers

This category of controllers comprises of separate series controllers controlled in a coordinated manner in the case of a multiline transmission system. It can also be a unified controller in which the series controllers perform the reactive power compensation in each

line independently. An example of this controller is the Interline Power Flow Controller (IPFC) in which the dc terminals of the controller converters are connected together [1].

2.4 Combined Series-Shunt Controllers

This category is a combination of separate series and shunt controllers operated in a coordinated manner. Hence, they are capable of injecting current into the line using the shunt part and injecting series voltage using the series part of the respective controller. An example of this controller is the Unified Power Flow Controllers (UPFC). A UPFC can inject a series voltage that is not in quadrature with line current, thus behaving as a phase shifting transformer that also provides shunt voltage compensation. Figure 2.5 represents a combined series and shunt control system where reactive power is injected into the system via the shunt controller and the line impedance is modified via the series controller. Figure 2.6 represents the phasor diagram of the series-shunt controller.

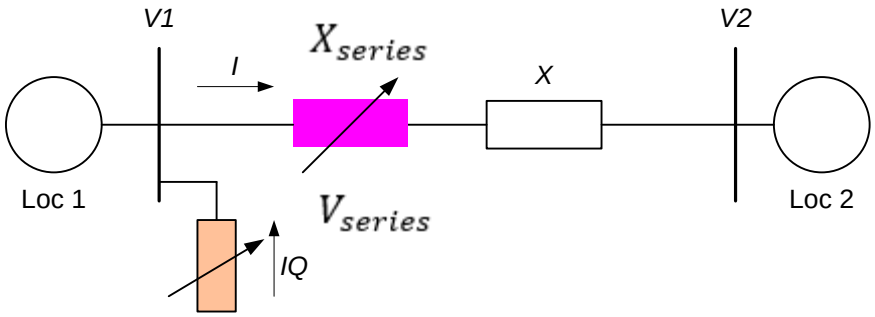

Figure 2.5: Series - shunt control of FACTS device [1]

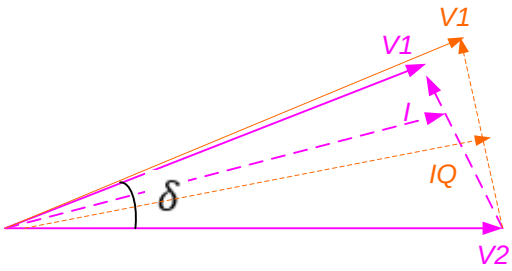

Figure 2.6: Phasor diagram of the series - shunt control of FACTS device [1]

In recent years, FACTS devices such as STATCOMs and SVCs have been widely utilized by electric utility companies to accomplish reactive power control. To enhance the performance of these devices, there is a need to combine them with real power sources to improve dynamic stability of the transmission system and to prevent cascading outages. Before discussing the enhanced configuration, the benefits of shunt compensation in the form of SVCs and STATCOMs in electric utility applications are covered.

2.5 Benefits of SVC and STATCOM in Electric Utility Applications

Static VAR Compensators are shunt connected controllers used extensively to control the ac voltage in transmission networks. Power electronic equipment such as the TCR and TSC have gained a significant market, primarily because of well-proven robustness to supply dynamic reactive power with fast response time and with low maintenance [14]. With the advent of high-power Gate Turn-Off thyristor (GTO) and transistor devices such as IGBTs, a new generation of power electronic equipment, STATCOMs, began to be applied in the early 1990s for power system applications [15][16].

2.5.1 Basic Description of an SVC

The SVC regulates the voltage by controlling the amount of reactive power absorbed from or injected into the power system. For example, it generates reactive power by switching capacitor banks when the system voltage is low, or loads are inductive. Consequently, the reactive power demand of the lagging load is supplied by the SVC – relieving the distribution or transmission lines from delivering it. Thus, the voltage drop on the line decreases and the voltage at the load terminals shall improve. Likewise, the SVC

absorbs reactive power when the system voltage is high, or loads are capacitive. In this case, the SVC uses the reactors to consume the VARS from the system, thereby lowering the system voltage.

Typically, an SVC comprises one or more banks of fixed or switched shunt capacitors or reactors, of which at least one bank is switched by thyristors. The SVC consists of the following elements:

- Thyristor-Controlled Reactors (TCR), air-cored
- Thyristor Switched Reactors (TSR) - optional
- Thyristor Switched Capacitors (TSC) - optional
- Harmonic filters
- Mechanically switched capacitors or reactors (MSC or MSR) (switched by circuit breaker)

The primary benefits of SVCs are the ability to provide continuous dynamic support. The TCR element varies the reactive power by controlling the thyristor's firing instants and accordingly, the current that flows in the reactance.

The TSC consists of capacitor bank sections switched by thyristors. A discrete cycle by cycle variation of the reactive power can be attained, but not a continuous change like that of a TCR. Nonetheless, by providing a suitably large number of small sections, the required resolution of reactive power variation for a single step can be achieved. In both the TCR and the TSC, the control of the SVC is based on measuring the reactive component of load current at the instant of voltage zero. Then, the measured current is used to determine the firing angle or turn ON/OFF for the TSC, so that the SVC absorbs or injects the amount of reactive power required for compensation.

The harmonic filters are high-power passive filters utilized to smooth the current waveforms resulting from undesired odd-order harmonics generated by the TCR. Since the filters themselves are capacitive at 60 Hz, they also export MVARs to the power system.

The mechanically switched capacitors (MSCs) provide steady-state VARs and they are typically switched by circuit breakers.

Figure 2.7 shows a possible basic representation of a Static VAR Compensator. The compensators include the TCR, TSC, harmonic filters and MSCs. The harmonic filters (for the TCR-produced harmonics) are capacitive at fundamental frequency. The TCR is typically larger than the TSC blocks so that continuous control is realized.

Other possibilities are fixed capacitors (FCs) and TSRs which are switched cycle by cycle and don't provide harmonics. Usually a dedicated step-up transformer is used, with the compensator equipment at medium voltage [14]. The transmission side voltage is controlled, and the MVAR ratings are referred to the transmission side. The rating of an SVC can be symmetrical or asymmetrical to meet the required power system demands. An example of a symmetrical rating for a transmission application is + 500 MVAR (capacitive) and -500 MVAR (inductive). Also, an example of an asymmetrical rating is +600 MVAR (capacitive) and -500 MVAR (inductive).

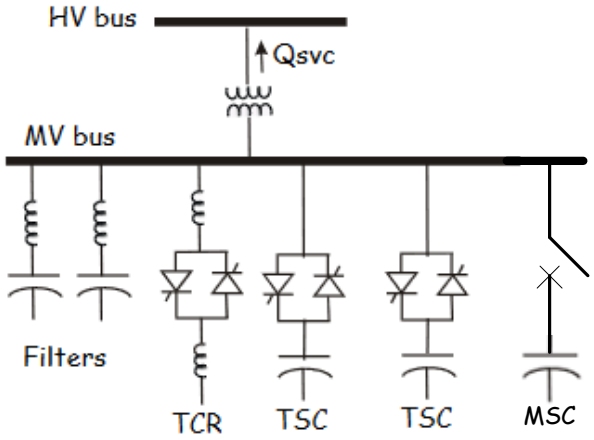

Figure 2.7: Basic representation of an SVC [14]

In transmission applications, the SVC is used to regulate the grid voltage. If the power system's reactive load is capacitive (leading) and the voltage is too high, the SVC will use TCRs to consume VARs from the system, lowering the system voltage. Under inductive (lagging) conditions, the capacitor banks are switched in by the SVC controls, thus providing a higher system voltage. By connecting the TCR, which is continuously variable, along with a capacitor bank step, the net result is continuously variable leading or lagging power.

By means of phase angle variation when switching the thyristors in the TCR, the reactor may be variably switched into the circuit and so provide a continuously variable inductive scheme used in VAR absorption from the electrical network [17]. The switching scheme used in TCRs generate undesirable odd-order harmonics and so as noted above, banks of high-power filters are usually provided to reduce lower order harmonics and smooth the current waveform. Addition of filters increases the footprint of SVCs compared with those of STATCOMs. The reduced space need is a chief advantage of STATCOMs.

2.5.2 Basic description of a STATCOM

A STATCOM is a voltage sourced converter-based device which converts a dc input voltage into an ac output voltage in order to compensate the active and reactive needs of the system [18][19]. The STATCOM consists mainly of:

- Semiconductor switching devices such as IGBTs in VSC circuit topology
- dc capacitor for small energy storage to make the dc bus a stiff voltage source
- ac coupling reactor for ac voltage harmonic suppression and to make the ac system appear as a current stiff.

Figure 2.8 shows a simplified diagram of a STATCOM. The leakage inductance of the transformer acts as the ac coupling reactor. Many different VSC topologies can be used. This dissertation will use the MMC topology from Figure 1.1 [14, 15].

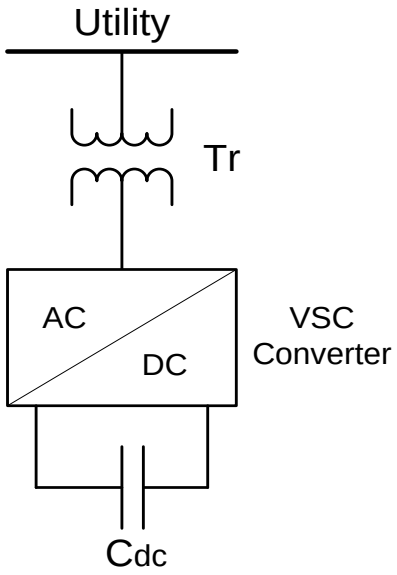

Figure 2.8: Simplified diagram of a STATCOM

The voltage sourced converter is the main building block of the STATCOM. Modern VSCs for utility applications use IGBT semiconductor switches.

When viewing the VSC from the dc side, assume the dc capacitors are charged at a controlled voltage. The capacitor voltage is used to synthesize ac voltage as shown in Figure 2.8. The angle difference between the created ac voltage waveform and the ac system voltage can transfer energy to and from the grid, to control charge on the dc capacitor. The VSC is able to perform independent control of active and reactive power with suitable controls, able to implement black start capabilities given an energy supply on the dc link. This makes the VSC suitable for connection to weak ac networks. Figure 2.9 shows a simplified principal arrangement of a STATCOM.

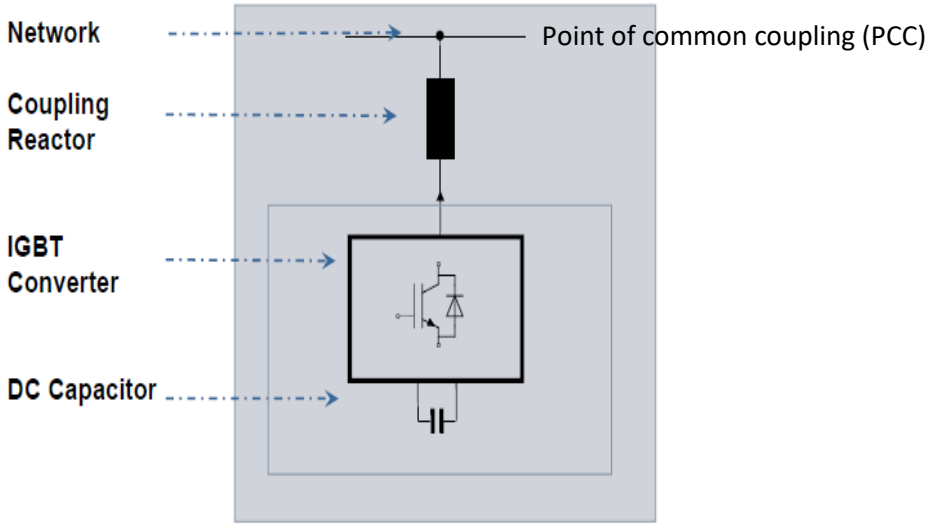

Figure 2.9: Simplified Principal Arrangement of STATCOM

The STATCOM control normally keeps the converter voltage in phase with the grid voltage in normal operation. When the amplitude of the converter voltage is higher than the grid voltage, the STATCOM acts like a capacitor or an over-excited synchronous machine and generates reactive power to the grid. On the contrary, when the amplitude of the converter voltage is lower than the grid voltage, the STATCOM acts like an inductor or an under-excited synchronous machine and absorbs reactive power from the grid. The maximum amount of

reactive power generated or absorbed depends on the switching control of the VSC, as well as on the dc bus voltage, which is controllable by the VSC, within limits. Figure 2.10 shows an illustration of the basic operation of a STATCOM connected to an electric grid.

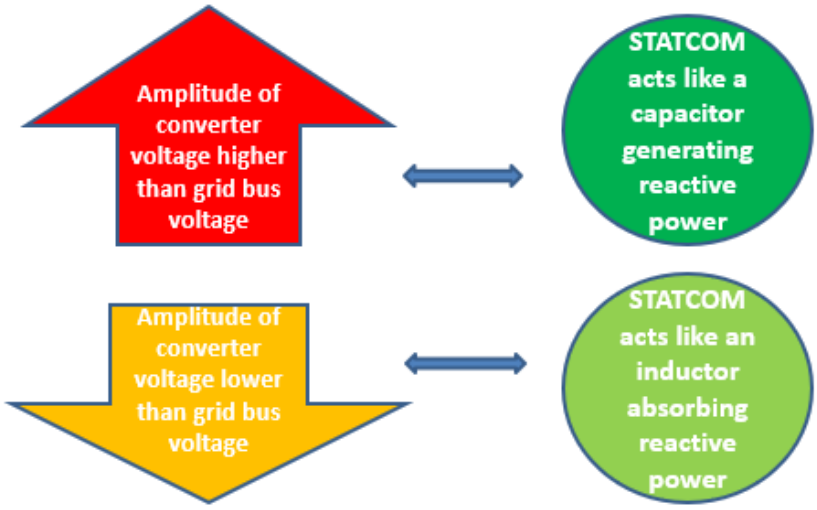

Figure 2.10: Basic operation of the STATCOM

The STATCOM operation is based on the principle of injection or absorption of reactive current at the point of common coupling (PCC) to the power network. Although the SVC and STATCOM are both used in electric power applications for reactive power compensation, the STATCOM has better characteristics than the SVC for low voltage conditions.

Both the STATCOM and the SVC can regulate current over a set range, as will be discussed later. Outside the control range, the SVC looks like a fixed impedance. The compensating current of the STATCOM does not depend on the voltage level of the PCC since it is not dictated by voltage over an impedance, thus the compensating current capability is not lowered as the voltage drops. This can be an advantage in a few situations.

Other reasons for preferring a STATCOM instead of an SVC are somewhat faster performance, smaller footprint and the ability to provide both short term active and steady state reactive power, thereby providing additional control.

In recent years, costs for STATCOMs have come down as have switching losses with adoption of MMC topologies. These take away part of the chief advantages of SVCs, making STATCOMS increasingly attractive.

Inherently, STATCOMs have a symmetrical rating with respect to inductive and capacitive current, and as a result for reactive power; for example, +500 MVAR (capacitive) and -500 MVAR (inductive). For asymmetric ratings, STATCOMs need a complementary reactive power source. This can be realized for example with mechanically switched capacitors [14].

Table 1.1 provides a comparison of the MMC STATCOM and the SVC installation characteristics. The choice of either device would depend on the specific needs of the power system.

Table 2.1: Comparison of MMC STATCOM and SVC

CHARACTERISTICS	STATCOM	SVC
Application	Fast dynamic compensation and voltage recovery during faults	Fast dynamic compensation and voltage recovery during faults
Switching Device and Design	IGBT, VSC, cascaded	Thyristor, series
Response time	1.5 - 2 cycles	2 - 3 cycles
Equipment Harmonics	Normally insignificant with MMC topology. Harmonically self-compensated; filters needed with 2 or 3-level VSC using PWM	TCR is source of harmonics (ac filters required). If TSR is used instead, no harmonics are present
Losses	Higher than SVC; reduced significantly with MMC	Lower than STATCOM
Installation Space	50% - 60%	100%
Equipment Location	More indoor	More outdoor
Maintenance Rate	20 - 30 hrs per year	40 - 50 hrs per year
Modular Unit	Yes	No
Installation Cost	Overall lower than SVC	Overall higher than STATCOM
Range	Symmetrical	Asymmetrical
V/I characteristics	Superior undervoltage performance	Good overvoltage performance
Control range	Symmetrical output: Adjustable range	Adjustable by branch ranges
Redundancy	Inbuilt redundancy in power modules	Inbuilt redundancy in thyristor valves

Siemens, ABB and GE are the main vendors of transmission level STATCOM devices. In [20], a marketing document by Siemens covers a multitude of benefits of the SVC PLUS, their name for STATCOM with MMC technology. The benefits include:

- Improved dynamic stability of transmission systems
- Increased power quality; reduction in risk of voltage collapse and blackout
- Highly efficient flicker reduction in distribution applications

- Low harmonic generation and low noise emissions, when using MMC technology
- Minimized engineering efforts due to standardized component design
- Fast, efficient, modular, and cost-effective solution

2.5.3 The MMC-based STATCOM at a Glance

The MMC-based STATCOM uses voltage sourced converter technology based on a modular converter design. Given enough levels, the MMC provides a nearly ideal sinusoidal-shaped voltage waveform on the ac side. Therefore, there is little (if any) need for high-frequency filtering and no need for low order harmonic filtering. The MMC topology allows for low switching frequencies, with small changes in voltage at each switching instance, which reduces system losses. The MMC technology provides a high degree of flexibility in converter design and station layout. The MMC STATCOM uses robust, proven standard components, such as typical AC power transformers, reactors, capacitors, and industrial class IGBTs (Insulated Gate Bipolar Transistors) that are widely used for traction and industrial drives. This design reduces the time and resources required for project development. The relatively low number of components simplifies design, planning, and engineering tasks [20].

An MMC STATCOM or SVC can help system operators meet the demands of increasingly distributed generation sources and liberalized markets. Power producers and system operators all over the world are faced with increasing demands for bulk power transmission, low-cost power delivery, and high system operational security. At the same time, congestion and bottlenecks cause limitations in power transmission. A STATCOM or SVC can provide a solution to such problems when properly sized and located. MMC

STATCOM design can be customized more easily than SVC or conventional STATCOM to meet individual reactive power demands.

Figure 2.11 shows waveforms of the MMC design compared with conventional two-level and three-level designs. In Figure 2.11c, the ac voltage waveform of the four-level STATCOM is a close approximation of the reference sinusoidal waveform, compared to the waveforms in Figures 2.11a and 2.11b. This is because the four-level STATCOM has more submodules connected in series, performing multiple switching steps. Increasing the number of switching steps improves the voltage waveform.

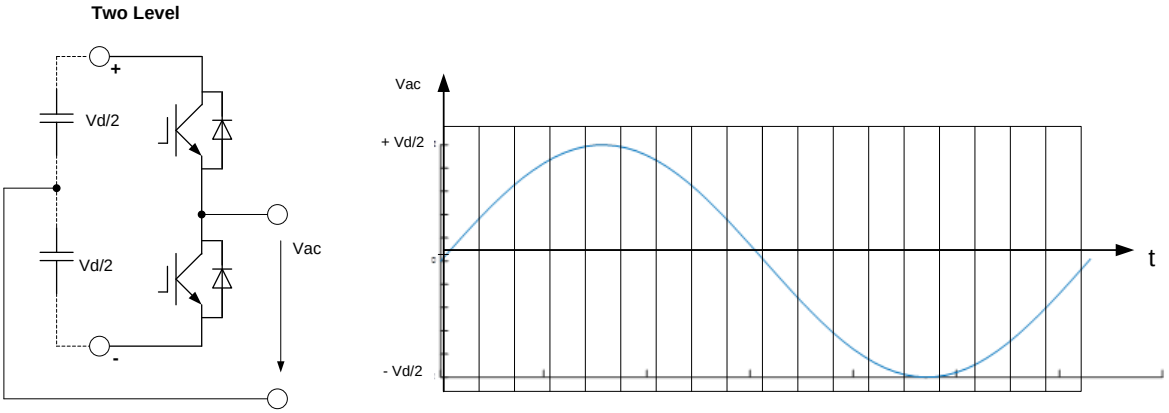

(a) Two-level PWM VSC design with switched ac waveform and fundamental component voltage

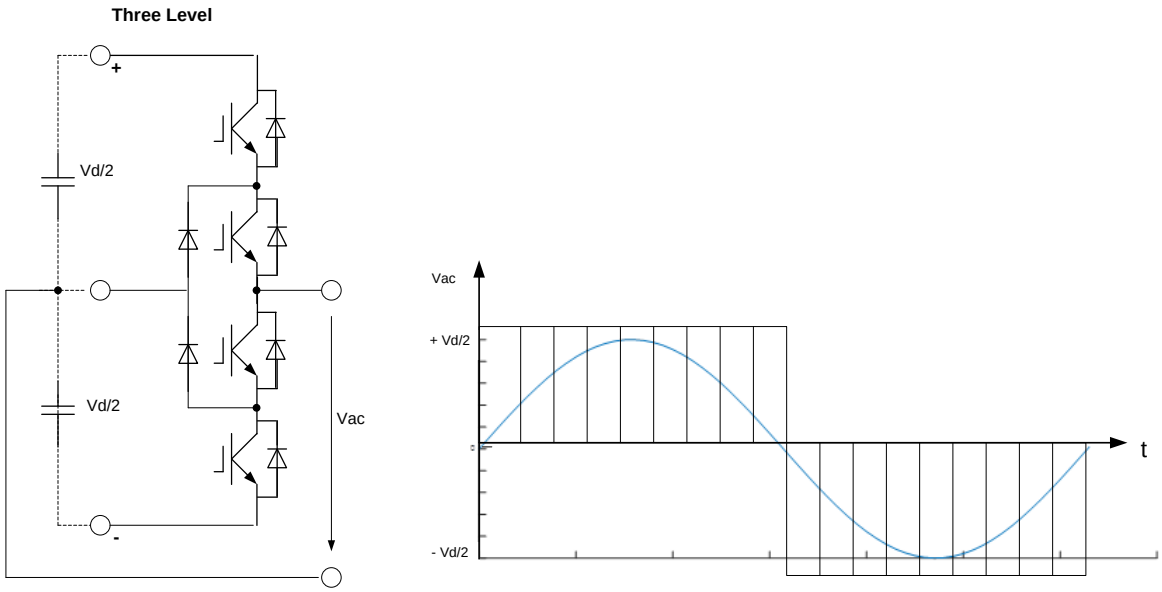

(b) Three-level PWM VSC design with switched ac waveform and fundamental component voltage

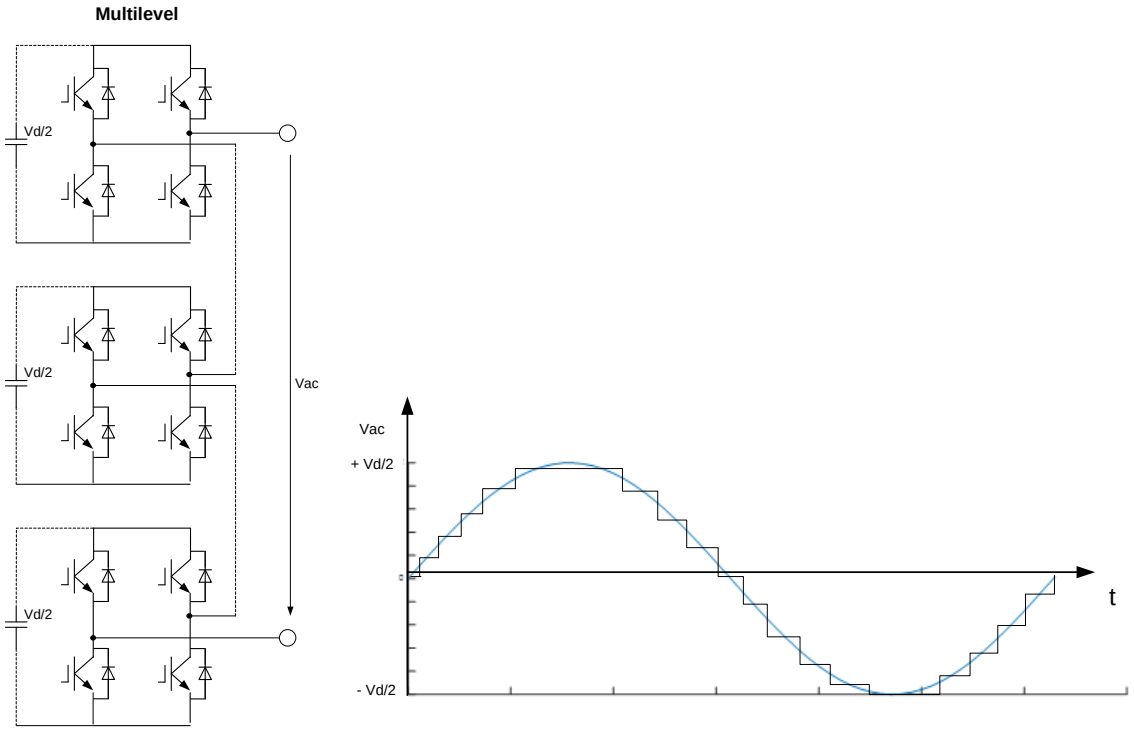

(c) Four-level STATCOM design with switched ac waveform and fundamental component voltage

Figure 2.11: Waveforms of a two-level, three-level and four-level STATCOM [20]

Figures 2.12 and 2.13 compare the voltage regulation ranges and the V/I characteristics of a STATCOM and SVC. As voltage decreases, the shaded region of the STATCOM extends to the bottom left (capacitive side). The ac portion is a benefit for STATCOMS. Similarly, as voltage increases, the shaded region of the SVC extends to the top right (inductive side). The ac portion is a benefit for SVC. This shows that the STATCOM shows better capacitive voltage performance and the SVC shows better inductive voltage performance (Figure 2.12). Similarly, the V-I characteristic curves of the STATCOM and SVC show that the continuous operating area of the STATCOM is larger than that of the SVC due to very low voltage operation capabilities. This is primarily of benefit for supporting voltage recovery from faults.

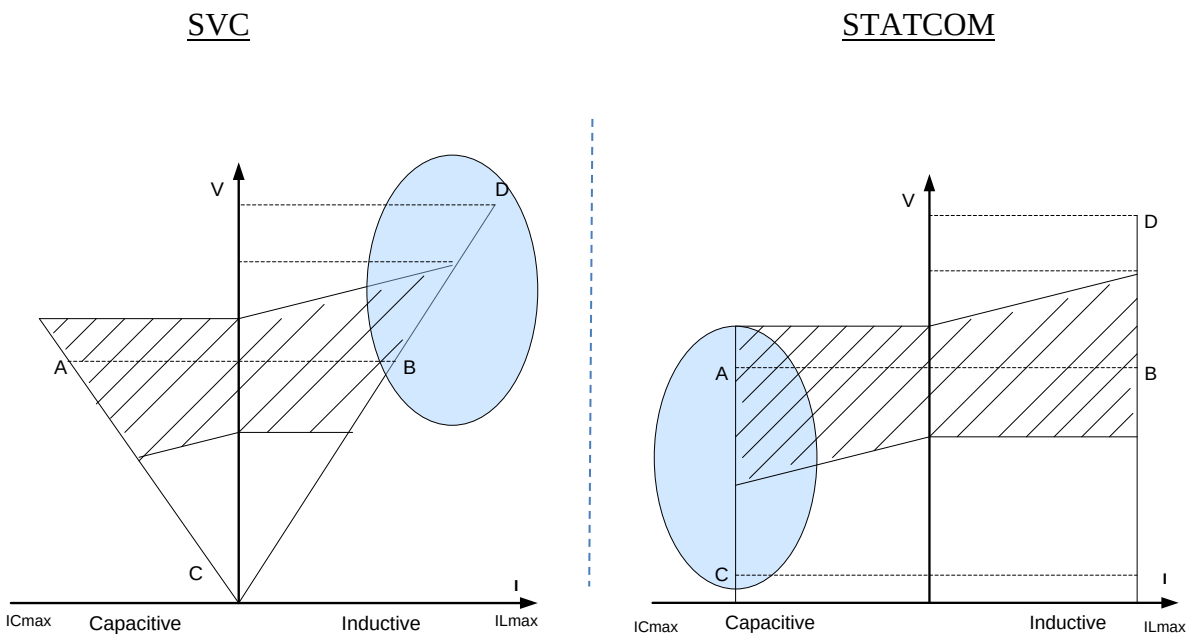

Figure 2.12: High and low voltage operating ranges of STATCOM versus SVC [20][21]

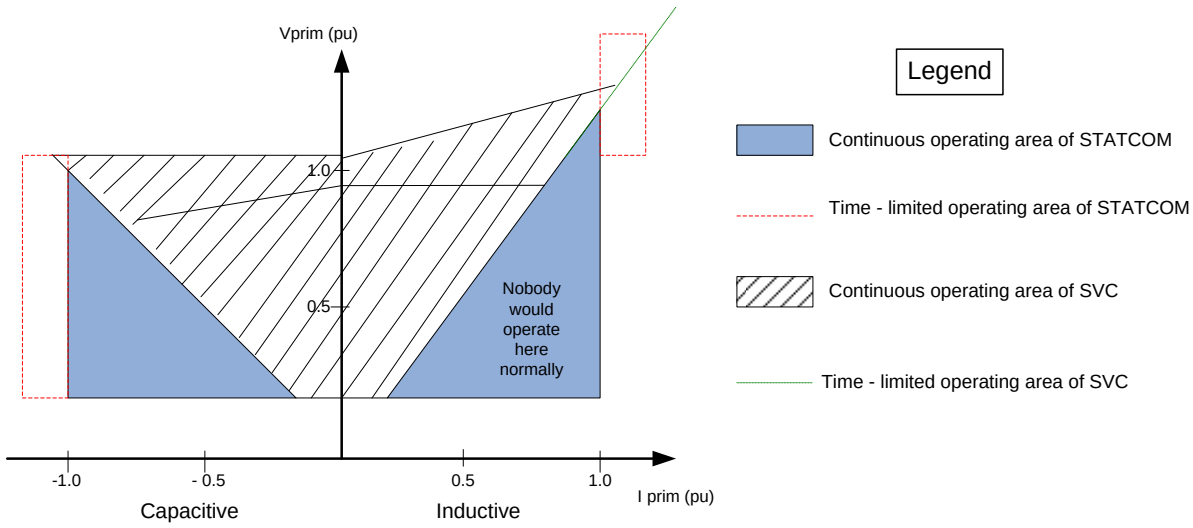

Figure 2.13: V/I characteristics of STATCOM versus SVC [20][21]

2.5.4 Performance Characteristics of STATCOM and SVC

2.5.4.1 V-I Characteristics

Figure 2.14 shows the ability of the STATCOM to regulate current along the voltage slope. The lower end of the slope is in the capacitive portion of the graph because at lower voltages, the STATCOM performs better in this portion by injecting capacitive current to regulate voltages.

The STATCOM can be specified with an increased transient current rating in both the capacitive and the inductive-operating regions. The maximum attainable transient overcurrent in the capacitive region is determined by the maximum current turn-off capability of the converter switches and converter cooling system [22]. The transient overload rating can be available both in the capacitive and inductive ranges only if specified when starting projects, as vendors don’t add the cooling for that for free.

In practice, the semiconductor switches of the converter are not lossless, so either the energy stored in the dc capacitor is eventually used to meet the internal losses of the converter and the dc capacitor voltage diminishes, or power is drawn from the ac system to supply the losses [22].

In the SVC characteriestics shown in Fgure 2.12, the capacitive output current changes linearly with ac voltage magnetude once the low voltage limit of the control range is hit, when the thyristors are not gated and all the capacitors are switched in.

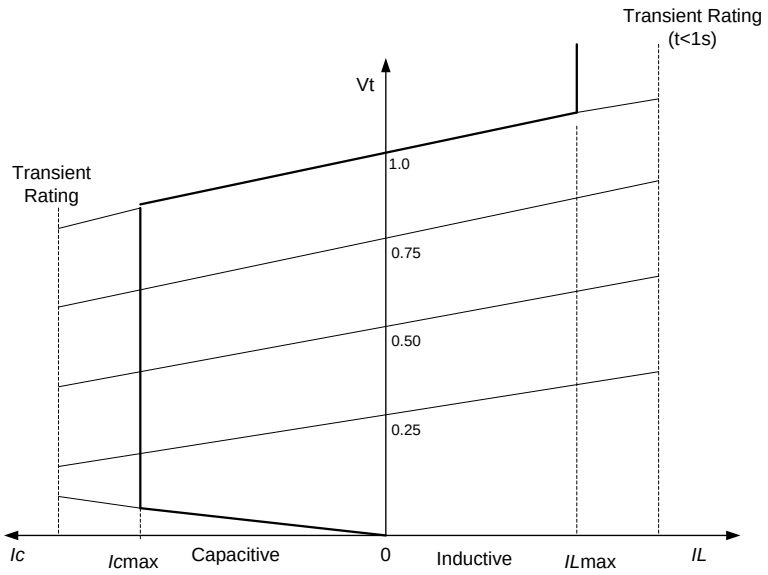

Figure 2.14:V-I characteristics of a STATCOM [22]

In the V-I characteristic of the SVC, the transient overload capability is only in the inductive range, but not in the capacitive range as shown in Figure 2.15.

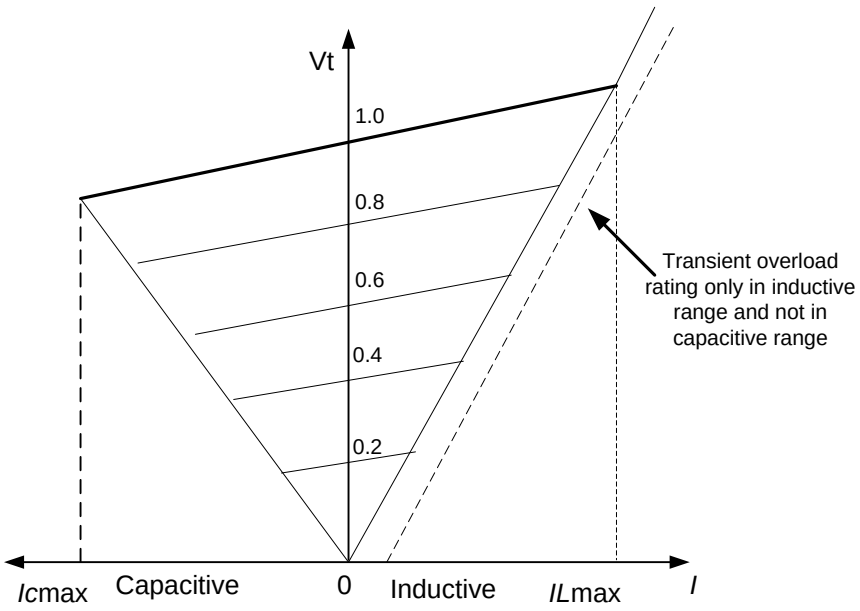

Figure 2.15: V-I characteristics of an SVC [23][24]

2.5.4.2 V- Q Characteristics

Figure 2.16 shows a simplified diagram of a STATCOM connected to a utility system. The output current of the STATCOM is proportional to the magnitude and angle difference of the converter and the utility voltages.

V_1 is the voltage of the system, V_2 is the terminal ac voltage of the VSC or STATCOM, X_{21} is the series reactance of the coupling transformer and δ is the angle of V_1 with respect to V_2. V_2 is the fundamental component of the VSC terminal voltage and δ is controlled by the converter.

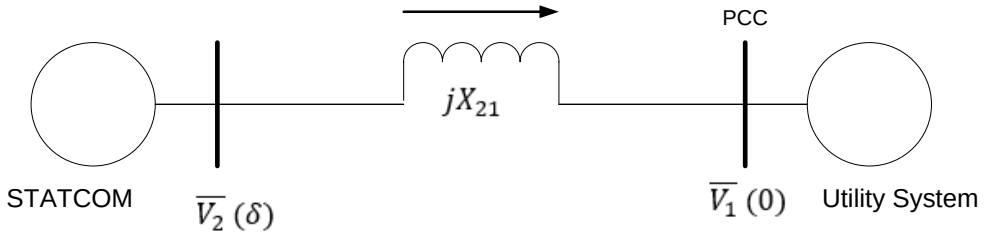

Figure 2.16: STATCOM and simple utility system equivalent circuit

In power systems, transmssion lines or coupling transformers typically have a series reactance given by $R + \omega L$. The X/R ratio is approximately 10 – 12 times (or bigger in transformers). Since the reactance (X) is significantly larger than the resistance (R) in a power system, in the example that follows, R is neglected to simplifythe calculation. By definition, series reactance has no R.

Assuming the voltage angle of the STATCOM, δ, is larger than the voltage angle of the utility system, power will flow from the STATCOM to the utility system.

For simplicity, the circuit impedance and current flow are given by:

$$\overline{Z_{21}} \approx jX_{21} \tag{2.3}$$

$$\overline{I_{21}} = \frac{\overline{V_2} - \overline{V_1}}{\overline{Z_{21}}} \tag{2.4}$$

The active power injected by the STATCOM is given by:

$$P_{21} = Re(\overline{V_2} * \overline{I_{21}}^{*}) \tag{2.5}$$

which, upon substituting (2.4) in (2.5) and simplifying results in:

$$P_{21} = \frac{|V_2|.|V_1| sin\ (\delta - 0)}{X_{21}} \tag{2.6}$$

The reactive power (Q_{21}) injected by the STATCOM to the utility system is given by:

$$Q_{21} = Im(\overline{V_2} * \overline{I_{21}}^{*}) \tag{2.7}$$

Substituting (2.4) into (2.7) and simplifying results in:

$$Q_{21} = \frac{|V_2|^2}{X_{21}} - \frac{|V_2|.|V_1| \cos(\delta - 0)}{X_{21}} \tag{2.8}$$

During steady-state operation as a STATCOM, the voltage V_2 generated by the VSC is in phase with V_1 ($\delta = 0$) so that only reactive power is flowing (P = 0). If $|V_2|$ is lower than $|V_1|$, Q is flowing from V_1 to V_2 (STATCOM is absorbing reactive power). On the reverse, if $|V_2|$ is higher than $|V_1|$, Q is flowing from V_2 to V_1 (STATCOM is generating reactive power.

2.6 Summary

FACTS devices are classified into series, shunt, combined series-series or combined series-shunt controllers. Series controllers connected in series with the transmission line are meant to inject voltage in series with the line. If the voltage is in phase quadrature with the line current, reactive power could be supplied or consumed. These devices can vary the line impedance and impact the magnitude of power transferred. An example of a series controller is the Static Series Synchronous Compensator.

Shunt controllers connected in parallel with the line are meant to inject current into the PCC. If the current is in phase quadrature with the line voltage, the voltage at the PCC could be increased or decreased. Examples of shunt controllers include STATCOMs and SVCs. Combined series-series and series-shunt controllers are capable of injecting both current and voltage into the system to vary the amount of reactive power in the power system.

In recent years, STATCOMs and SVCs are predominantly used to dynamically control reactive power injection into the system and reactive power absorption from the system. Compared with the SVC, the STATCOM has the main benefit of small footprint requirements for installation. The VSC is the main component of the STATCOM. The VSC allows the STATCOM to be designed with MMC. The larger the number of converter submodules, the higher the power output capability of the MMC STATCOM and the smoother the output voltage waveforms.

The STATCOM and SVC have different ranges of voltage regulation and V-I characteristics. The STATCOM demonstrates better capacitive voltage performance and the SVC demonstrates better inductive voltage performance. Also, in STATCOMs, transient overload rating is available for both the capacitive and inductive ranges while in SVCs, transient overload rating is only available in the inductive range.

Chapter 3: Power Converter Technology

3.1 Definition of Power Converters

A power converter is an electronic device or circuitry that changes power from one form to another for efficient power transfer. A power inverter transfers power from direct current (dc) to alternating current (ac) [25]. Since the power in an inverter is produced by the dc source, it is required that the dc power source be stable and capable of supplying approximate voltage and current for the intended power demands of the system.
The input voltage depends on the design and purpose of the inverter. Common dc voltage levels include:

- 12V to 48V for smaller consumer and commercial inverters for home energy systems
- 200V to 400V for photovoltaic solar panels
- 300V to 450V for electric vehicle battery applications in vehicle-to-grid systems
- Tens of kilovolts for VSC based FACTS
- Hundreds of kilovolts for high-voltage direct current (HVDC) power transmission systems.

There are two basic designs of converters for producing household ac voltage from a voltage dc source. The first design uses a dc-dc boost converter to increase dc voltage and then converts it to ac voltage via an inverter. The second design converts dc voltage to ac via an inverter and then uses a line-frequency transformer to increase the output voltage [26].

An HVDC converter transfers electric power between high voltage alternating current and high voltage direct current. HVDC is used as an alternative to alternating current for transmitting electrical energy over long distances or between ac power systems of different

frequencies [27]. HVDC converters are bidirectional as they can convert either from ac to dc (rectification) or from dc to ac (inversion). Electronic converters for HVDC are divided into two main categories.

- Line-commutated converters (LCC) made with electronic switches that have controlled turn-on and uncontrolled turn-off. LCC used the mercury valves for switching until the 1970s but now uses thyristors [28].
- Voltage-sourced converters (VSC) made with switching devices that exhibit controlled turn-on and turn-off. Modern VSCs now use the IGBTs for fast switching [29].

As of 2012, both the line-commutated and voltage-source technologies have seen significant application; with line-commutated converters used mainly where very high capacity and efficiency are needed, and voltage-sourced converters used mainly for interconnecting very weak ac systems, for connecting large-scale offshore wind-power to the grid, or for HVDC interconnections that are likely to be expanded to become multi-terminal HVDC systems in future. The market for voltage-source converter HVDC is growing fast, driven partly by the surge in investment in renewable power, with one particular type of converter, the modular multilevel converter emerging as a front-runner due to its benefits of lower harmonics, lower losses and modularity [30].

In STATCOM applications, the voltage-sourced converter is the main building block in a STATCOM. The VSC enables the STATCOM to regulate the local voltage magnitude of a utility grid by controlling reactive power injection to the grid when the terminal voltage magnitude of the VSC is higher than that of the local grid, or by absorbing reactive power from the local grid when the voltage magnitude of the VSC is lower than that of the local

grid. This can be achieved by keeping the dc voltage constant and controlling the reactive output current directly by controlling the converter output voltage through pulse width modulation (PWM) or some other direct voltage control scheme. PWM is a technique that compares a high frequency waveform (carrier signal) with a slow-varying waveform (modulation signal) for switching. The PWM technique is used in this dissertation.

3.2 Voltage Sourced Converters Overview

The VSC is built from of half-bridge switch submodules. Each submodule is composed of self-commutating switches in antiparallel connection with diodes. The dc system that provides a voltage source to the VSC dc bus capacitor can be a supercapacitor, a battery unit, photovoltaic or wind generation system or an ac/dc converter system [31].

Figure 3.1 shows a schematic diagram of the full-bridge, single-phase, two-level VSC (also known as an H-bridge converter). Two half-bridge VSCs are connected in parallel through their dc sides to realize the full bridge converter. One advantage of interfacing the ac side with full bridge converters is that for a given dc voltage, the synthesized ac voltage is twice as large and more efficient in comparison with half bridge VSC. The fundamental component of the ac-side voltage of a full bridge converter is usually controlled based on a pulse width modulation technique [31].

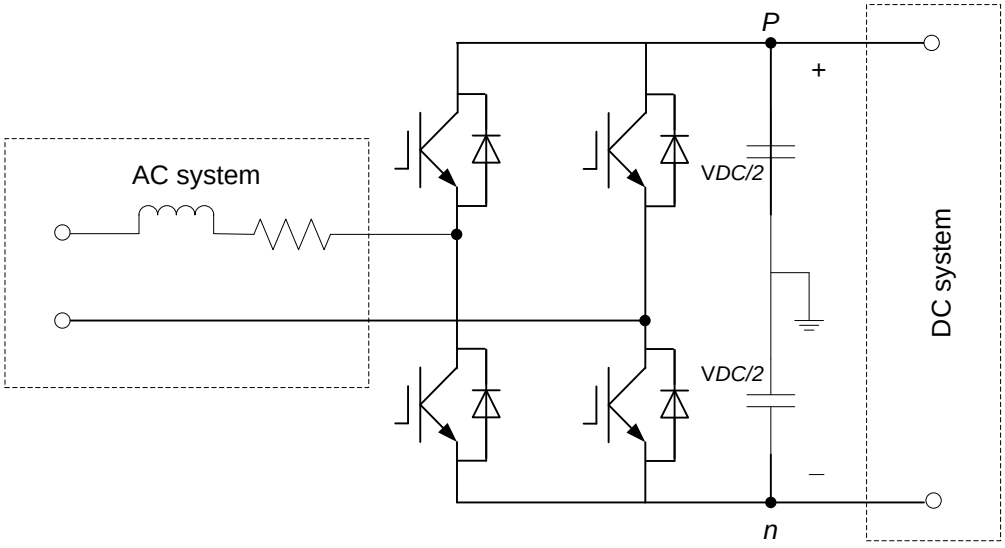

Figure 3.1: Schematic diagram of the single-phase, full-bridge, two-level VSC

The switching device and configuration for transmission applications has seen remarkable evolution from the 1940s with mercury valves, to thyristor valves in the 1970s and to applying voltage-sourced converters in the 1990s, with improvements, reliability, controllability, compactness, and ease of system interface. Figure 3.2 shows a representation of the evolution of switch converters.

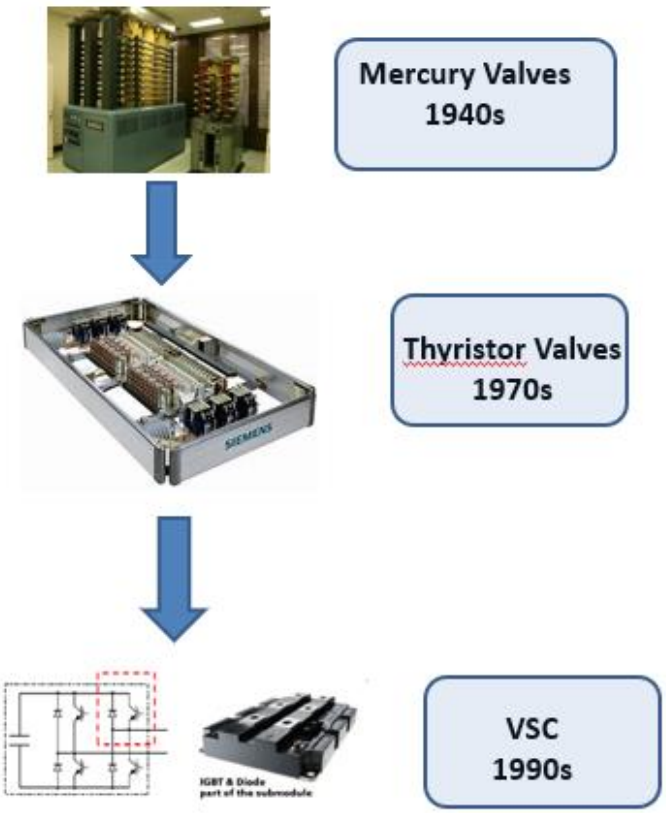

Figure 3.2: Evolution of switch converters for HVDC and FACTS [3]

With the application of VSC technology to transmission applications, it is important to understand the control schemes of VSCs, and for this work, more specifically for STATCOMs, the challenges in incorporating a real power source such as an energy storage system to the dc link.

3.3 Control Schemes For STATCOMs

There are challenges in designing a reliable and stable STATCOM with an energy storage system, and effectively controlling the device to achieve the objectives for the system applications. There are two typical STATCOM control schemes:

- Indirect control method (older method)
- Direct control method

1) The indirect control method controls the reactive output current indirectly by controlling the dc capacitor voltage via controlling the angle of converter output voltage;
2) The direct control method keeps the dc voltage constant and controls the reactive output current directly by controlling the converter ac voltage magnitude through pulse width modulation or some other direct ac voltage control scheme. With the emergence of high voltage devices that could be connected in series, the advent of multilevel converter topologies and variant PWM technologies, the direct control method has been widely utilized. It is also the focused control method in this dissertation [32].

3.3.1 PWM Switching Scheme for two level VSC

PWM can be implemented using numerous techniques. The simplest technique to compares a high frequency periodic triangular waveform, the carrier signal, with a slow-varying waveform known as the modulating signal [31]. The intersection of the carrier and modulating signals determine the switching instant of the IGBT switches. Figure 3.3 illustrates the PWM process where the switching function of a switch is defined as:

$$S(t) = \begin{cases} 1, & \text{if the switch is commanded to conduct} \\ 0, & \text{if the switch is turned off} \end{cases}$$

Once the modulating signal is smaller than the carrier signal, Switch S1 is turned off and the Switch 4 turn-on command is issued. Switch 4 will only turn ON if the command is issued. Similarly, once the modulating signal is greater than the carrier signal, Switch S1 turned-on command will be issued and Switch 4 will receive a turn-off command. This PWM strategy controls switching in the ac direct voltage control method. Real converters include a blanking time where neither switch is turned on to prevent shorting the dc link [31].

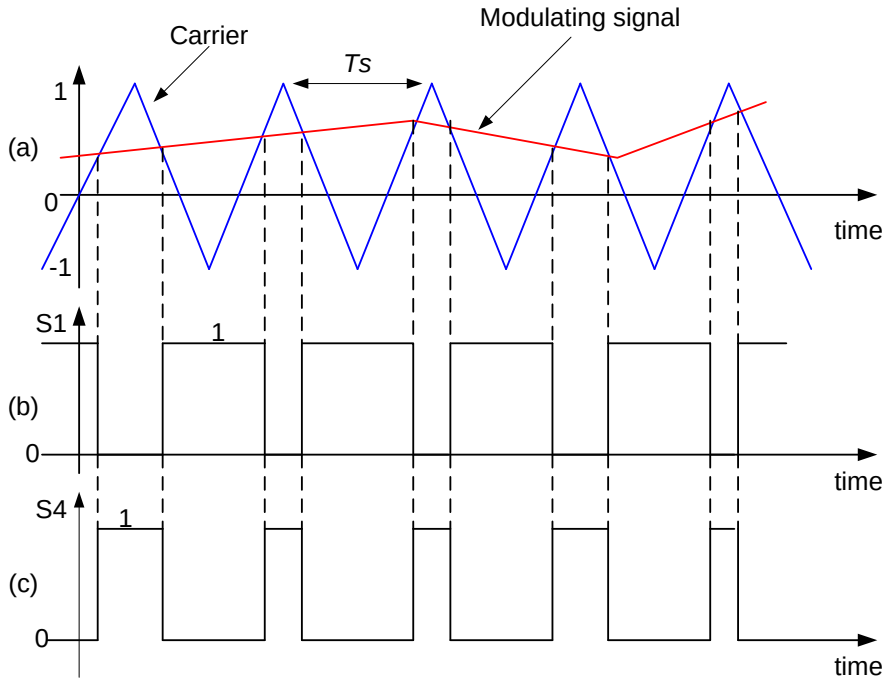

Figure 3.3: Carrier-based PWM switching technique [31]

Where Figure 3.3 shows the following:

(a) Carrier and modulating signals;

(b) Switching function of S1;

(c) Switching function of S4;

A complete two level, three-phase PWM VSC would consist of three of the single-phase half-bridge modules with modulating functions consisting of sinusoids shifted by 120 degrees between phases. Frequency control in a PWM converter is accomplished by changing the frequency of the input modulating voltage. A PWM converter switches states many times during a single cycle of the resulting output voltage. This rapid switching means that PWM converters require fast components such as IGBTs for proper operation. IGBTs

are preferred components for building high voltage, high MVA converters due to their combination of high-speed turn-on/turn-off and high-power switching capabilities [33].

3.3.2 Real and Reactive Power Control of STATCOM

To control the real and reactive power, $P_s(t)$ and $Q_s(t)$, that the VSC exchanges with the ac system, the dc side of the VSC is connected in parallel with a dc voltage source. Figure 3.4 shows a VSC system that will be used to describe the real and reactive power control scheme [31].

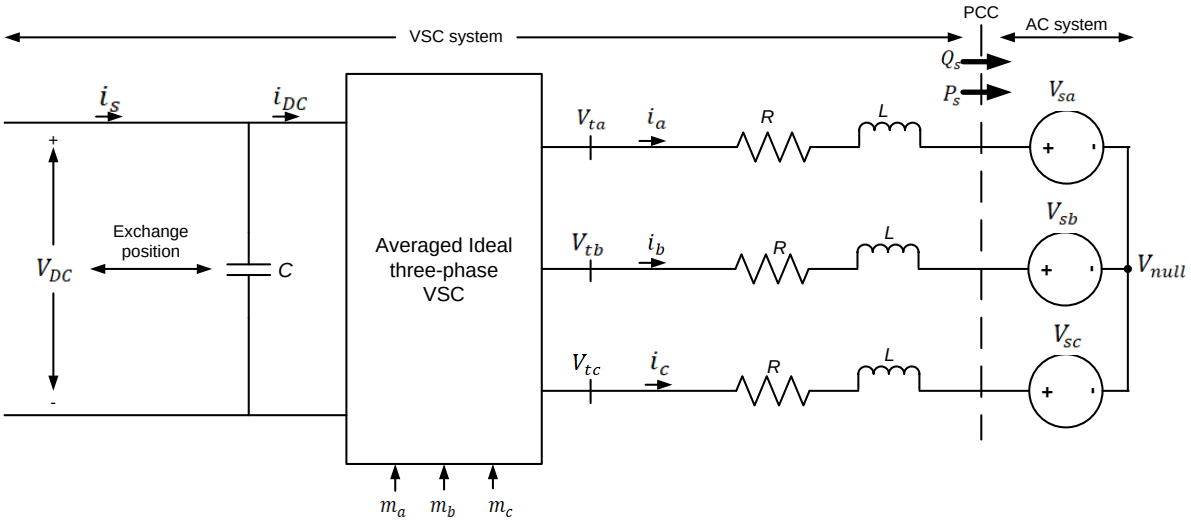

Figure 3.4: VSC real and reactive power Controller

There are two commonly used methods to control the P_s and Q_s transfer at the PCC for high power applications as seen in Figure 3.4: voltage-mode control and current-mode control.

The voltage-mode method was used in early high voltage and power VSC applications such as in FACTS controllers and some industrial applications [34][35][36]. In the voltage-mode control method, the real and reactive power are controlled, respectively, by the phase angle and the amplitude of the VSC ac-side terminal voltage relative to that of the PCC or ac

side voltage [37]. If the phase angle and amplitude of V_{tabc} and that of V_{sabc} are close to each other, the real and reactive power are almost decoupled, and two independent compensators can be employed for their controls, as seen in Figure 3.5. The main disadvantage of this control is that there is no closed control loop on the VSC line current, and therefore, the VSC is not protected against overcurrent, and the current may undergo large current excursions if the power commands are rapidly changed or faults occur in the ac system or between the converter and the PCC [31].

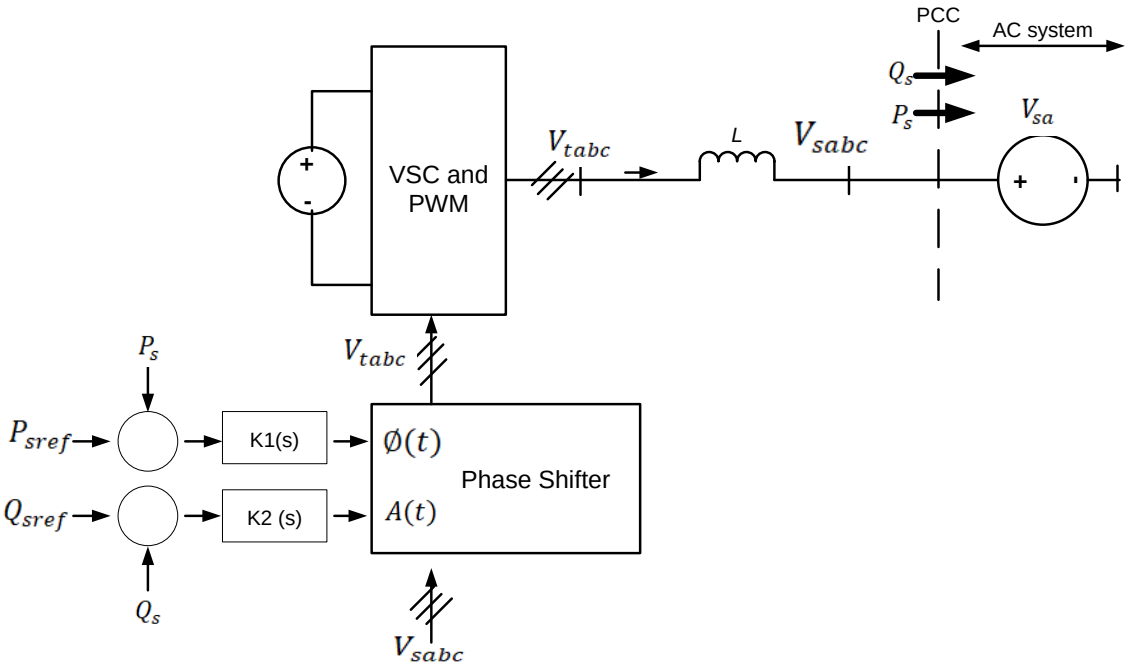

Figure 3.5: Voltage-mode control of real and reactive power for VSC

In the ac current-mode control method, the real and reactive power controllers determine current references for fast current regulators implemented in the synchronous dq reference frame. In this method, the VSC line current is tightly regulated by the dedicated current-control scheme, synchronized to the ac voltage at the PCC. Therefore, the VSC is protected against overcurrent [31].

In this dissertation, the current control mode method is performed in the synchronous dq-frame. The synchronous dq-frame control has many advantages, one of which is that the control variables are dc quantities in steady-state, resulting in easier control design, compared to tracking sinusoidal quantities. Figure 3.6 shows a schematic diagram of a current-mode real and reactive power controller in the synchronous dq-frame.

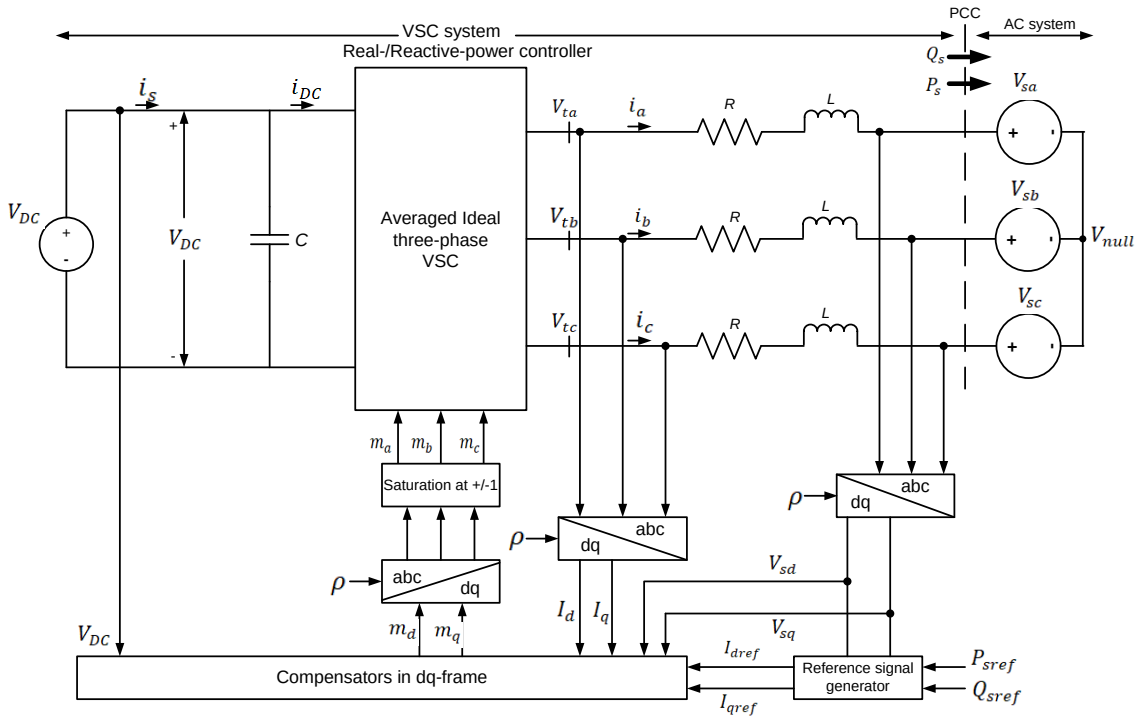

Figure 3.6: Current-mode control of real and reactive power for VSC [31]

The P_s and Q_s quantities are controlled by regulating the line current components I_d and I_q determined from I_{dref} and I_{qref}. First, the feedback and feed-forward signals are transformed to the dq-frame and then processed by compensators to produce the modulating signals in dq-frame. Finally, the modulating signals are transformed to the abc-frame and fed to the VSC. The reference commands I_{dref} and I_{qref} limited by saturation blocks are used to protect the VSC [31].

3.3.3 Dynamic Model of Real and Reactive Power Controller

From Figure 3.6, the ac system voltage at the PCC can be represented as [31]:

$$V_{sa}(t) = \overline{V_s} \cos\ (\omega_0 t + \theta_0) \tag{3.1}$$

$$V_{sb}(t) = \overline{V_s} \cos\ (\omega_0 t + \theta_0 - \tfrac{2\pi}{3}) \tag{3.2}$$

$$V_{sc}(t) = \overline{V_s}\ \cos\ (\omega_0 t + \theta_0 - \tfrac{4\pi}{3}) \tag{3.3}$$

Where $\overline{V_s}$ is the peak value of the line-to-neutral voltage, ω_0 is the AC system (source) frequency, and θ_0 is the source initial phase angle.

The space-phasor differential equation of the dynamics of the AC side of the VSC can be expressed as:

$$\tfrac{Ld\vec{\imath}}{dt} = -(R)\vec{\imath} + \overrightarrow{V_t} - \overrightarrow{V_s} \tag{3.4}$$

Assuming the space-phasor equivalent of V_{s-abc} is $\overrightarrow{V_s}(t)\ = \overline{V_s}\ e^{j(\omega_0 t+\theta_0)}$

Substituting $\overrightarrow{V_s}\ = \overline{V_s} e^{j(\omega_0 t+\theta_0)}$ in (3.4) gives:

$$\tfrac{Ld\vec{\imath}}{dt} = -(R)\vec{\imath} + \overrightarrow{V_t} - \overline{V_s} e^{j(\omega_0 t+\theta_0)} \tag{3.5}$$

To express (3.5) in dq-frame, we substitute $\vec{\imath} = i_{dq} e^{j\rho}$ and $\overrightarrow{V_t} = V_{tdq} e^{j\rho}$ in (3.5)

$$\tfrac{Ld\vec{\imath}}{dt} = -(R) i_{dq} e^{j\rho} + V_{tdq} e^{j\rho} - \overline{V_s}\ e^{j(\omega_0 t+\theta_0)} \tag{3.6}$$

Assuming $f_{dq} = f_d + j f_q$ and simplifying further, the real and imaginary components can be expressed as:

$$\tfrac{Ldi_d}{dt} = \left(\tfrac{Ld\rho}{dt}\right) i_q - (R) i_d + V_{td} - \overline{V_s} \cos\ (\omega_0 t + \theta_0 - \rho) \tag{3.7}$$

$$\frac{Ldi_q}{dt} = \left(\frac{Ld\rho}{dt}\right) i_d - (R)i_q + V_{tq} - \overline{V_s}\sin(\omega_0 t + \theta_0 - \rho) \quad (3.8)$$

If $\rho(t)$ transforms the quantities to the synchronous rotating reference frame, the values V_{td}, V_{tq}, i_d and $i_q$are constant in steady-state as the product terms involving V_s in the equation. The mechanism used here to ensure $\rho(t) = \omega_0 t + \theta_0$ synchronized with the PCC is a phase-locked loop (PLL).

Figure 3.8 shows the schematic diagram of a 3-phase implementation of a PLL [31]. The PLL transforms V_{sabc} to V_{sdq} and adjusts the rotational speed of the synchronous dq-frame transformation through a PI controller, such that V_{sq} is forced to zero in the steady state when synchronized. The result is that $\rho = \omega_0 t + \theta_0$ and $V_{sd} = \overline{V_s}$.

The integrator in Figure 3.7 is realized by means of the voltage-controlled oscillator (VCO). The VCO is a resettable integrator whose output, ρ (t), is reset to zero whenever it reaches 2π [31].

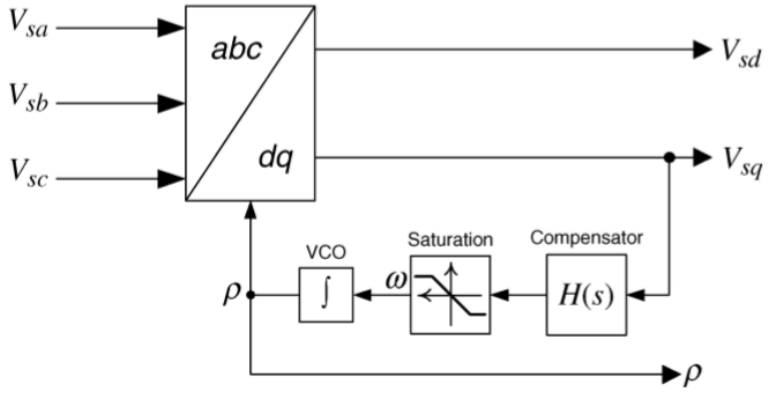

Figure 3.7: Schematic diagram of the PLL [31]

3.4 Modular Multilevel Converter History and Benefits

Modularity, in general, refers to a technique to develop comparably large systems by combining smaller subsystems. For power converter topologies, a cascaded connection of converter cells is an interesting solution to reach high voltage with high quality waveforms with minimum complexity [38]. The term multilevel converter was created with three-level converter designed for traction applications [5]. Subsequently, several multilevel converter topologies have been developed [39][40][41][42].

Since the 1990s, multilevel inverters have slowly gained prevalence in the high MVA power electronics industry. Compared with conventional inverters, multilevel inverters have two distinguished features that make them more suitable for high MVA applications requiring good waveform quality:

- Reduced switching losses
- Standard building block; meaning that vendors don't need a custom converter and filter design for every application

3.5 Multilevel Inverter Topologies

Multilevel inverters have been developed and utilized in various topologies. Three typical topologies are: diode-clamped multilevel converters, flying capacitor multilevel converters, and cascaded multilevel converters. Each of these topologies has applications they are well suited for. Overall, the cascaded topology has several advantages over the diode-clamped and flying capacitor topologies for transmission level applications. Some of

the advantages are that the cascaded topology with half bridge submodules needs fewer components compared with diode-clamped and flying capacitor inverters. Cascaded converters have reduced switching losses at high voltages compared to the other two designs. Due to modular design and maybe weight, the price of the cascaded inverter is less than those of the other two inverters for high voltage applications. But that applies to all three and requires modifications to the design. Soft switching is possible by some of the new switching methods [43].

The general concept of multilevel inverters involves producing an ac waveform from voltage steps created by utilizing a bank of series capacitors or separated dc sources [44]. Multilevel inverters perform power conversion in multiple voltage steps, which improves waveform quality and lowers total harmonic distortion (THD) in output voltage, and lowers switching losses. With these advantages, multilevel inverters have been gaining considerable popularity in recent years for high voltage transmission applications [45]. One of the challenges of multilevel inverters is simplifying the complex control scheme as the number of levels increases.

Figure 3.7 shows the three multilevel inverter topologies mentioned above. In recent years, the cascaded multilevel inverter topology has been the most prevalent of the three topologies for transmission applications. It consists of a combination of power modules in series and parallel. This configuration does not need extra capacitors and diodes for clamping. The output waveform is quite sinusoidal in nature with a sufficient number of levels or application of PWM and does not need filtering. One of the major issues of the cascaded topology is that the separate dc sources may seem to create an increase in the number of components and a burden to the system. This issue has been resolved by having

fewer dc sources and a separate DC (SDC) topology has also be proposed [46]. On the other hand, the separate dc sources make multilevel inverters suitable for integrating battery energy storage, solar, wind and other sources of renewable energy.

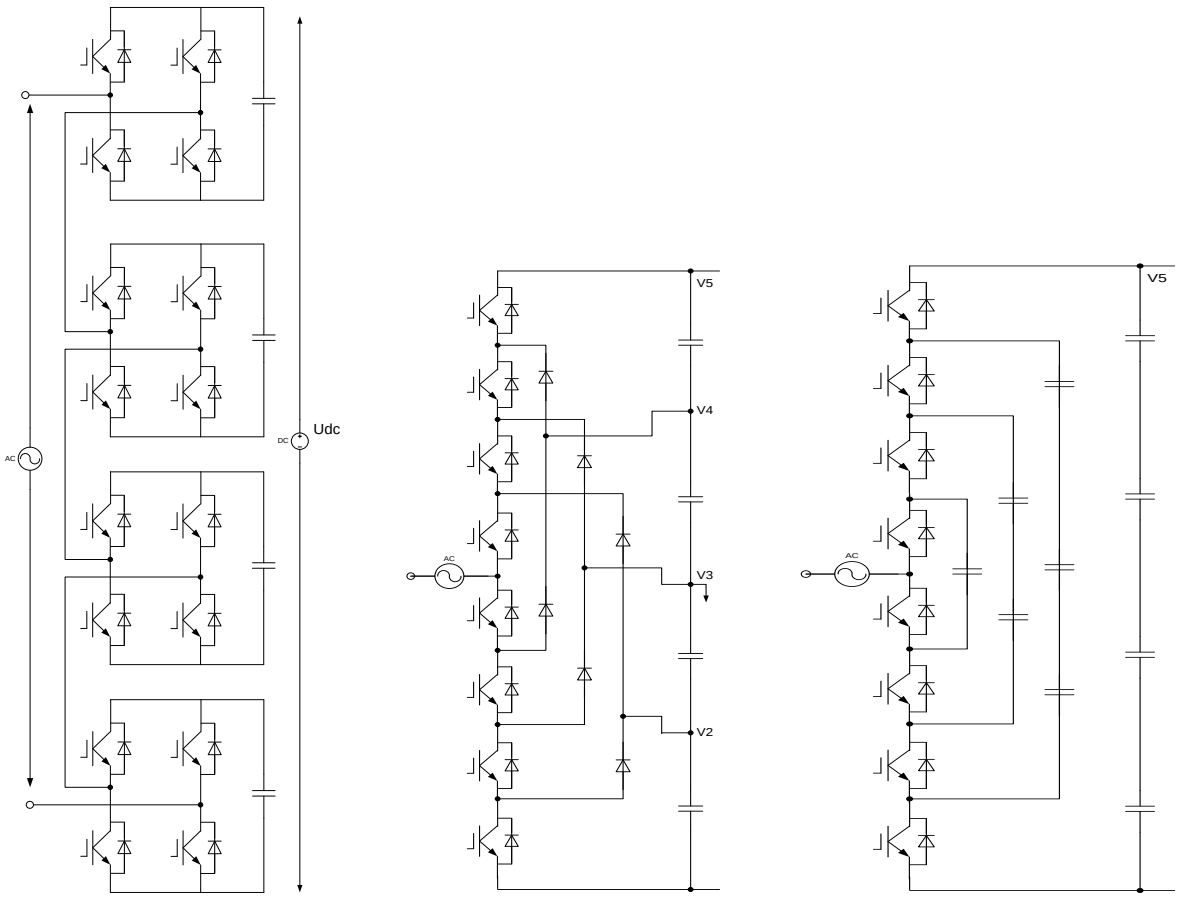

(a) Cascaded full bridge (b) Diode-clamped (c) Flying capacitor

Figure 3.7:Multilevel Inverter Topologies

3.6 Equivalent Circuit of Half Bridge VSC

Figure 3.8 shows an equivalent circuit of a half-bridge submodule-based multilevel VSC. A bidirectional, single-pole, multi-throw switch is a key element of the multilevel model. By controlling the way in which the switch is connected to a portion of the string of

capacitors, a number of output voltage levels can be synthesized. To generate a negative output voltage, the reference of the output can be connected to different segments of the capacitor string [38].

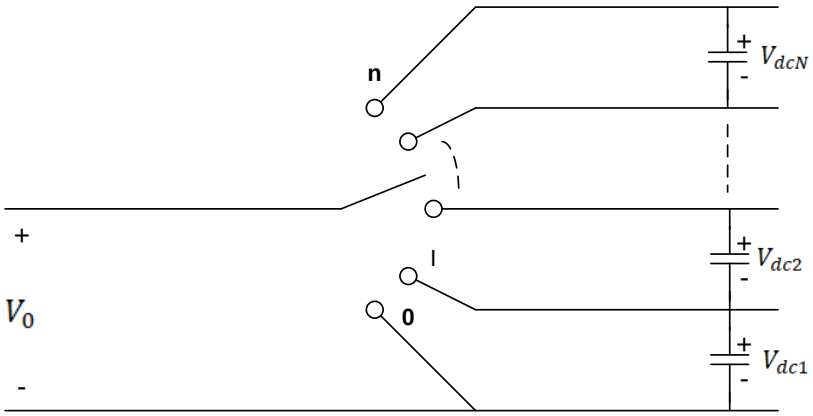

Figure 3.8: Equivalent circuit of multilevel voltage-sources converter

3.7 Sinusoidal Approximation of Multilevel Converter

Figure 3.9 illustrates an example of a multilevel converter output voltage waveform. In this figure, the waveform shown has a peak-to-peak voltage of 1.0 kV. In this case, the multilevel converter produces a fair approximation to a sinusoidal waveform. The multilevel converter output stepped waveform contains sharp transitions. This phenomenon results in harmonics at multiples of the switching frequency, which can be eliminated by filters. With enough levels and the resulting relatively small steps, the internal impedances of the converter and its line connections and their relationship to the loads tends to filter much of the switching frequency harmonics, without much further filtering effort. Filters may be unnecessary, depending on the load and line topology.

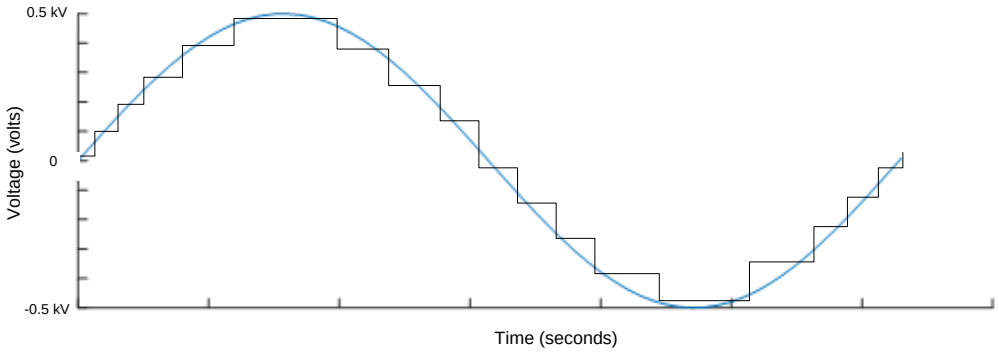

Figure 3.9: Example multilevel sinusoidal approximation [47]

Both the size of voltage steps and related voltage gradient are minimized if the AC voltage generated by the converter can be selected in small increments. Having smaller voltage increments at each switching instance also reduces losses. This is accomplished by increasing the number of submodules connected in series. Reducing the voltage step size also reduces harmonic voltage distortion [3].

Although the MMC-based STATCOM can provide the needed reactive power support in high voltage applications, the ability to support real power control is limited due to limited energy storage capability of the submodule dc-link capacitors. This energy storage deficiency can be mitigated by connecting an energy storage system (ESS) in parallel with the dc-link capacitor [7]. Combining the MMC STATCOM with an energy storage system would provide capability to dynamically inject both real and reactive power to the medium or high voltage grid, for better power quality and stability [5][6][7][11][48]. Energy storage would also provide improved flexibility for integration of renewables to the electric grid. An enhanced modular multilevel converter based STATCOM with hybrid energy storage system (E-STATCOM/BE3SC) is proposed, which will be described in more detail in Chapter 4. In addition to dynamically controlling real and reactive power, the proposed enhanced STATCOM design also reduces the depth of discharge (DOD) of a battery and

prolongs the battery life by combining with an appropriately sized supercapacitor. This additional benefit of adding supercapacitors improves upon what has been presented in other papers that combine STATCOMs with ESS.

Chapter 4: MMC-based STATCOM with Hybrid Energy Storage

4.1 Introduction of the E-STATCOM/BE3SC

An MMC STATCOM connected to a hybrid battery energy storage and supercapacitor system can control both active and reactive power flow, providing more flexibility and versatility in power transmission operations as shown in [5][48]. Recent technological advances make it more reasonable to utilize STATCOMs with a hybrid combination of battery and supercapacitors (HESS), in high power applications.

Combining an MMC STATCOM, battery and supercapacitors allows active power output and power input control. The design is an ideal tool for providing fast frequency response in the first few seconds of a major grid disturbance. While the STATCOM part provides inductive or capacitive reactive power, the electrical energy in the battery and supercapacitors is injected into the grid in order to secure the grid from needing load shedding or even prevent a blackout. Adding supercapacitors is potentially an economical solution to combine with batteries, to provide fast responding high power density storage. Due to the low losses and easy maintenance, improved energy efficiency can be achieved with supercapacitors.

Figure 4.1 shows a basic diagram of the proposed E-STATCOM/BE3SC, and Figure 4.2 shows a single-phase, two-submodule topology of the E-STATCOM/BE3SC design which are described in greater details in the next section. The design in Figure 4.1 consists of a dc-capacitor connected in parallel with the VSC and is used to build the ac voltage. The figure does not show the MMC submodules. A hybrid combination of battery and supercapacitor is connected in parallel with the dc-capacitor via bidirectional dc-dc converters to efficiently

control real and reactive power to and from the ac system, based on the control of the VSC. The bidirectional dc-dc converter allows two directional power flow to charge and discharge the energy storage system based on the system needs. One of the applications employed in this dissertation is to measure the grid frequency and send an active power command to allow the flow of power from the grid to the ESS (charging) when the grid frequency is above a set point, or to allow the flow of power from the ESS to the grid (discharging) when the grid frequency is below a set point. Details of this control scheme will be discussed in Chapter 6. The VSC consists of fast switching IGBTs which allow exchange of power between the ESS and the grid as well as controlling reactive power injection.

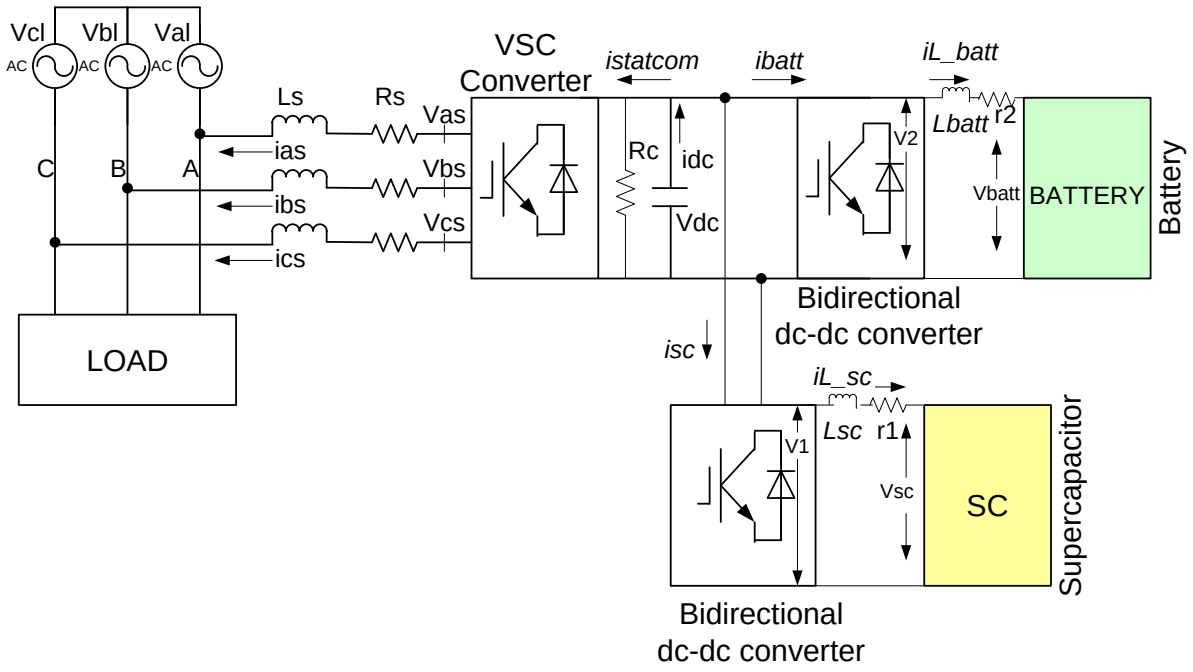

Figure 4.1: Basic diagram of an E-STATCOM/BE3SC

The design in Figure 4.2 shows a single-phase, two-submodule, full bridge topology of the enhanced STATCOM with a hybrid combination of battery and supercapacitor energy storage. Each submodule consists of four IGBTs switches with antiparallel diodes arranged in the form of an "H" (sometimes called H-bridge). The submodules are connected in series to

increase the power capability and flexibility of the design as well as to improve AC waveforms. Among other benefits, this makes the design suitable for high and medium voltage transmission applications. Hundreds of submodules can be connected in a multilevel topology for improved waveforms. Some transmission applications have seen designs that consist of over 400 submodules of converter for each of the three phases [31]. For ease of simulation, this dissertation will use 22 modules for each MMC STATCOM branch and PWM switching. The ESS is comprised of batteries and supercapacitors connected through bidirectional dc-dc converters and can be connected across the dc link capacitor of each submodule. Each ESS has a dedicated bidirectional dc-dc converter to facilitate sizing and flexibility of control. For simplicity, the HESS is connected to only 2 of the 22 modules of the MMC STATCOM.

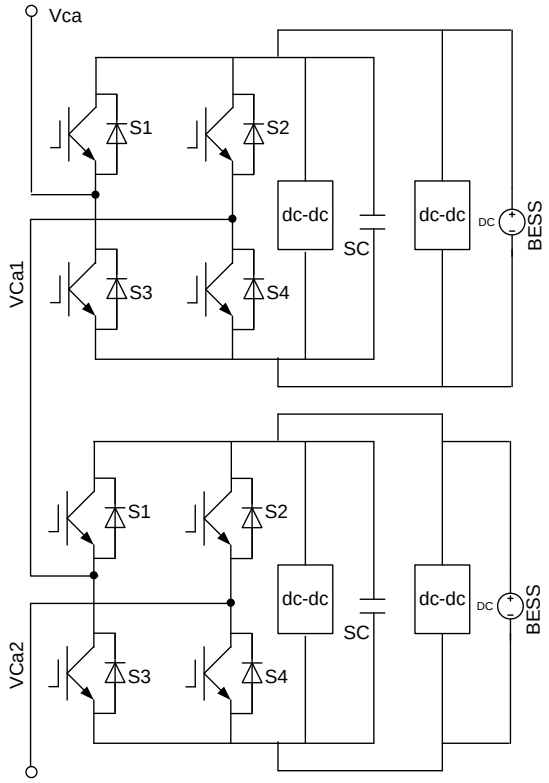

Figure 4.2: Single-phase, two-submodule topology of E-STATCOM/BE3SC

4.2 Overview of the E-STATCOM/BE3SC Design

The proposed design, which is capable of both dynamic real and reactive power control on the electric grid, consists of five basic elements:

- Voltage Sourced Converter (VSC)
- dc capacitor
- ac coupling reactor
- Hybrid Energy Storage System (battery and supercapacitor) (HESS)
- dc-dc converter stages

The voltage sourced converter, dc capacitor and ac coupling reactors are components of the MMC STATCOM. The HESS, battery-supercapacitor hybrid, provides a source for real power control and the STATCOM provides a source for reactive power control. The battery and supercapacitor energy storage devices are each connected via dc-dc bidirectional converters to the dc link capacitor. The advantage of adding the dc-dc converter is to efficiently control the real power outputs of the storage devices individually for optimum operation.

Using Figure 4.1 and references [49] and [50], the following expressions represent the STATCOM mathematical responses for the ac side (4.1) – (4.3) and the dc side (12) behavior:

$$L_s \frac{d}{dt} i_{as} = -R_s i_{as} + V_{as} - V_{al} \tag{4.1}$$

$$L_s \frac{d}{dt} i_{bs} = -R_s i_{bs} + V_{bs} - V_{bl} \tag{4.2}$$

$$L_s \frac{d}{dt} i_{cs} = -R_s i_{cs} + V_{cs} - V_{cl} \tag{4.3}$$

$$\frac{d}{dt}\left(\frac{1}{2}CV_{dc}^2(t)\right) = -[V_{as}i_{as} + V_{bs}i_{bs} + V_{cs}i_{cs}] - \frac{V_{dc}^2(t)}{R_c} \quad (4.4)$$

Where:

R_s = Series resistance of the transformer windings

L_s = Transformer leakage inductance

R_c = Resistance in parallel with DC − link capacitor; represents a switching loss term

V_{as}, V_{bs}, V_{cs} = STATCOM three phase output voltages at converter terminal

V_{al}, V_{bl}, V_{cl} = Bus voltages at point of interconnection

i_{as}, i_{bs}, i_{cs} = STATCOM AC currents

The ac currents are transformed to the synchronous two-axis reference using the Park's transformation. The state equations of the VSC can be represented in the synchronous reference frame using (13) [14].

$$\frac{d}{dt}\begin{bmatrix} i_{ds} \\ i_{qs} \\ V_{dc} \end{bmatrix} = \begin{bmatrix} -\frac{R_s}{L_s} & \omega & \left(\frac{K}{L_s}\right)cos\alpha \\ -\omega & -\frac{R_s}{L_s} & \left(\frac{K}{L_s}\right)sin\alpha \\ \left(-\frac{3K}{2C}\right)cos\alpha & \left(-\frac{3K}{2C}\right)sin\alpha & -\frac{1}{R_c} \end{bmatrix}\begin{bmatrix} i_{ds} \\ i_{qs} \\ V_{dc} \end{bmatrix} - \frac{1}{L_s}\begin{bmatrix} V_{dl} \\ V_{ql} \\ 0 \end{bmatrix} \quad (4.5)$$

Where:

i_{ds}, i_{qs} are the STATCOM synchronous reference frame direct and quadrature axis currents, respectively, V_{di}, V_{qi} are the synchronous reference frame direct and quadrature axis voltages corresponding to V_{al}, V_{bl}, V_{cl} at the point of interconnection as the high side of the transformer

V_{dc} is the voltage across the dc link capacitor,

α is the phase rotating angle ($\alpha = \omega t$)

ω is the angular speed at system normal frequency

As discussed in Chapter 3, Section 3.3, the synchronization circuit regulates the converter voltage $V_{qi} = 0$.

Therefore, the real and reactive power equations can be written, respectively, as:

$$P_l = \frac{3}{2} V_{dl} i_{ds} \tag{4.6}$$

$$Q_l = \frac{-3}{2} V_{dl} i_{qs} \tag{4.7}$$

The STATCOM real and reactive control strategy can be obtained from these equations.

The DC side current equation can be written as [11]:

$$i_{dc} = c \frac{d}{dt} V_{dc} + \frac{V_{dc}}{R_c} \tag{4.8}$$

4.3 Mathematical Representation of E-STATCOM/BE3SC Control

The bidirectional dc-dc converters in Figure 4.1 control the amount of power supplied or received by the battery and supercapacitor. The dc-dc converters are controlled relative to the dc link voltage of the inverter module, V_{dc} which is regulated by the STATCOM so that there will be no change in the STATCOM control strategy [11]. The STATCOM control chooses an active power command which would cause V_{dc} to change and cause the dc-dc converter to charge or discharge the ESS. Details of the control strategy are presented in Chapter 6.

The following equations can be utilized to calculate the current drawn by the dc-dc converter connected to the battery and the dc-dc converter connected to the supercapacitor [11].

From Figure 4.1, the differential equation for the voltage of the DC bus is given by the expression:

$$C\frac{d}{dt}V_{dc} = i_{dc} - \frac{V_{dc}}{R} \tag{4.9}$$

(C is the capacitance of the DC link capacitor)

$$i_{dc} = i_{batt} + i_{SC} + i_{statcom} \tag{4.10}$$

From (4.9) and (4.10)

$$C\frac{d}{dt}V_{dc} + \frac{V_{dc}}{R_c} = i_{batt} + i_{SC} + i_{statcom} \tag{4.11}$$

$$i_{batt} = C\frac{d}{dt}V_{dc} + \frac{V_{dc}}{R_c} - (i_{SC} + i_{statcom}) \tag{4.12}$$

$$i_{SC} = C\frac{d}{dt}V_{dc} + \frac{V_{dc}}{R_c} - (i_{batt} + i_{statcom}) \tag{4.13}$$

Where:

i_{batt} is the current drawn by the dc-dc converter connected to the battery

i_{SC} is the current drawn by the dc-dc converter connected to the supercapacitor

Assuming m_1 and m_2 are the modulation functions of the respective dc-dc converters, L_{sc} and L_{batt} are the dc-dc converter filter inductances and r_1 and r_2 are the respective internal resistances of the smoothing inductors, the average model of the dc-dc converters can be represented by equations (4.14) and (4.15):

$$V_1 = m_1 V_{dc} \tag{4.14}$$

$$V_2 = m_2 V_{dc} \qquad i_{SC} = \frac{1}{m1} i_{L_{sc}} \tag{4.15}$$

(Where subscript 1 denotes SC and subscript 2 denotes battery)

The current through the battery is a product of the modulating function and the current through the smoothing inductor of the battery.

$$i_{batt} = \frac{1}{m2} i_{L_{batt}} \tag{4.16}$$

The average model equivalent for the energy storage systems in Figure 4.1 can be represented in terms of the voltage across the supercapacitor by the relationship in (4.17) and voltage across the battery by (4.18)

$$L_{sc} \frac{d}{dt}\, i_{L_{sc}} + r_1 i_{L_{sc}} = V_1 - V_{sc} \tag{4.17}$$

$$L_{batt} \frac{d}{dt}\, i_{L_{batt}} + r_2 i_{L_{batt}} = V_2 - V_{batt} \tag{4.18}$$

The supercapacitor voltage V_{sc} delivered to the system is given by:

$$V_{sc} = r_{sc} i_{sc} + \frac{1}{C_{sc}} \int i_{sc} dt \tag{4.19}$$

From [51] and columbic algorithm, the state of charge (SOC) of the supercapacitor and battery can be calculated as:

$$SOC_{sc}\% = \frac{V_{sc}}{V_{sc_{max}}}\, x\, 100 \tag{4.20}$$

$$SOC_{batt}\% = SOC_{batt\_init}\% + \int \frac{(i_{batt}\, \eta)}{C_n}\, dt\, x \frac{100}{3600} \tag{4.21}$$

(Since 1Watt-hour = 3,600 Joules, the term in (4.21) is divided by 3,600 to convert it to Watt-hours.)

Where:

r_{sc}, C_{sc} are the internal resistance and capacitance of the supercapacitor, respectively

V_{sc}, $V_{sc_{max}}$ are the supercapacitor voltage and maximum supercapacitor voltage, respectively

η is the Faradaic efficiency

C_n is the storage capacity of the battery

4.4 Principles of Operations of MMC with Separate DC Sources

An MMC configured with separate dc sources is discussed here. Figure 4.3 shows the basic structure of a three-phase Y-configured VSC made from cascaded inverters with separate DC sources. In this application, each separate dc source is associated with a single-phase full bridge VSC. The ac terminal voltages of submodule inverters are connected in series [45].

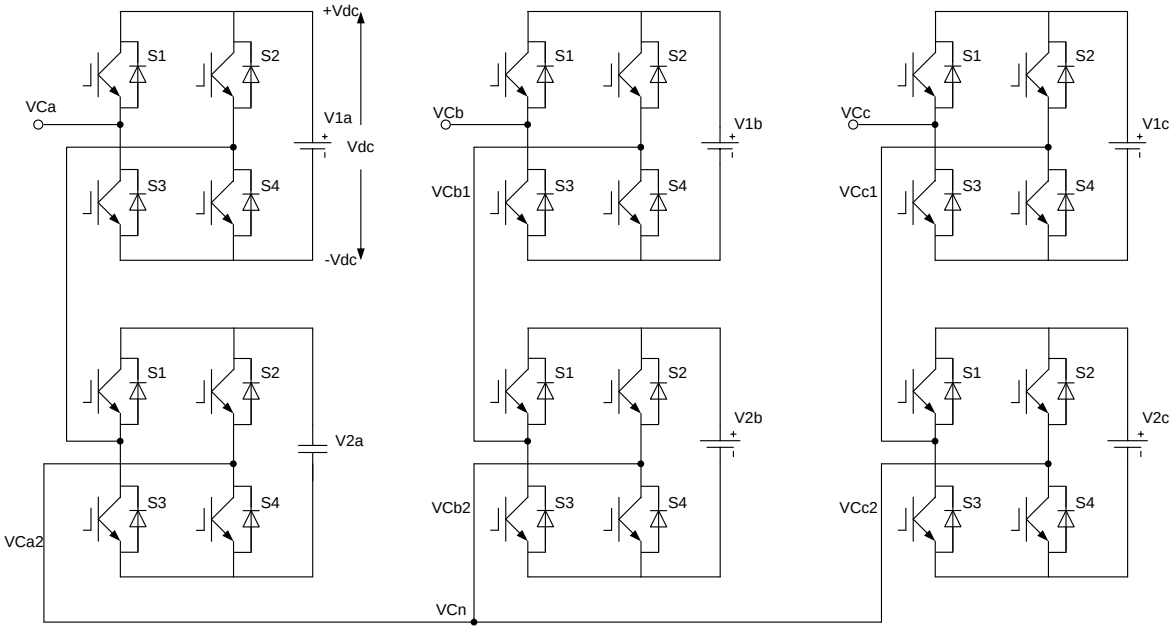

Figure 4.3: MMC with separate dc sources

Different combinations of switch positions for each single-phase full bridge inverter determine three different levels of voltage output levels:

$+V_{dc}$, 0, $-V_{dc}$

This is made possible by connecting the DC sources to the ac side via the combination of the four semiconductor power devices (IGBTs). Two switching combinations are present for 0 volts, S_1 and S_2 closed, connecting the ac output V_1 to positive dc voltage rail or S_3 and S_4 closed, connecting the ac output V_1 to negative dc voltage rail [46]. The other combinations are (from Figure 4.3):

- by turning ON S_1 and S_4, $V_1 = +V_{dc}$;
- by turning ON S_2 and S_3, $V_1 = -V_{dc}$;

Similarly, the ac output voltage for each level can be obtained in the same manner with appropriate submodules.

The challenges of this hybrid design are to ensure that the battery and supercapacitor devices are adequately sized to maintain the desired power system stability. The power electronic devices will similarly need appropriate voltage and current ratings. This will be covered is Chapters 6 and 7. Also, it is important to ensure that total harmonic distortion meets an acceptable minimum when selecting the number of levels and the VSC switching scheme.

4.5 Total Harmonic Distortion (THD) Calculation

4.5.1 THD Calculation

In designing the enhanced STATCOM it is important to ensure that THD is reasonably low. The tradeoff is with number of levels, switching control scheme and losses. THD is a calculation that determines how much distortion in a voltage or current is due to harmonics

in the signal. THD is an important aspect in power systems with power converters. The lower the THD, the smoother the ac waveform.

THD is defined as the ratio of equivalent root mean square (RMS) voltage of all the harmonic frequencies (from the second harmonic on) over the RMS voltage of the fundamental frequency (the fundamental frequency is the main frequency of the signal, i.e., the frequency that you would identify if it were a pure sinusoid. Equation (4.22) shows commonly used mathematical definition of THD (note that voltage is used in this equation, but current could be used instead) [52]. Assume no non-integer harmonics are present.

$$THD \approx \frac{\sum_{n=2}^{K} V_{n_{rms}}^2}{V_{fund_{rms}}} \tag{4.22}$$

$V_{n_{rms}}^2$ is the RMS magnitude of the nth harmonic

$V_{fund_{rms}}$ is the RMS magnitude of the fundamental frequency voltage

Since the amplitudes of the harmonics are needed to calculate the THD, Fourier analysis can be used to help determine individual harmonics. The Fourier terms must be calculated to determine the magnitudes of the fundamental frequency and the harmonics up to predetermined maximum frequency [52].

Figure 4.4 shows an example of a 1 kHz frequency spectrum of a distorted sine wave. The amplitudes of even-numbered harmonics and harmonics above the 15th are nearly 0 in this specific case, so they are not included in the calculation. The 1st harmonic is the fundamental frequency while the 3rd, 5th ,7th… harmonics are the frequencies of the distorted sinewave. The bigger the fundamental frequency, the smaller the THD. The amplitudes of the distorted sinewave are tabulated in Table 4.1 and plotted in Figure 4.4.

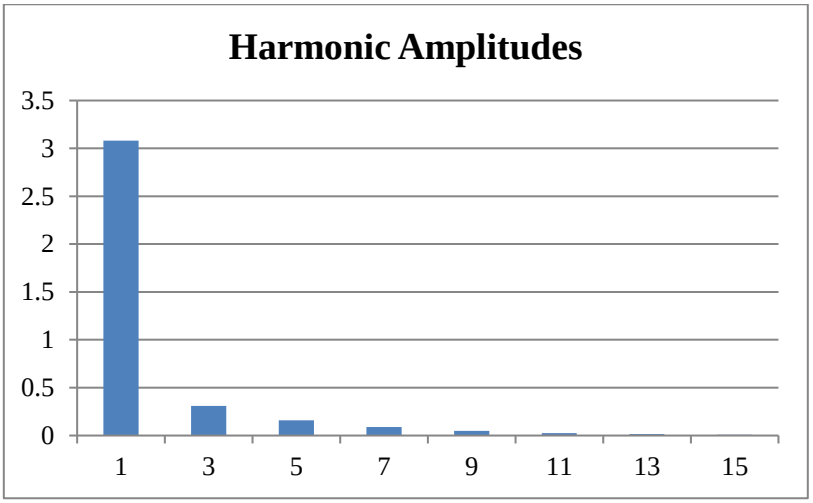

(a) Bar chart

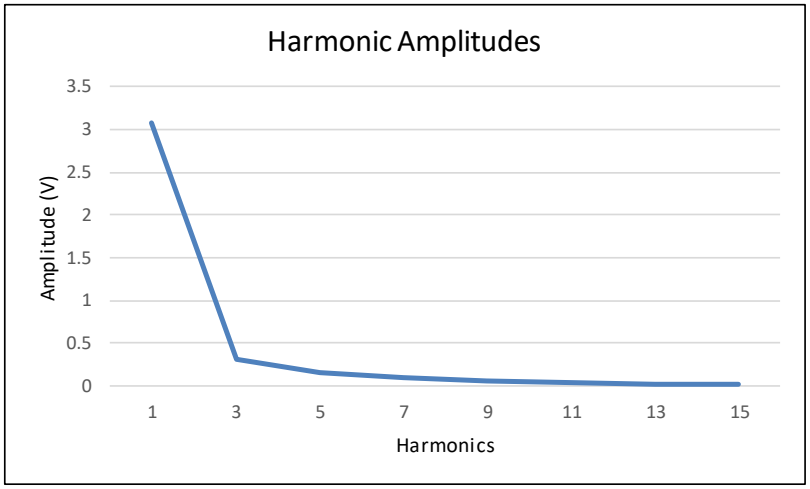

(b) Line chart

Figure 4.4: Harmonic amplitude charts [52]

Table 4.1: Amplitudes of harmonics of distorted sine wave

Harmonic	**Amplitude (V)**
1	3.08
3	0.308
5	0.159
7	0.09
9	0.0487
11	0.0253
13	0.0164
15	0.01

THD can be calculated from (4.23)

$$THD = \frac{V_{rms\,without-fundamental}}{V_{rms\,fundamental}} \tag{4.23}$$

Note that voltage amplitudes can be used in place of rms values since $V_{rms} = \frac{V_{peak}}{\sqrt{2}}$

$$THD = \frac{\sqrt{0.305^2+0.159^2+0.09^2+0.048^2+0.0523^2+0.0164^2+0.010^2}}{3.08} \text{ x } 100$$

$$\text{THD} = 11.8\%$$

4.6 Summary

In this chapter, the enhanced STATCOM with a hybrid combination of batteries and supercapacitors is discussed. This design allows the STATCOM to dynamically control injected real and reactive power transfer with the ac system. The design employs the use of MMC topology. Each module of the MMC has a coupling reactor, a dc capacitor, with the hybrid ESS connected in parallel through dc-dc converters. The bidirectional dc-dc converter for each of the ESS efficiently controls the power outputs of the ESS between the supercapacitor and the battery. The bidirectional dc-dc converter controls generate a power command that regulates real power exchange between the ESS and the STATCOM, and therefore with the grid. The STATCOM controls also command the exchange of reactive power between the STATCOM and the grid to maintain system voltage stability.

The full bridge MMC topology consists of multiple levels of submodules. Each submodule consists of four IGBTs and the modules are connected in series to increase the voltage capability as well as improving ac waveforms. For ease of simulation, this dissertation will use 22 modules per phase and implement a PWM scheme. The MMC is

implemented with separate dc sources, where modular hybrid ESS are connected to 2 of the 22 modules of the MMC STATCOM.

The MMC design will be done to ensure that THD is reasonably low and the output ac waveform is as close as reasonable to a sinusoid.

Chapter 5: Hybrid Energy Storage System (HESS)

5.1 Hybrid Energy Storage Systems

A hybrid energy storage system composed of batteries and supercapacitors has been recognized as a promising solution to mitigate life cycle degradation of batteries in electric vehicle applications, provide voltage regulation of the dc bus for the photovoltaic energy applications, used to smooth wind power fluctuations in power generation applications and provide stability in electric power systems [53][54][55][56].

In power system applications, the supercapacitor handles the fast charge/discharge operations to regulate the dc bus voltage it is connected to, while the battery handles slower charge/discharge operations at a steady rate over time. The benefits of the battery and supercapacitor complement each other when combined in power system applications.

The HESS takes advantage of the beneficial properties of supercapacitors and the batteries to offset the weaknesses of each.

5.1.1 Supercapacitor Description

Supercapacitors are also known as ultracapacitors, electric double-layer capacitors or electrochemical double-layer capacitors. A supercapacitor is a high-capacity capacitor with capacitance values much higher than other capacitors, bridging the gap between electrolytic capacitors and batteries. Supercapacitors typically store 10 to 100 times more energy per unit volume or mass than electrolytic capacitors, can accept and deliver charge much faster than batteries, and can tolerate many more charge and discharge cycles than batteries.

Supercapacitors are used in applications requiring many rapid charge/discharge cycles rather than long term compact energy storage: within cars, buses, trains, cranes, and elevators where they are used for regenerative braking, short term energy storage or burst-mode power delivery. Charge time for supercapacitors is typically cited as ranging from 1 to 10 seconds compared to 10 to 60 minutes or longer to reach a full charge on a battery. Typically, batteries have 500-1000 charge-discharge cycles in life while supercapacitors can reach up to one million cycles [57].

Unlike ordinary capacitors, supercapacitors do not use a conventional solid dielectric but rather, they have both electrostatic double-layer capacitance and electrochemical pseudocapacitance.

The high value of capacitance that is attainable through electrostatic double-layer capacitors (EDLC) is a result of the combination of double-layer capacitance and pseudocapacitance. Regular double-layer capacitance arises from the potential-dependence of the surface density of charges stored electrostatically (non-Faradaically) at the interfaces of the capacitor electrodes [59].

As illustrated in Figure 5.1, a double-layer capacitor device employs two double layers, one at each electrode interface, working one against the other on charge or discharge [58][59].

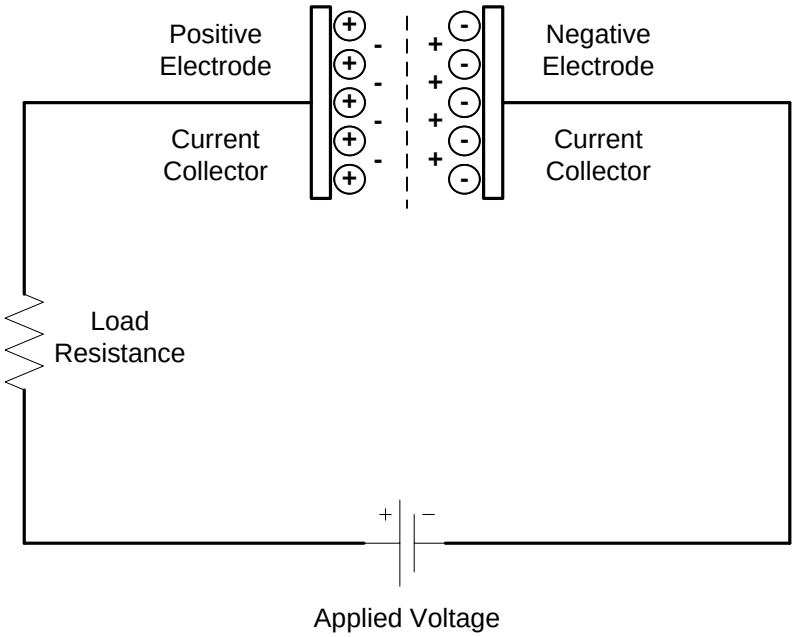

Figure 5.1: Schematic of an electrochemical double-layer capacitor

References [53][60][57][58][59] describe the construction and operation of supercapacitors in greater details.

Supercapacitors have the following benefits:

- Large capacitance
- Quick charge and discharge capabilities in bursts
- High power density compared to batteries
- Light weight
- Ability to charge and discharge over a very high cycle life without degrading.

However, there are disadvantages too, including cost and relatively low energy density. Also, supercapacitors have very small breakdown voltages per cell, which can pose problems for STATCOM applications.

5.1.2 Battery Description

A battery is a device consisting of one or more electrochemical cells with external connections provided to power electrical devices [61]. A battery system is made up of a set of low-voltage power modules connected in parallel and in series to achieve a desired electrical characteristic. Batteries are "charged" when they undergo an internal chemical reaction under a potential applied to the terminals. They deliver the absorbed energy, or "discharge," when they reverse the chemical reaction. Key factors of batteries for storage applications include high energy density, high energy storage capability, round trip efficiency, cycling capability, life span, and initial cost [62]. Several types of batteries such as lead-acid batteries, Nickel–cadmium battery, Nickel–metal hydride battery, Lithium-ion polymer battery, and Lithium-ion battery are in use. Lithium-ion batteries are the choice in many consumer electronics and have one of the best energy-to-mass ratios and a very slow self-discharge when not in use.

Due to the chemical kinetics involved, batteries cannot operate at high power levels for long time periods. In addition, rapid, deep discharges may lead to battery failure and early replacement of the battery, since heating resulting in this kind of operation reduces battery lifetime. There are also environmental concerns related to battery storage due to toxic gas generation during battery charge/discharge [7]. A discussion of management of hazardous materials in batteries is beyond the scope of this dissertation.

Batteries have the following benefits:

- Efficient compared to supercapacitors
- High energy density compared to supercapacitors

- Potential to supply bulk energy over a long period of time
- Becoming more affordable over time, depending on the specific type. Some

Some disadvantages of batteries are:

- Environmentally unfriendly
- Heavy weight compared to supercapacitor of equivalent peak power rating. (will be lighter than supercapacitors of equivalent energy rating)

5.1.3 Combining Batteries with Supercapacitors

Although these devices have limitations, the combining benefits cited provide some reasons why batteries and supercapacitors can be used to complement each other and can be used in conjunction for energy storage and active power injection in electric grid and other power applications. The batteries are used to fulfill the energy requirements for a distinctly long length of time, while the supercapacitors are used to fulfill the immediate electricity demands [55]. In photovoltaic or solar applications, a HESS system using supercapacitors to meet short term ramping can help prolong the state of charge of the batteries and makes energy available during peak demand periods in the night when there is no solar energy available. This would help mitigate the “intermittency” issues which have plagued the renewable energy industry.

5.2 The Ragone Plot

The performance of energy storage options regarding their specific energy and power densities can be compared using a graph called a Ragone plot. It consists of two axes: energy density and power density. The capabilities of different energy storage devices are plotted on

the graph according to their respective characteristics, allowing analysis of performance characteristics at a glance [63].

Figure 5.2 shows a Ragone plot that compares the performances of a range of energy storage devices. It shows that supercapacitors (ultracapacitors) can deliver high instantaneous power but their energy density is very limited. On the other hand, batteries can store larger amounts of energy but have a relatively low power density. The sloping lines on the Ragone plots indicate the relative time to get the charge in or out of the device. At one extreme, power can be pumped into, or extracted from capacitors in microseconds.

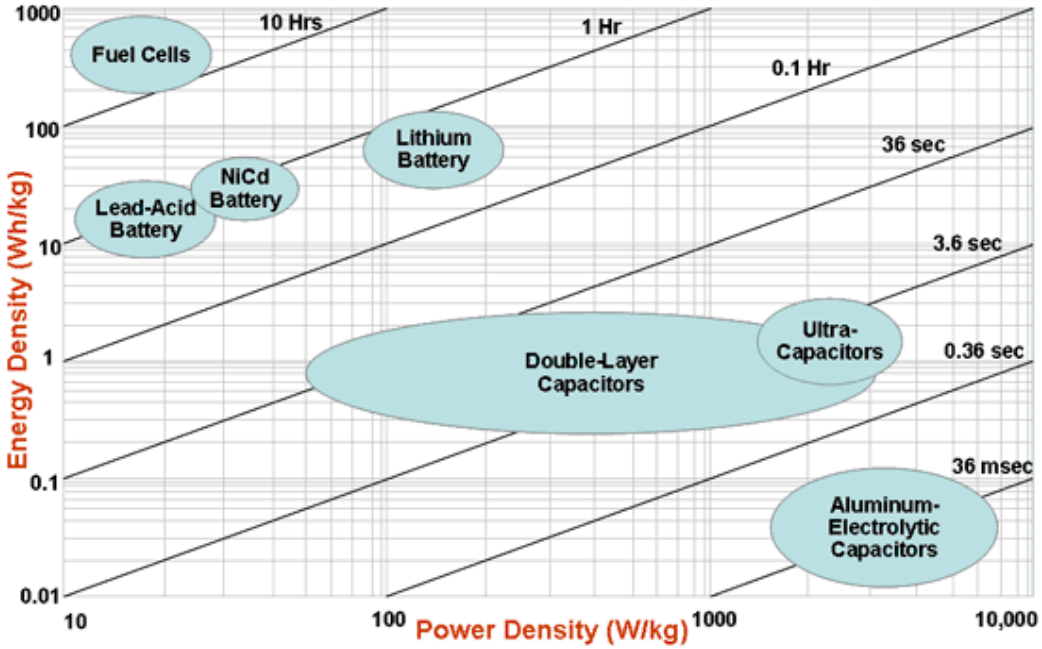

Figure 5.2: Ragone plot showing performance of a range of electrochemical devices [57]

5.3 Sizing Energy Storage System for the E-STATCOM/BE3SC

In Figure 5.3, the ESS are each coupled to individual bidirectional dc-dc converters to facilitate individual adjustments of voltage or current to control power output. In this

dissertation, the hybrid ESS are connected to two submodules based on the system needs, as shown in Figure 5.3.

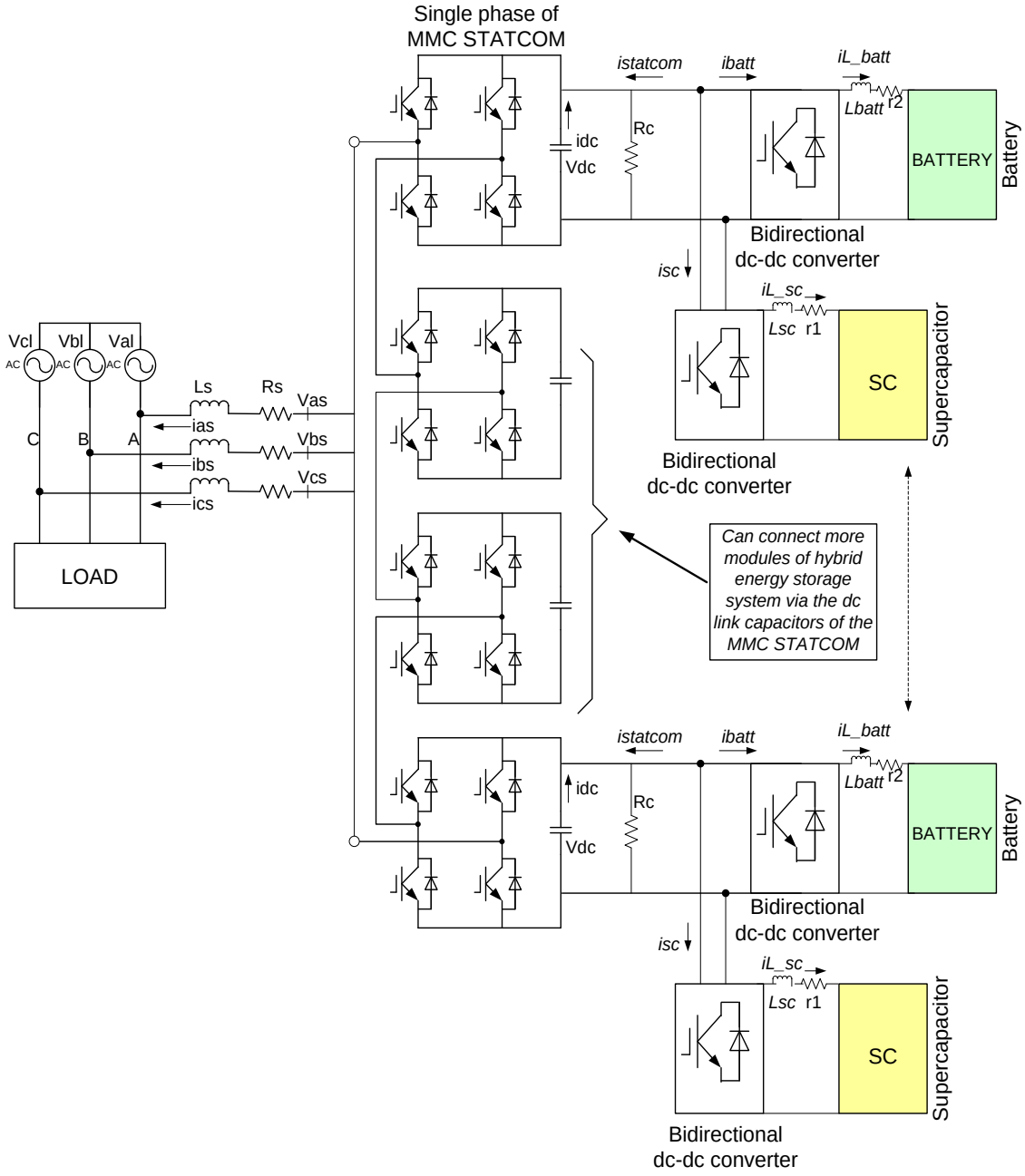

Figure 5.3: Basic diagram of an E-STATCOM/BE3SC with 4 MMC submodules per phase

Application of the HESS introduces complex sizing, energy management and integration problems [54]. In electric vehicle applications, the sizing objective of HESS is to find the

appropriate number of supercapacitor banks and battery cells that minimize cost and maximize efficiency of system or maximize the battery life [54]. In wind power generation applications, the sizing method is based on the magnitude of average fluctuation of wind profiles of a specific wind station which consequently creates fluctuations in the generated wind power [53]. In electric power transmission systems, proper sizing of the HESS is based on specific operational needs that can't be addressed with less costly alternatives.

In the battery-supercapacitor hybrid design, it is imperative to size the battery and supercapacitor devices adequately in order to get the acceptable quality of performance in terms of net stored energy and peak power and also increase the lifetime of the battery [53][64].

5.3.1 Energy Stored in a Supercapacitor

The energy stored in a supercapacitor (E_{sc}) depends on the capacitance and the square of the voltage applied to the terminals.

$$q = C_{sc}V \tag{5.1}$$

$$C_{sc} = \frac{\varepsilon A}{d} \tag{5.2}$$

$$E_{sc} = \frac{1}{2}C_{sc}V^2 \tag{5.3}$$

Where:

$\mathrm{C_{sc}} = \text{Capacitance of the supercapacitor}$

$\mathrm{q} = \text{Stored Charge}$

$\mathrm{V} = \text{Voltage applied across the plates}$

$\mathrm{D} = \text{Distance between the capacitor plate}$

$\mathrm{\varepsilon} = \text{dielectric constant}$

5.3.2 Supercapacitor Model

Many equivalent models have been developed for supercapacitors, but the ladder model shown in Figure 5.4 [65] is the equivalent circuit for a supercapacitor that is chosen for this research [67].

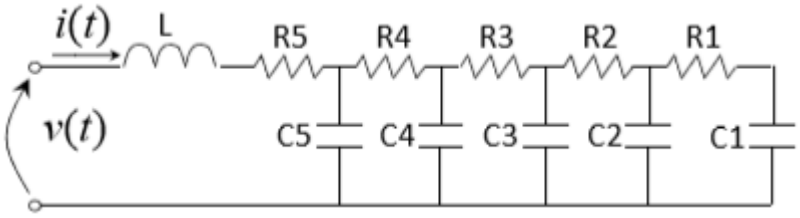

Figure 5.4: Equivalent circuit of supercapacitor ladder [65]

5.3.3 Battery Model

Batteries are characterized in terms of power density, energy density and life cycle [53]. Figure 5.5 [66] shows the equivalent model of a Lithium ion battery used in this analysis [67].

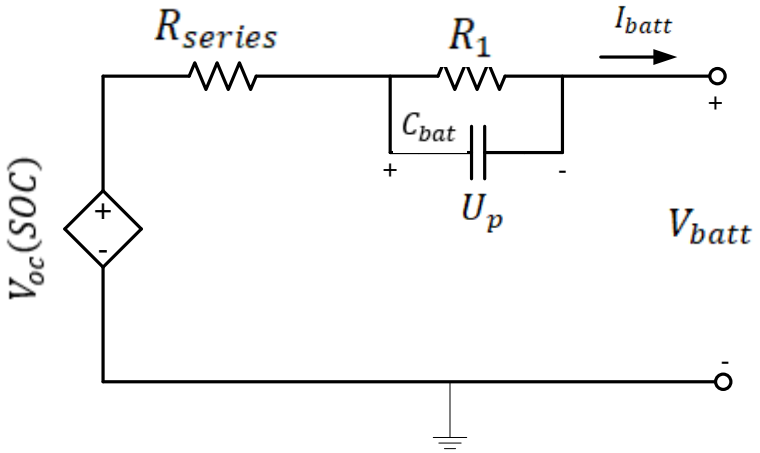

Figure 5.5: Equivalent circuit of Lithium Ion Battery used in the Research [66]

Where:

V_{oc} is the no load voltage of the battery

R_{series} is the internal series resistance of the battery

R_1 and C_{bat} are the polarization resistance and capacitance, respectively

I_{batt} is the battery current

U_P is the voltage across the capacitor plates

The model consists of a single voltage source and a combination of resistors and a capacitor. After 200 to 1000 cycles of charge/discharge which may take around 4 to 5 years in the application at hand, the batteries may need to be replaced [53]. If more advanced technology of Lithium-ion phosphate batteries is used, the batteries may last around 10 years with 7000+ charge-discharge cycles [68]. Future applications of the proposed design will utilize this advanced technology.

The HESS design focuses on controlling charging and discharging behavior to improve current output quality and increase battery life. When batteries work continuously, the cells warm up and the internal resistance increases which results in more losses [53]. Also, frequent deep depth of discharge (DOD) can degrade the life of the battery for many battery chemistries. A control scheme can resolve the loss issues and prevent the deep DOD by controlling the battery operation by taking advantage of supercapacitors. This can be accomplished by controlling the upper and lower bounds of the supercapacitor's SOC to adjust the energy distribution of the battery to the system and thus the current to and from the battery. For example, when the battery DOD is more than 50%, the controller increases the lower bound of the supercapacitor's allowable SOC. This will help the battery be discharged less.

5.4 Battery and Supercapacitor Power and Energy Equations

In a HESS system, the supercapacitor can be sized with respect to power, considering equations (5.4) and (5.5) [53]:

$$i(t) = C_{sc}\frac{dV(t)}{dt} \tag{5.4}$$

$$P(t) = V(t) * i(t) \tag{5.5}$$

To size the supercapacitor with respect to energy, consider equations (5.6) and (5.7) below:

$$E_{ex} = \int_0^{\tau} P(t)dt \tag{5.6}$$

$$E(t) = \frac{1}{2}\, C_{sc}V(t)^2 \tag{5.7}$$

E_{ex} is the energy exchanged with time t, E is the instantaneous energy stored by the supercapacitor.

Assume that the maximum voltage discharge of a supercapacitor can be up to approximately 80% of its maximum voltage. The maximum exchange energy ($E_{\Delta\max}$) of a supercapacitor is calculated as shown in (5.8) [69]:

$$E_{\Delta sc-\max} = \frac{1}{2}C_{sc}(V_{max}^2 - V_{min}^2) \tag{5.8}$$

Increasing $E_{\Delta sc-\max}$ decreases the operating time of the batteries in a hybrid system and can also result in need for smaller batteries in the design [53].

Where:

$\mathrm{C_{sc}} = \text{Capacitance of the supercapacitor}$

$\mathrm{V} = \text{Voltage applied across the terminals}$

V_{max} = Maximun allowable voltage

V_{min} = Minimun allowable voltage

Similarly, equation (5.9) shows that the battery size is proportional to the power rating of the system, P_{rated}, dc-link voltage, $V_{dc-link}$, total duration of battery charge (TDC); and it is inversely proportional to the supercapacitor size, C_{sc} [53].

$$C_{bat} \propto \frac{(P_{rated} * TDC * V_{dc-link})}{C_{sc}} \tag{5.9}$$

$$P_{rated} = \frac{C_{bat} * C_{sc}}{TDC * V_{dc-link}} \tag{5.10}$$

Assuming a 10% safety factor for the calculated capacity of the supercapacitor, the energy stored in the HESS can be calculated from Equation (5.11).

$$E_{HESS} = P_{rated} * TDC * 10\% \tag{5.11}$$

$$E_{HESS} = \frac{C_{bat} C_{sc}}{TDC.V_{dc-link}} TDC * 10\% \tag{5.12}$$

$$E_{HESS} = \frac{C_{bat} C_{sc}}{V_{dc-link}} * 10\% \tag{5.13}$$

$$E_{sc} = E_{HESS} * SC\% \tag{5.14}$$

Where:

SC% is the percentage of the HESS energy stored in the supercapacitor.

5.5 Supercapacitor Charge and Discharge Characteristics

The charge and discharge time of a supercapacitor is similar to that of any ordinary capacitor. However, high charging and discharging currents can be achieved due to the

minimal internal resistance offered by the supercapacitor. While batteries generally take a long time to be fully charged, supercapacitors can be charged to full stable state of charge in under two minutes assuming supply can provide sufficient current [70].

Figures 5.6, 5.7 and 5.8 show the SOC, voltage and current characteristics, respectively, of a 10,000 Farad supercapacitor charged over a period of 0.3 seconds, through a 1 mΩ series resistor from a 480V supply. This is the rating of the capacitor used in the research.

Rated Capacitance (C_{rated}) = 10,000 F

Rated voltage (V_{rated}) = 480 V

Initial charge = 240 V (50%)

Equivalent dc series resistance (R_{series}) = 1 $m\Omega$

Time = 0.3s

Notice that after 0.3 seconds, the supercapacitor discharges via an external load to roughly 232.5 V.

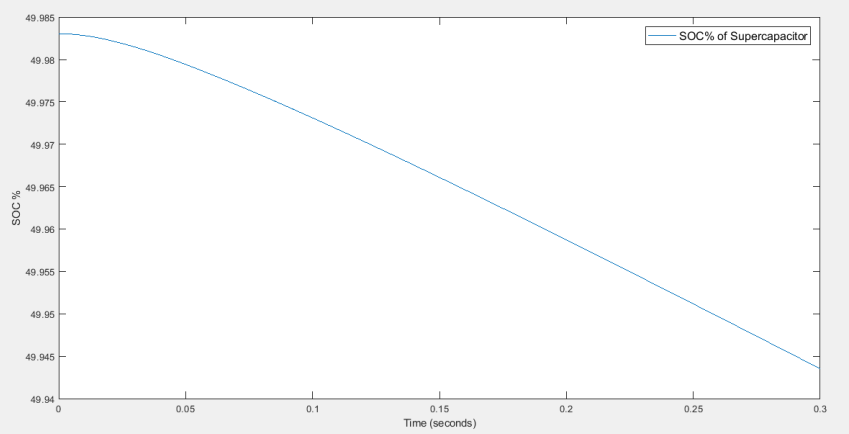

Figure 5.6: Supercapacitor SOC for a 10,000 F supercapacitor

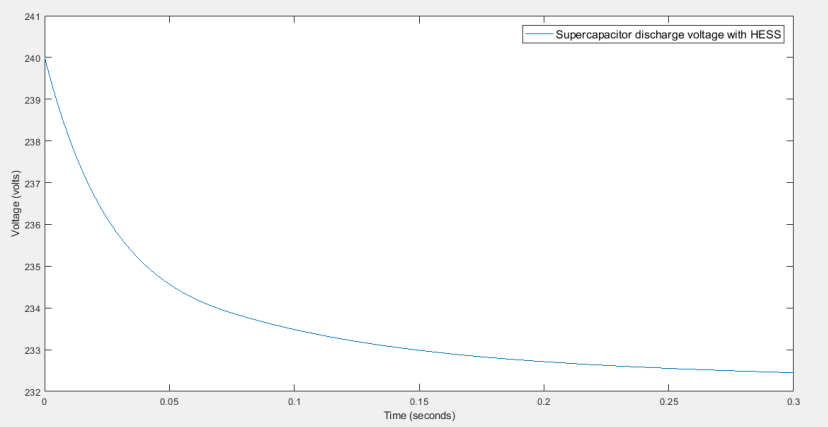

Figure 5.7: Supercapacitor discharge voltage for a 10,000 F supercapacitor via an external load

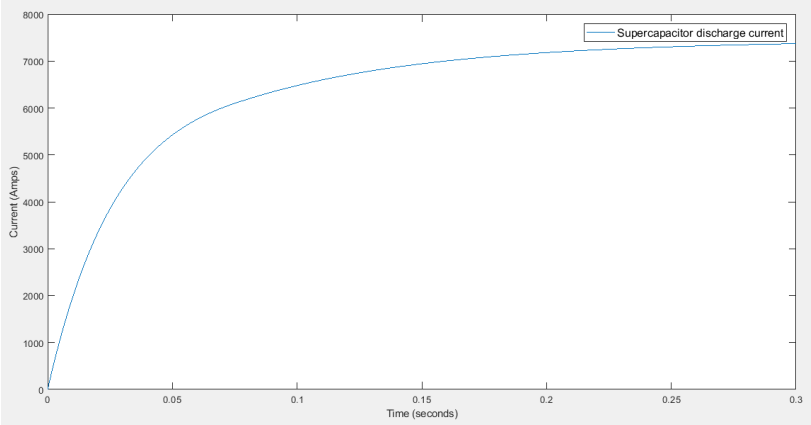

Figure 5.8: Supercapacitor discharge current for a 10,000 F supercapacitor via an external load

Since the capacitance for supercapacitors is larger than that for regular capacitors, the charge is much larger for supercapacitors, but it takes correspondingly longer for supercapacitors to attend full charge compared to regular capacitors, due to the higher capacitance. However, charging faster or providing more energy faster means the external circuit has to be able to supply more power. This can be a limiting factor.

The charging time of a supercapacitor can be mathematically calculated from the following relationship [71]:

$$\frac{Q}{Q_{max}} = 1 - e^{(\frac{t}{RC})} \quad (5.15)$$

Where:

Q = Charge in supercapacitor (Coulombs)

Q_{max} = Maximum charge capacitor can hold (Coulombs)

t = time elapsed (seconds)

R = Internal resistance of circuit (Ohms)

C = Capacitance of capacitor (Farads)

RC = Time Constant (seconds)

5.6 Battery Characteristics

Battery performance depends on how the battery is used and on the environmental conditions under which it is use. These conditions are rarely, if ever, specified in mass market advertising. Some of the parameters used to characterize batteries and how their performance varies with temperature are discussed below [57].

5.6.1 Battery Discharge Curve

Energy cells have been developed for a wide range of applications using a variety of different technologies, resulting in a wide range of available performance characteristics. There are several types of batteries, including Lithium ion, Lead acid, Nickel-zinc, etc. The Lithium ion battery is widely used at present due to its lower self-discharge rate, faster charge rate, and longer life, compared to its counterparts. When specifying a battery to match the performance requirements of an application, the voltage discharge characteristics for the different types of batteries should be taken into account. The actual voltage appearing

at the terminals at any time, as with any cell, depends on the load current, internal impedance of the cell, temperature, state of charge and age of the battery [57].

Battery C-rate refers to the rate at which a battery is charged or discharged or the value of ampere hour rating. For example, a 40 Ah rating battery has the following discharge current ratings:

- 0.5 C-rate = 0.5 x 40 = 20 Amps
- 1 C-rate = 1 x 40 = 40 Amps
- 2 C-rate = 2 x 40 = 80 Amps

Figure 5.9 shows an example from applying a Matlab model (parallel_battery_SC_boost_converter) used in this dissertation [67]. The battery discharge characteristics of a Lithium Ion battery with a maximum capacity of 2500 Ah, and a nominal discharge current of 1,187 Amperes are presented in this dissertation. The second graph shows how the discharge rate varies with different discharge currents. Overall, the higher the current, the faster the discharge rate.

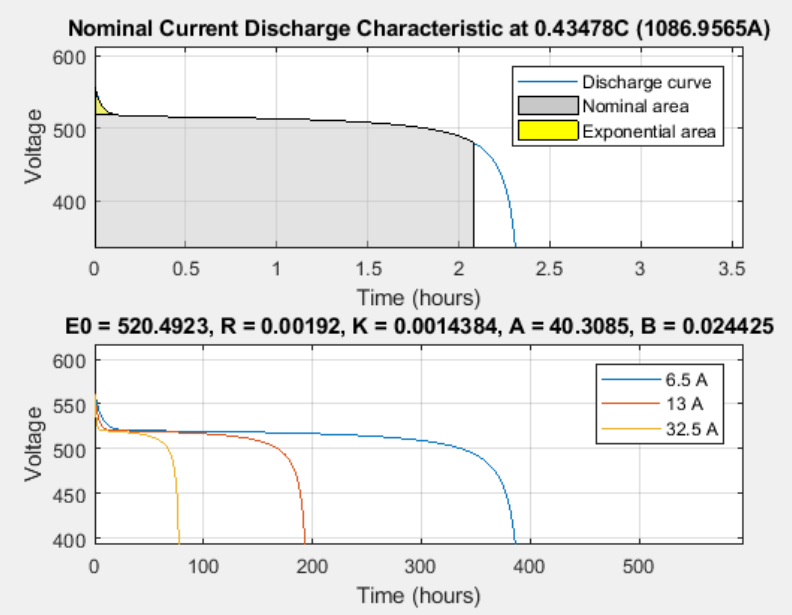

Figure 5.9: Battery discharge characteristics for a Lithium Ion battery [67]

5.6.2 Battery Temperature Characteristics

Battery performance can change dramatically with temperature. At a lower temperature, batteries with aqueous electrolytes may see the electrolyte itself freeze, setting a lower limit on the operating temperature. At low temperatures Lithium batteries suffer from Lithium plating of the anode, causing a permanent reduction in capacity. At the upper extreme temperature, the active chemicals may break down, destroying the battery. In between these limits the cell performance generally improves with temperature. Figure 5.10 shows how the performance of Lithium ion batteries deteriorates as the operating temperature decreases.

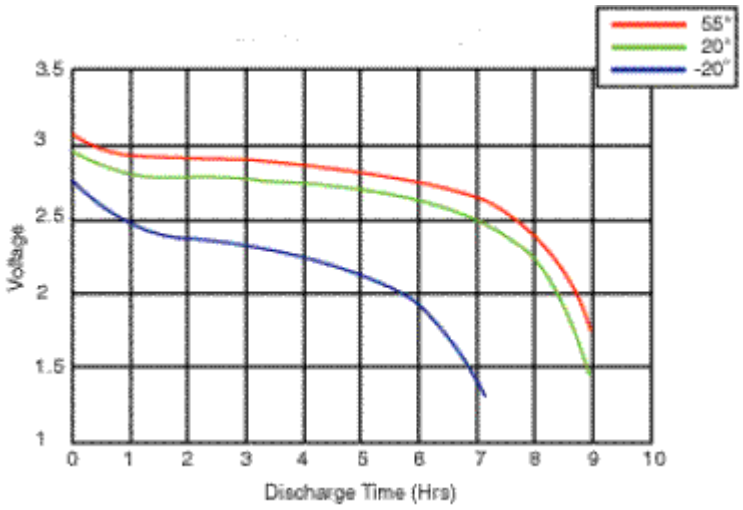

Figure 5.10: Performance of Lithium ion batteries at different operating temperatures [57]

The Arrhenius equation in (5.16) defines the relationship between temperature and the rate at which a battery chemical action proceeds. It shows that the rate increases exponentially as temperature rises.

$$k = A\, e^{-E_A/RT} \tag{5.16}$$

Where

k = rate at which the chemical reaction proceeds

A = frequency factor related to the frequency of collisions between molecules, usually taken as a constant over small temperature variation ranges.

e = mathematical constant = 2.71828

E_A = activation energy. A constant representing the minimum energy needed for the reaction to occur.

R = Universal Gas Constant

T = temperature in degrees Kelvin

RT = average kinetic energy of the reaction

5.6.3 Battery State of Charge (SOC) and State of Health (SOH)

Knowing the amount of energy left in a battery compared with the energy it had when it was full gives the user an indication of how much longer a battery will continue to perform before it needs recharging. It is a measure of the short-term capability of the battery. Using the analogy of a fuel tank in a car, the State of Charge (SOC) estimation is often called the "Gas Gauge" or "Fuel Gauge" function [57].

To avoid battery failure and keep the battery lifetime intact, a Battery Management System (BMS) needs to control its use by considering several parameters of such as State of Charge and State of Health (SOH). The State of Charge provides the percentage of battery capacity, while the State of Health estimates the long-term battery health [72].

Mathematical equations for the Thevenin battery models are as follows [73]:

$$u_p' = -\frac{u_p}{C\,R_1} + \frac{I_{batt}}{C_p'} \tag{5.17}$$

$$V_{batt} = V_{oc} - U_p - I_{batt}\,R_{series} \tag{5.18}$$

$$V_{batt}(s) - V_{oc}(s) = I_{batt}(s)\left(R_{series} + \frac{R_1}{1+sR_1C}\right) \tag{5.19}$$

5.6.4 Battery Life

That batteries have a finite life is due to occurrence of the unwanted chemical or physical changes to, or the loss of, the active materials of which they are made. Otherwise they would last indefinitely. These changes are usually irreversible, and they affect the electrical performance of the individual cells. Battery performance deteriorates over time

whether the battery is used or not. This is known as "calendar fade." Performance also deteriorates with usage and this is known as "cycle fade." [57].

a) Battery Calendar Life

There are two key factors influencing calendar life, namely temperature and time, and empirical evidence shows that these effects can be represented by two relatively simple mathematical dependencies. As derived from the Arrhenius Law formula in equation (5.16), the rate at which a chemical reaction proceeds doubles for every 10 degrees rise in temperature. In this case it applies to the rate at which the slow deterioration of the active chemicals increases. Similarly, the $t^{1/2}$ (or $\sqrt{t}$) relationship represents how the battery internal resistance also increases with time, t. The graph in Figure 5.11 illustrates these effects [57].

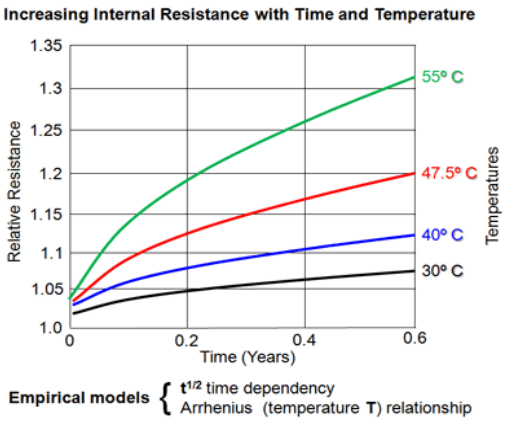

Figure 5.11: Battery calendar: Increasing internal resistance with time and temperature [57]

b) Battery Cycle Life

Battery cycle life is defined as the number of complete charge - discharge cycles a battery can perform before its effective capacity falls below 80% of its initial rated capacity. Key factors affecting cycle life are time, t , and the number, N, of charge-discharge cycles

completed. Another significant factor is the Depth of Discharge (DOD) applied to the battery, which is a simple reciprocal mathematical relationship, but there are many more complex factors which can also influence performance. The relation between the cycle life and the depth of discharge appears to be logarithmic as shown in Figure 5.12. In other words, the number of cycles yielded by a battery goes up exponentially for applications with consistently applied shallow DOD [57].

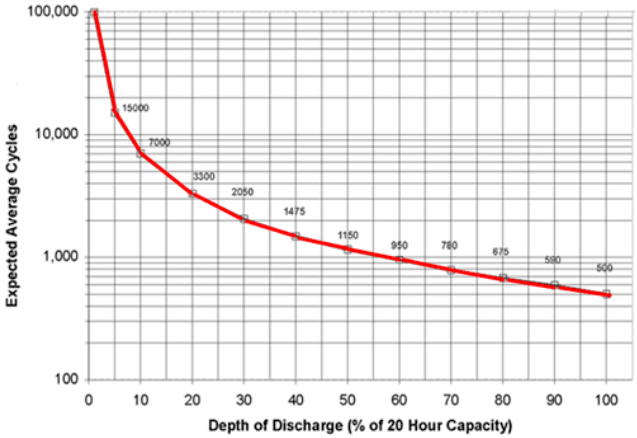

Figure 5.12: Depth of discharge versus cycle life for Lithium ion battery [57]

The lifetime of the battery also depends on several other parameters, such as peak current, transients of the peak current, the number of peak currents, temperature, charge and discharge cycles, etc.

Although battery life can be extended by preventing or reducing the cause of the unwanted parasitic chemical effects in the cells through the conditions described above, the battery life can also be extended by connecting with a supercapacitor, to limit exposing the batteries to the most stressful conditions.

The “power_battery_aging” example in Matlab is used to illustrate the impact of aging due to cycling on a 12.8V, 40Ah Lithium-ion battery. The battery is submitted to several discharge-charge cycles at ambient temperature of 25 degrees celcius, and at various depths

of discharge and discharge rates over 1000 hours. As observed from the plots in Figure 5.13, the impact of DOD and discharge rate on the battery life is as described.

Overall, the battery ages rapidly as the DOD (inverse of SOC) and discharge rate increases, and this quickly reduces the battery capacity [74][75].

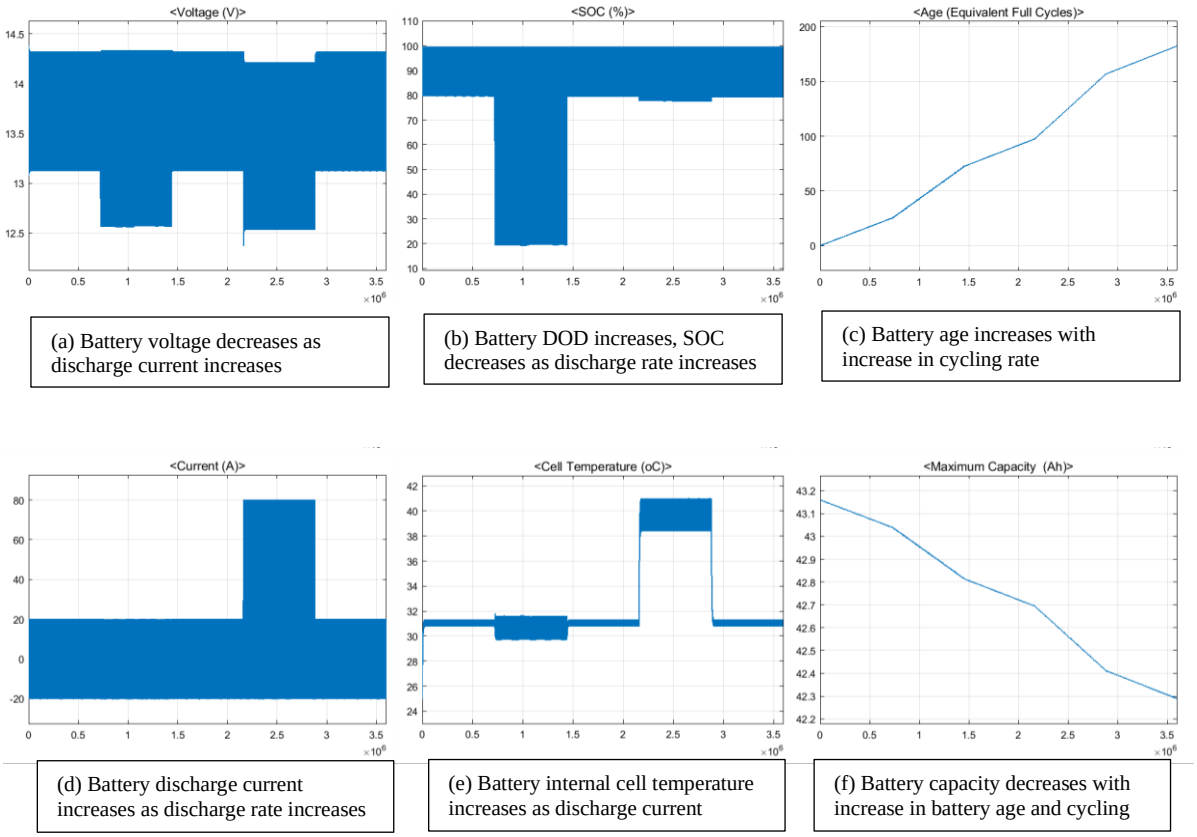

Figure 5.13: Impact of battery aging due to charge-discharge operations [74][75]

5.6.5 State of Health

The State of Health (SOH) is a "measurement" that reflects the general condition of a battery and its ability to deliver the specified performance compared with a fresh battery. It takes into account such factors as charge acceptance, internal resistance, voltage and self-discharge [57]. It is a percentage of the ratio of the present actual battery capacity to the maximum battery capacity. The actual capacity is determined by the DOD, cycling rate, age,

discharge current, battery cell temperature as discussed earlier. The higher the actual battery capacity, the higher the SOH of the battery and vice versa.

The state of health can be calculated from the expression below [76].

$$SOH_c = \frac{C_{act}}{C_{cap}}\ x\ 100\% \tag{5.20}$$

Where:

SOH_c is the value of state of health

C_{act} is the present actual capacity

C_{cap} is the battery maximum capacity

During the lifetime of a battery, its state of health deteriorates over time whether the battery is used or unused, until eventually, the battery is no longer useful or dead. As mentioned earlier, this is known as battery cycle fade and battery calendar fade, respectively. The SOH is an indication of the point which has been reached in the life cycle of the battery and a measure of its condition relative to a fresh battery. This state is also impacted by the DOD and the cycle usage.

Battery manufacturers do not specify the SOH because they only supply new batteries. The SOH only applies to batteries after they have started their ageing process either on the shelf or once they have entered service. The SOH definitions are therefore specified by test equipment manufacturers or by the user [57].

5.6.6 Sizing the Energy Storage System

There are several approaches in sizing energy storage systems. Section 5.4 showed relevant equation used in the sizing ESS. Chapter 6 will cover more on sizing the ESS for the application.

In this dissertation, a modular HESS is used to generate real power to the grid to improve system performance. In this dissertation, HESS can be increased by adding more modules. Having standard sized modules will lower application cost compared to customizing for every application. This is a selling point for MMCs with a large number of modules.

The HESS also helps to regulate the transmission system frequency during certain conditions. Since the 500 kV grid system described in Chapter 7, Section 7.3 has a lot of solar generation, there are cloudy days when solar generation is reduced, varied rapidly or lost. When there is a loss of solar generation in the area, say approximately 1.26 GW, this may result in low system frequency which may result in load shedding. Operation engineers may have roughly 24 seconds (0.0067 hours) to address the situation before shedding load. The amount of energy storage needed for this grace period is roughly 1.26 GW x 0.0067 hours = 8.4 MWh.

The hybrid energy storage system used in this dissertation is connected to two submodules per phase based on the total power and energy needs (standard sized modules). Energy storage system may not be needed on all submodules. This could impact harmonic behavior of the system. The two HESS submodules have a total energy supply capacity of 2.8 MWh per phase. The 3-phase HESS has a total energy supply capacity of 3 x 2.8 MWh = 8.4 MWh and this is needed to avoid possible load shedding on the grid.

The battery is designed for roughly 1.2 MWh for the two submodules modules, per phase, and the supercapacitor is designed for roughly 1.6 MWh for the two submodules per phase.

The reason for sizing the supercapacitor higher than the battery is to allow the supercapacitor to handle more of the charge/discharge operations in order to increase the battery life.

Below are calculations of the HESS used in this dissertation.

Battery energy sizing per submodule per phase is calculated below:

Rated capacity = 1,250 Ah

Nominal voltage = 480 V

Battery energy = 1,250 Ah * 480 V = 0.6 MWh

Supercapacitor energy sizing per submodule per phase is calculated below:

Nominal voltage = 480 V

Rated capacitance = 5,000 F

Number of parallel capacitors = 5

Total capacitance = 25,000 F

Supercapacitor energy = $\frac{0.5*25{,}000*480^2}{3600}$ = 0.8 MWh

The energy supply capacity of the HESS per submodule, per phase is:

0.6 MWh + 0.8 MWh = 1.4 MWh

For simplicity, only two HESS submodule per phase are used in this simulation.

The energy supply capacity of the HESS for two submodules, per phase is:

$$2 \times 1.4 \text{ MWh} = 2.8 \text{ MWh}$$

For the 3-pahse power system, the total energy supply capacity of the HESS is:

$$3 \times 2.8 \text{ MWh} = 8.4 \text{ MWh}$$

Note that the residual charge (and voltage) that should be left in the battery and supercapacitor when completely discharged (to improve lifespan), should be considered when sizing the HESS.

5.7 Summary

In this chapter, the design of a hybrid energy storage system, composed of batteries and supercapacitors, is discussed. The HESS takes advantage of the beneficial properties of the supercapacitors and batteries to offset their weaknesses. Although these devices have limitations, the combining benefits provide some reasons why they can be used to complement each other. The supercapacitors have benefits of quick charge/discharge capabilities, high power density and high cycle life without degradation. The batteries have benefits of high efficiency, high energy density, and capability to supply bulk power over a long period.

In the HESS design, it is imperative to size the batteries and supercapacitors appropriately, to get the acceptable quality of performance and improve the lifetime of the battery.

When connected to a power grid, the HESS can perform real power exchange with the grid, to improve stability. It is important to adequately control the amount of real power injected to the grid, or absorbed from the grid, to improve stability. This control can be achieved by connecting the HESS with bidirectional dc-dc converters.

Chapter 6: Bidirectional dc-dc Converter Control in Battery-Supercapacitor Hybrid Energy Storage System

6.1 Introduction

This chapter is from a conference paper accepted for presentation at the 2020 IEEE PES Innovative Smart Grid Technologies conference meeting in Washington, DC, in February 2020 [77]. The paper will be published in the conference proceedings.

In recent years, the application of batteries has seen rapid increases in use in electric vehicles, photovoltaic generation, wind power generation, peak load shaving and power system stability applications. Power system disturbances caused by equipment outages may result in system instability as power supplied by the grid generators may no longer match the load demand. This may result in unacceptable frequency fluctuations, cascading outages or even local blackouts, if a remedial action is not taken promptly. Batteries are increasingly used to enhance performance of power systems to enable better leveraging clean energy sources. However, high numbers of rapid, deep charge/discharge battery operations result in battery degradation and eventually reduce the battery life span. Another energy storage technology is the supercapacitor (SC) [78][79]. Combining a supercapacitor with a battery provides a superior energy storage system where the supercapacitor can respond to very fast charge/discharge operations and the battery can respond more slowly but with larger net energy transfers. However, the supercapacitor technology provides design challenges due to its lower energy density compared to batteries [80]. This paper proposes the design of an energy storage system (ESS) that will combine batteries, supercapacitors, and bidirectional dc-dc converters for use in a power system dynamic compensation application. The two energy storage systems

are each coupled to individual bidirectional dc-dc converters to facilitate individual adjustments and sizing [81].

The bidirectional dc-dc converters control the flow of power between the energy storage system and the grid. If the grid frequency exceeds a maximum set point, the controller allows flow of power from the grid to the ESS. This excess energy charges the appropriate energy storage system based on the energy transfer needed. Similarly, if the grid frequency drops below a minimum set point, the controllers allow the flow of power from the energy storage system to the grid. In this paper, the maximum and minimum frequency set points are 60.2 Hz and 59.8 Hz, respectively; the desired grid frequency is 60 Hz. The bidirectional dc-dc converters allow for both energy storage elements to discharge and recharge within their limits [80]. The system is designed such that the supercapacitor charges/discharges first before the battery. This reduces battery activity and prolongs its life. In the case where power is flowing from the ESS to the grid, if the supercapacitor is completely discharged and the grid frequency is still below the minimum set point, the battery will start discharging while the supercapacitor will start charging. A single hybrid energy storage system might not be able to solve the frequency deviation, but many working in a similar fashion could do so.

As a precautionary measure to avoid cascaded outages, some utility companies install Under Frequency Load Shedding (UFLS) schemes to drop load blocks if the system frequency decreases below the minimum threshold for over 6 cycles. Dropping customers is not a preferred alternative. The design presented in this paper will mitigate the need to drop customers during such unacceptable frequency fluctuations by using the energy storage system.

Section II of this paper presents a basic block diagram of the proposed control scheme and a brief description of the functionality of the bidirectional dc-dc converter controls.

6.2 Basic Design

The design shown in Figure 6.1 consists of a battery and a supercapacitor, each connected to a dedicated bidirectional dc-dc converter, which are in turn connected to a common inverter. These could possibly each be separate submodules in a modular multilevel converter (MMC). The two ESS are each coupled to separate bidirectional dc-dc converters to facilitate flexibility of charge and discharge controls, as well as other adjustments. This ensures that the output power of the battery and supercapacitor are controlled independently, which in turn controls the charge/discharge operations. The alternate charge and discharge operations of the battery and supercapacitor would prolong the availability cycle of stored energy and extend battery life. The bidirectional dc-dc converter shown in Figure 6.2 consists of self-commutated power electronic switches S1 and S2 made from power MOSFETS or IGBTs, an inductor L to smooth current ripple, and a capacitor C for filtering voltage ripples and smoothing output waveforms. The capacitor maintains the dc voltage level at the converter output, while the inductor acts as a smoothing reactor for the converter current [82]. The current source represents the current injected by or drawn by the Voltage Sourced Converter (VSC) in Figure 6.1 and the resistor, R, approximates the converter losses.

To mitigate the impacts of frequency instability, the control scheme is designed such that the system frequency is continuously measured, and signals are sent to a comparator to compare the measured and the reference frequency (60 Hz) as shown in the flow chart in Figure 6.3. If there is a change in frequency, the error is passed through a Proportional-Integral (PI) controller which continuously calculates the error value and applies a correction, based on the proportional and integral terms. If the power system frequency increases above 60.2 Hz, the PI

controllers, as shown in Figure 6.4 send a command to allow flow of power from the grid to the dc side to charge the ESS. Alternatively, if the grid power system frequency is less than 59.8 Hz, the controllers send a command to discharge the energy storage system. Figure 6.1 illustrates four possible power flow modes between the ESS and the grid.

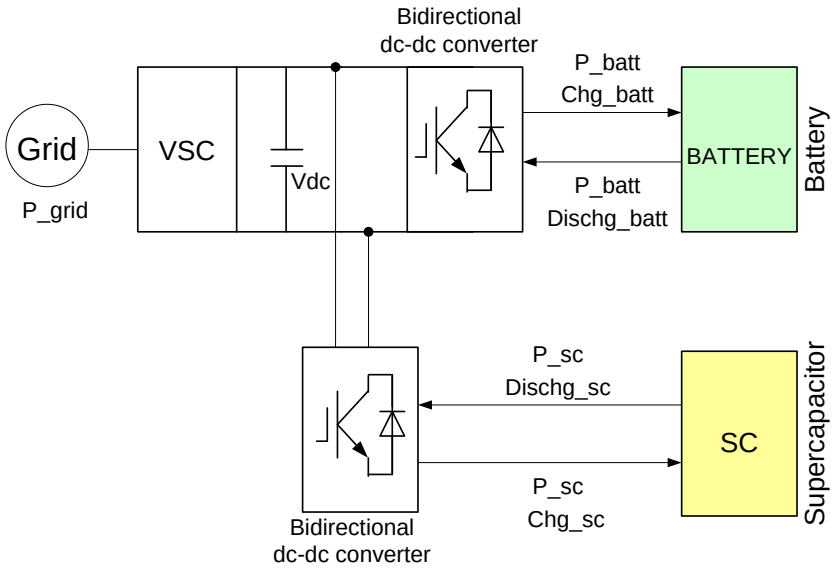

Figure 6.1: Basic design and power flow modes

6.3 Power flow Modes

Four main power flow modes are presented.

6.3.1 Charge Supercapacitor and Battery Mode

In this mode, the grid generation is more than the load demand and power flows from the grid to the ESS; the measured system frequency is higher than the maximum allowable frequency; $f_{mea} > f_{max}$

$$P_{grid} > P_{batt} + P_{\mathrm{sc}} \tag{6.1}$$

6.3.2 Discharge Battery and Supercapacitor Mode

In this mode, the grid generation is less than the load demand and power flows from the ESS to the load; the measured system frequency is lower than the minimum allowable frequency; $f_{mea} < f_{min}$

$$P_{grid} < P_{batt} + P_{\mathrm{sc}} \tag{6.2}$$

6.3.3 Charge/discharge mode

In this mode, the battery is used to restore the supercapacitor to the nominal state of charge following an event where it was used to respond to a system event. Since we want to discharge the supercapacitor first, there might be circumstances where the battery can be discharged slowly, and the supercapacitor charged to get the supercapacitor back to a preferred state of charge.

$$P_{batt} > P_{sc} \tag{6.3}$$

6.3.4 Normal mode

In this mode, the measured system frequency is within the acceptable range and the energy storage is not acting.

$$f_{min} \leq f_{mea} \leq f_{max} \tag{6.4}$$

There is a variation of the normal mode where the control scheme will allow both the battery and supercapacitor to be charged or discharge to their nominal state of charge in order to be ready for the next event or disturbance.

If the measured grid frequency is less than or equal to the reference frequency (60 Hz) but more than or equal to the minimum allowable frequency (59.8 Hz) as in (6.5), the control

scheme should allow the ESS to be at a nominal SOC of between 50% and 80%, to be ready to discharge and deliver power to the grid for the next event.

$$f_{min} \leq f_{mea} \leq f_{ref} \tag{6.5}$$

Similarly, if the measured grid frequency is less than or equal to the maximum allowable frequency (60.2 Hz) but more than or equal to the reference frequency (60 Hz) as in (6.6), the control scheme should allow the ESS to be at a nominal SOC of between 20% and 50%, to be ready to charge and absorb power from the grid for the next event.

$$f_{ref} \leq f_{mea} \leq f_{max} \tag{6.6}$$

The Probability of Power Supply Loss of the Grid (PPSLG) is chosen to evaluate the power supply reliability of the power system as defined in (6.7) [83].

$$PPSLG = \frac{\sum_{i=1}^{N} [P_{grid}(t_i) - (P_{batt}(t_i) + P_{sc}(t_i))]}{\sum_{i=1}^{N} P_{grid(t_i)}} \tag{6.7}$$

Where $t_i \sim t_N$ is the operating time of the power system. The assumption is that under normal conditions, the grid is operating 8,760 hours in a year, 24 hours a day. The lower the PPSLG, the higher the reliability of the power system and the more satisfied the customers are. The higher the PPSLG, the lower the reliability of the power system and the less satisfied the customers are.

6.4 Bidirectional dc-dc converter control

Figure 6.2 shows the schematic diagram of the bidirectional dc-dc converters used in this design. Bidirectional dc-dc converters are utilized to allow both directional power flow to charge and discharge the energy storage system. The battery and supercapacitor each have separate bidirectional dc-dc converters to facilitate individual control of the ESS. The

bidirectional dc-dc converter response should be fast enough to compensate for the slow dynamics of the ESS, especially the battery.

The controllers sense the measured frequency from the grid power system and compare it with the reference frequency. The error is passed through a PI block generating a reference modulating signal. This reference signal is compared with the PWM carrier signal in the operator box and the generated signal passed to the logic box. In the logic box, if the reference signal is greater than the PWM signal, switch commands are generated to switches S1 and S2 to perform the desired charge/discharge operation.

The novelty in this design is that each energy storage device has its own bidirectional dc-dc converter to increase resiliency and flexibility of control of charge/discharge operations. The downside is higher cost for separate bidirectional dc-dc converters. However, the benefits are expected to exceed the costs. The benefits of separate bidirectional dc-dc converters are: flexible control that allows the supercapacitor to discharge while the battery is charging, and vice versa, individual control and sizing based on the system needs, improved reliability and redundancy in case of equipment failure, eliminate need of installing several equipment in separate locations.

To improve the power transfer capabilities of the bidirectional dc-dc converter and to be able to handle the frequency variations, several bidirectional dc-dc converters and ESS can be connected in a modular multilevel converter topology. The MMC topology also has benefits of improved dynamic stability, increased power quality, reduced switching losses, as well as fast and efficient operations of the power system. Also, a high frequency transformer with a high turns ratio can be utilized to increase the output voltage of the converter.

The output voltage of the bidirectional dc-dc converter can be calculated as [89]:

$$V_{out} = \frac{N_s}{N_p} . V_{in} \tag{6.8}$$

Where N_s and N_p are the transformer secondary and primary turns, respectively.

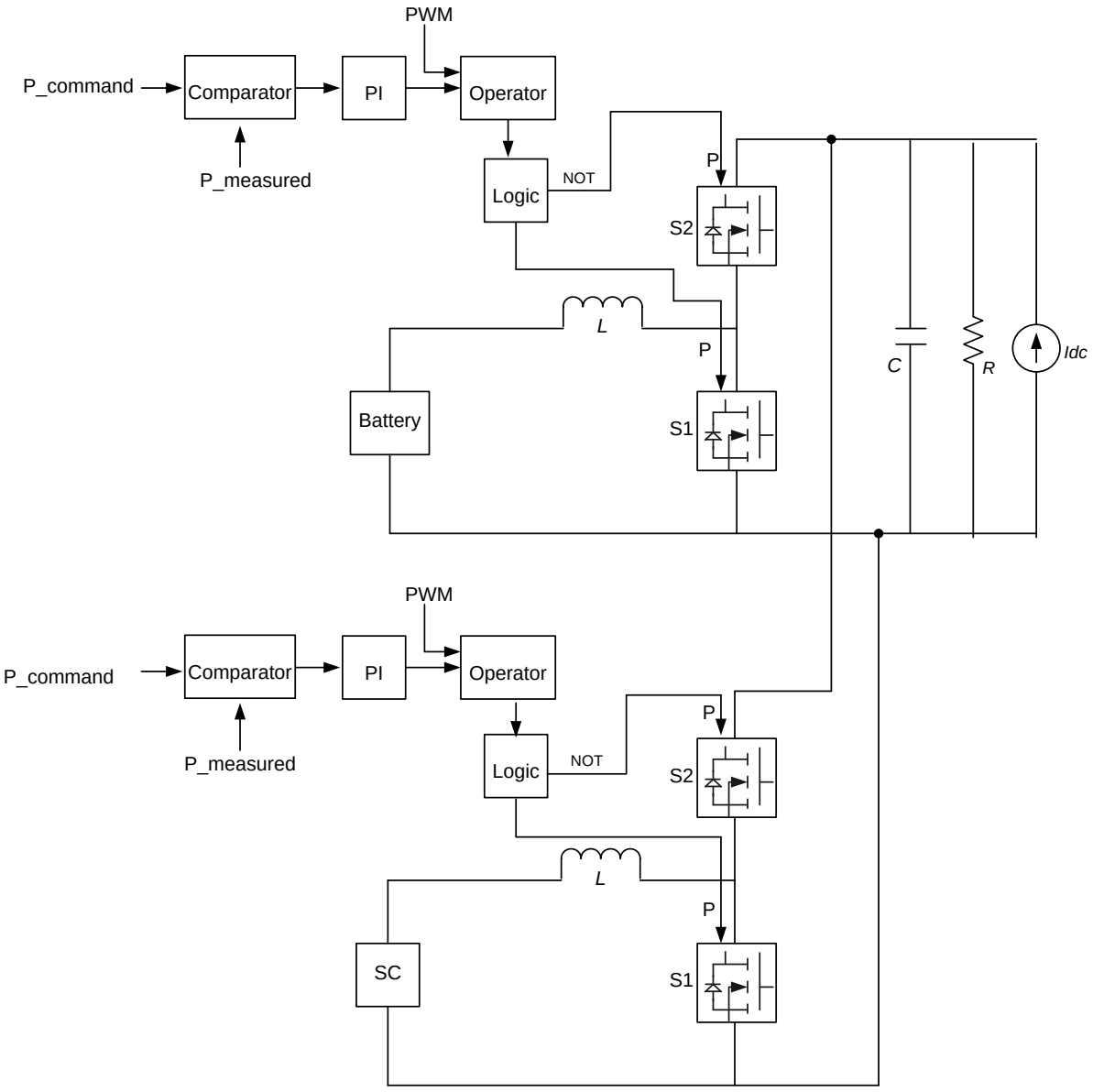

Figure 6.2: Bidirectional dc-dc converter for hybrid energy storage system (HESS)

6.4.1 Control strategy

Figure 6.3 shows a simplified block diagram of the control strategy.

Assume that the reference frequency, $f_{ref} = 60$ Hz, f_{min}=59.8 Hz and f_{max}= 60.2 Hz

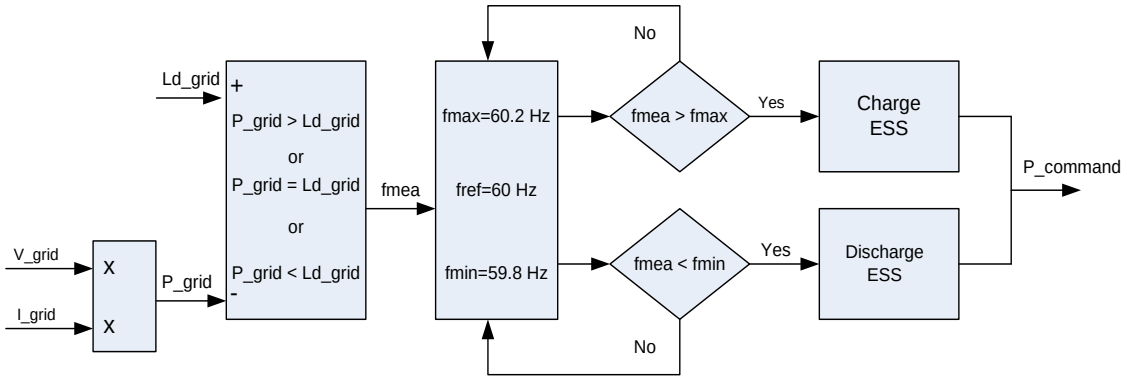

Figure 6.3: Control strategy

The $P_{command}$ is the required power command to keep the grid within an acceptable frequency range, between 59.8 Hz and 60.2 Hz. To generate the $P_{command}$, the controller senses the grid voltage, V_{grid} and grid current, I_{grid} and multiplies the components. The resulting grid power, P_{grid} which is equivalent to the grid power or generation capability, is compared with the grid load, Ld_{grid}. If P_{grid} is more than Ld_{grid}, the grid frequency increases; If P_{grid} is less than Ld_{grid}, the grid frequency decreases. Minimum and maximum frequency thresholds are set. If the measured frequency, f_{mea}, is greater than the maximum frequency threshold, f_{max}, OR f_{mea} is less than the minimum frequency threshold, f_{min}, a $P_{command}$ is generated to charge or discharge the ESS, respectively. If neither of these conditions is met, the controller will continue to sense and measure the grid frequency.

Figure 6.4 shows the control block diagram with the generated $P_{command}$ as input to each of the bidirectional dc-dc converters. The controller divides the $P_{command}$ by the measured ESS voltage, $V_{mea-ESS}$, to generate the reference current signal, $I_{command}$. The $I_{command}$ in

turn is compared with the measured ESS current, $I_{meas-ESS}$ and the error signal is passed through a PI controller, generating a PI output reference signal which is compared with a PWM signal in the operator box. The resulting modulated signal is passed through a logic block and if the $P_{command}$ conditions are met, the resulting signal is sent to the switches S1 and S2 of the bidirectional dc-dc converter to perform the appropriate charge/discharge operations.

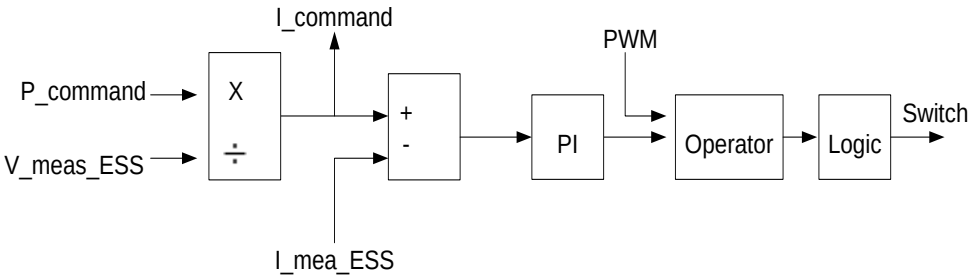

Figure 6.4: Control block diagram

6.5 Sizing the hybrid energy storage system

It is imperative to size the battery and supercapacitor adequately to satisfy the energy and power requirements of the grid and to prolong the battery life. Supercapacitor cells have low rated voltage and low energy density compared to batteries [84]. The cells are connected in series to increase the output voltage and in parallel to increase the capacity [85]. The more the number of cells, the higher the output voltage and capacity. The total number of cells is driven by the nominal voltage of each cell, rating of the bidirectional dc-dc converter and the power demand of the grid.

The battery and supercapacitor terminal voltages are restricted by the bidirectional dc-dc converter input voltage ranges [86]. In this control scheme, the bidirectional dc-dc converter

utilized has a high side operating voltage range of 60 V - 1200 V and a low side operating voltage range of 10 V - 1150 V [87].

The batteries are sized based on (6.9) and (6.10).

$$V_{batt}.N_{batt} \geq V_{hs-min} \tag{6.9}$$

$$V_{batt}.N_{batt} \leq V_{hs-max} \tag{6.10}$$

Where V_{batt} is the battery voltage of a single cell, N_{batt} is the number of series connected battery cells, V_{hs-min} and V_{hs-max} are the minimum and maximum high side operating voltages of the bidirectional dc-dc converter, respectively.

For example, the battery utilized in this control scheme has a nominal dc voltage of 48 V. Assuming each cell has a nominal dc voltage of 4.8 V, the number of series connected battery cells is 10. The high side voltage of the converter is the dc link voltage, which is roughly 1,100V.

For areas that have historical low frequency issues, the supercapacitor is set at an initial SOC of roughly 80%. This high initial SOC provides a good starting point in preparation for an event that has a high likelihood of requiring discharging the supercapacitor. The initial SOC is not set at 100% because the device won't have the capability to respond to high frequency conditions of the grid. Generally, the supercapacitor can be sized based on (6.11) and (6.12).

$$\text{SOC\% x } (V_{sc}.N_{sc}) \geq V_{ls-min} \tag{6.11}$$

$$\text{SOC\% x } (V_{sc}.N_{sc}) \leq V_{ls-max} \tag{6.12}$$

HESS sizing is based on combining battery energy and supercapacitor energy (6.13).

$$E_{batt} + E_{sc} = E_{Hess} \tag{6.13}$$

Where E_{batt} is the energy stored in the battery, E_{sc} is the energy stored in the supercapacitor.

The energy stored in a supercapacitor depends on the capacitance and the square of the voltage applied to the terminals and is calculated as in (6.11) (6.12) (6.14):

$$E_{sc} = \frac{1}{2} C_{sc} (V_{sc} * N_{sc})^2 \tag{6.14}$$

Increasing E_{sc} decreases the operating time of the batteries and results in smaller batteries in design [88].

C_{sc} can be calculated from (6.14) and (6.15), assuming the rated power P(t) of the system is known.

$$\mathrm{E_{sc}} = \int_0^{\tau} \mathrm{P(t)dt} \tag{6.15}$$

Similarly, the battery energy size E_{batt} is proportional to the rated power of the system P_{rated} and the percentage of time the battery is operating $PTBO$ (6.16).

$$E_{batt} = P_{rated} * PTBO \tag{6.16}$$

From (6.9), (6.10) and (6.16)

$$E_{batt} = (V_{batt}.N_{batt}) * I_{batt} * PTBO \tag{6.17}$$

Where I_{batt} is the current rating of the battery.

The proportion of battery and supercapacitor energy in the hybrid energy storage system is given as:

$$E_{sc} = X\% \,. E_{HESS} \tag{6.18}$$

$$E_{batt} = E_{HESS} - E_{SC} \tag{6.19}$$

Where X% is the percentage of supercapacitor energy in the HESS. The ESS is designed such that a higher percentage of the energy is attributed to the supercapacitor than the battery. The larger the supercapacitor energy, the smaller the battery energy and the smaller the battery design.

In this scheme, 60% of the HESS energy is stored by the supercapacitor.

$$E_{sc} = 60\% \,.\, E_{HESS}$$

The battery size is proportional to the rated power of the system, the dc link voltage, annual percentage of battery operating time, and inversely proportional to the supercapacitor size.

$$E_{batt}\, \alpha\, \frac{P_{rated}.BOT.V_{dc}}{E_{sc}.V_{rated-sc}}$$

Where BOT is the annual percentage of battery operating time. BOT, in addition to other factors, depends on the grid reliability and supercapacitor SOC.

The maximum power transfer capabilities and the maximum energy storage capabilities for the supercapacitor and the battery can be calculated from (6.20) (6.21)(6.22) and (6.23).

$$P_{max-sc} = \frac{V_{nominal}^2}{R_{eq-series}} \quad \text{(kW)} \tag{6.20}$$

$$E_{max-sc} = \frac{\frac{1}{2}C.V_{nominal}^2}{3{,}600} \quad \text{(kWh)} \tag{6.21}$$

$$P_{max-batt} = V_{\frac{nominal}{R_{internal}}}^2 \quad \text{(kW)} \tag{6.22}$$

$$E_{max-batt} = P_{rated}.t \quad \text{(kWh)} \tag{6.23}$$

Where P_{max-sc} and $P_{max-batt}$ are the maximum power capabilities of the supercapacitor and battery, respectively; E_{max-sc} and $E_{max-batt}$ are the maximum energy storage capabilities of the supercapacitor and battery respectively; $R_{eq-series}$ is the equivalent series resistance, $R_{internal}$ is the internal resistance, $V_{nominal}$ is the nominal voltage, P_{rated} is the rated power and t is the operating time.

The HESS is sized based on the needs of the grid. The grid consist of solar generators which are not available during a cloudy day. Solar generation is typically available between 12 noon and 5 pm. In a cloudy day, solar generation decreases and may cause a deficiency of 500 MW generation. This translates to roughly 500 MW x 5 hours = 2500 MWh of energy unavailable and it may result in a frequency drop below 59.8 Hz. To avoid dropping load, the energy storage system is sized to deliver 3000 MWh to account. This size will also account for possible losses. Tables 6.1, 6.2 and 6.3 show the supercapacitor, battery, and bidirectional dc-dc converter parameters, respectively.

When connecting the batteries or supercapacitors in series, we assumed perfect sharing among the series connected batteries or supercapacitors in strings. The balancing mechanisms are outside the scope of this research.

Table 6.1: Supercapacitor specifications

Nominal DC voltage	480 V
Rated capacitance	1,000 F
Energy storage capacity	32 kWh
Initial SOC	50%
Equivalent DC series resistance	1 mΩ

Table 6.2: Battery specifications

Nominal DC voltage	48 V
Battery capacity	450 Ah
Energy storage capacity	22 kWh
Initial SOC	50%
Internal resistance	1.1mΩ
Nominal discharge current	195 A
Cut-off voltage	36 V
Type	Lithium-ion

Table 6.3: Bidirectional dc-dc converter specifications

Inductance L (battery)	1 mH
Inductance L (SC)	100 mH
Output capacitance C	1,000 μF
Equivalent inverter losses	1 kΩ

6.6 Simulation results

The simulation results of the bidirectional dc-dc converter for the battery and supercapacitor are analyzed in this section. Power of the battery is limited by a rate limiter block; therefore, the transient power is supplied to the DC bus by the supercapacitor. The simulation time is 20 seconds and the simulation time step is 25μs.

The scheme is modelled such that the required power will output a repeating sequence of numbers specified in time-value pairs.

Figures. 6.5, 6.6 and 6.7 show plots of the dc link voltage of the bidirectional converter connected with the supercapacitor alone, battery alone and the hybrid energy storage system, respectively. In this scenario, the battery and supercapacitor are both discharging. Notice that in Figure 6.7, the dc link capacitor voltage is higher when the battery and supercapacitor are combined than when the battery alone is connected as in Figure 6.6. With the battery alone

connected to the converter, the dc link voltage is roughly 800 V. With the supercapacitor combined with the battery, the dc link voltage is roughly 1,100 V. When this high dc link voltage is input to the inverter, it helps to improve the stability of the grid during low frequency situations.

Notice that the dc link voltage waveform of the HESS in Figure 6.7 is similar in shape to the combined waveforms of the supercapacitor alone and the battery alone, in Figures 6.5 and 6.6, respectively.

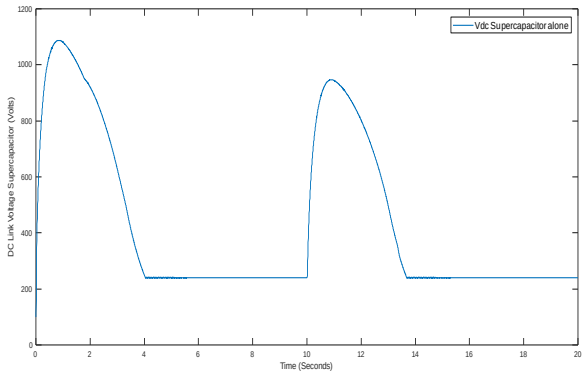

Figure 6.5: DC link voltage for supercapacitor connected alone

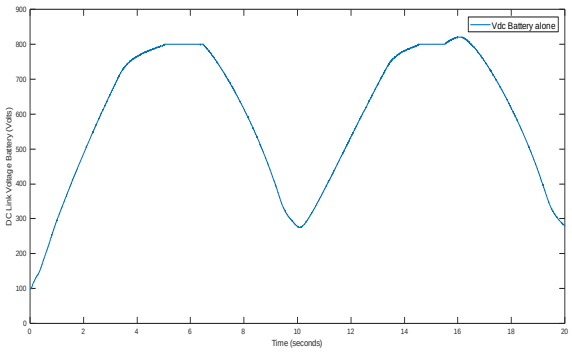

Figure 6.6: DC link voltage for battery connected alone

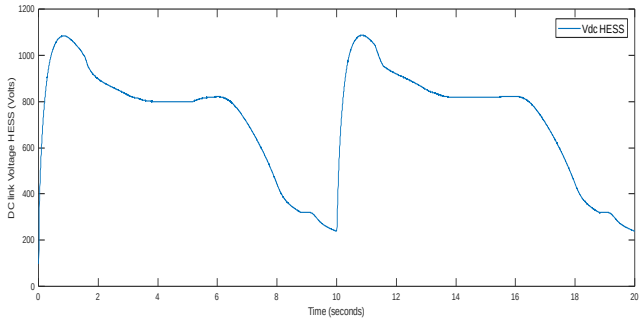

Figure 6.7: DC link voltage of hybrid energy storage system (HESS)

Figure 6.8, 6.9 and 6.10 show the battery in charge mode, the supercapacitor in discharge mode, and the discharge current of the HESS, respectively.

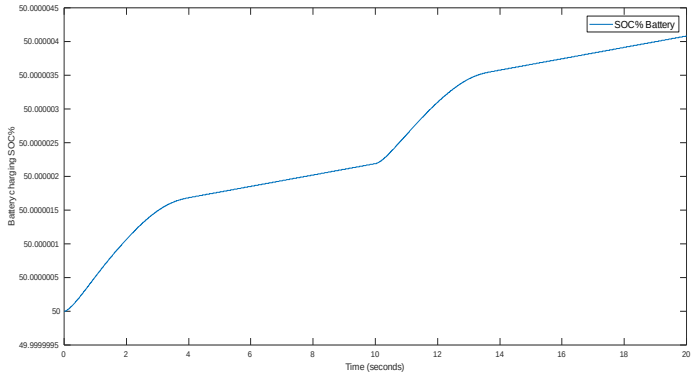

Figure 6.8: Battery charging

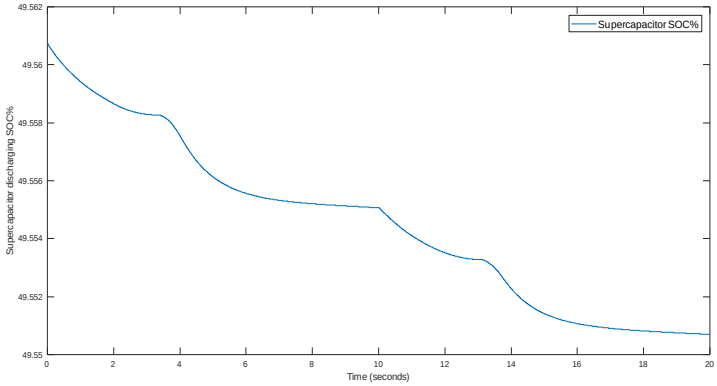

Figure 6.9: Supercapacitor discharging

In the discharge mode, the current is negative while in charge mode, the current is positive. The change in current is due to the inverter control of the dc link voltage. When the voltage increases due to discharging the ESS, it will transfer more power to the grid, changing the current in the current source.

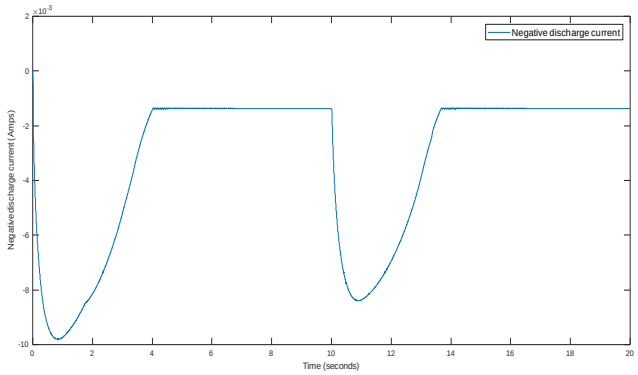

Figure 6.10: Negative discharge current of HESS

6.7 Summary

Batteries and supercapacitors are increasingly used to enhance performance of power systems due to benefits of high energy density and high-power density, and better leveraging clean energy sources. In this design, the ESS is controlled to generate or absorb power during unacceptable frequency fluctuations. The two energy storage devices are each coupled to separate bidirectional dc-dc converters to allow flexible control of the battery and supercapacitor operations. Each of the battery and supercapacitor control schemes can be adjusted independently based on the needs of the grid.

The bidirectional dc-dc converters enable bidirectional control of power flow between the energy storage system and the grid and enable efficient charging and discharging of the energy storage system. The controllers sense the measured grid frequency and compare it with the

reference frequency. If the measured frequency is not within an acceptable frequency range, the controllers send a command to charge or discharge the appropriate energy storage system. This enhances the dynamic performance of the grid and maintains the grid frequency within the desired range.

A single hybrid energy storage system might not be able to solve the frequency deviation, but many working in a similar fashion could do so. Combining several modules of the hybrid energy storage system in a modular multilevel converter topology will increase the power capability of the system and make them suitable for such frequency variation mitigations in medium or high-power transmission applications.

These modular multilevel converters can be combined with Static Synchronous Compensators (STATCOMs) and other Flexible AC Transmission Systems (FACTS) devices, to dynamically control the exchange of both real and reactive power with the grid, to enhance stability. The STATCOM provides reactive power compensation while the HESS provides real power compensation. Renewable energy sources such as solar and wind generation can be connected to the MMC and the energy can be stored in the HESS and used later.

This scheme provides a cost-effective solution for modern power systems as power generation, energy storage and power compensation devices can all be installed in one location, rather than installing several standalone systems at different locations.

Chapter 7: Enhanced STATCOM Model Implemented in Matlab/Simulink

7.1 Introduction

This chapter will describe how the enhanced STATCOM design was implemented in Matlab/Simulink. The enhanced STATCOM model was implemented by building modular multilevel converter submodules in combination with battery and supercapacitor energy storage system. Built-in models were used in some cases by adding components and modifying controls to meet requirements. A typical 500 kV system in the Western Electricity Coordinating Council (WECC) region that has experienced very high and low voltage issues during normal and abnormal conditions was modelled. The system was tested with the Positive Sequence Load Flow (PSLF) software and the results are consistent with the system modelled in Matlab. The enhanced STATCOM was connected to the 500 kV system. In addition, bidirectional dc-dc converter controls were designed to manage the charging and discharging operations of the batteries and supercapacitors. The following sections describe how the enhanced STATCOM project was implemented and how the model was validated.

7.2 The 500 kV Grid Model

The 500 kV grid is modelled to approximate a real life situation currently experienced in a 500 kV system in the WECC. The local 500 kV grid used in the simulation consists of four major substations separated by between 60 miles and 150 miles from each other and with compensation consisting of FACTS devices such as shunt capacitors and shunt reactors. There are also generators and loads connected to the underlying 230 kV system.

- Shunt capacitors are connected to some of the substation buses to generate reactive power to the grid and increase bus voltage
- In other substations, shunt reactors are connected to the substation buses to absorb reactive power and reduce bus voltage

Installing multiple FACTS devices poses a challenge to operate the system and this can result in complex interactions. The proposed enhanced STATCOM will mitigate these challenges and risks by using a single installation and provide dynamic real and reactive power support to the grid. The design will have a centralized device location to dynamically regulate voltages, frequencies and stability of the power system area in question.

The area of study is a solar generation-rich area and experiences high and low voltage issues during both normal and abnormal conditions. The total generation in the local area simulated is roughly 3,170 MW and the total load is 3,100 MW. Total transmission losses are approximately 70 MW under normal conditions. Figure 7.1 shows a simplified single line diagram of the 500 kV system simulated in PSLF and in Matlab/Simulink.

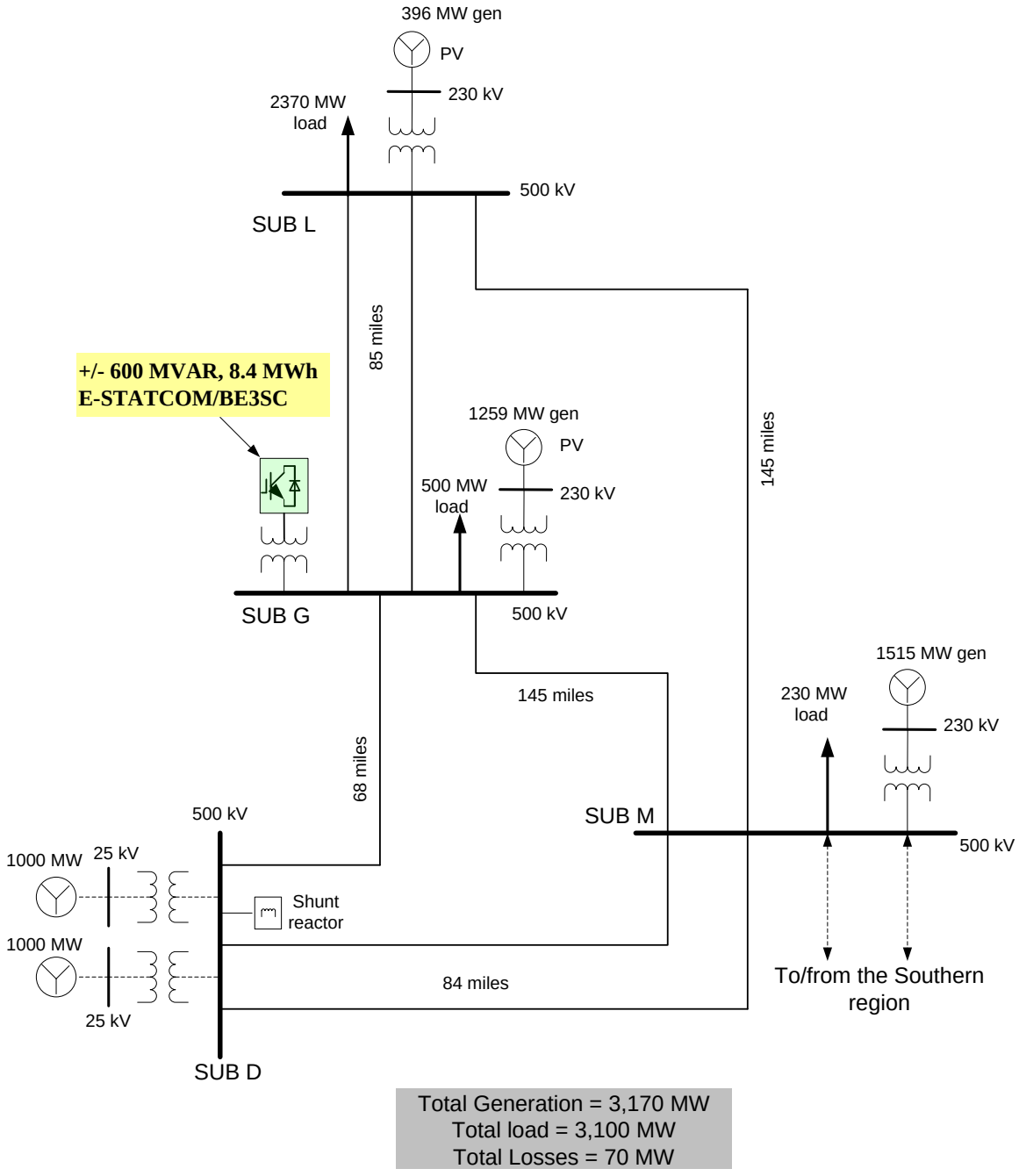

Figure 7.1**:** 500 kV system studied

The 500 kV system experiences voltages as high as high as 1.12pu (554 kV) due to high PV generation. The normal operating voltage range in the 500 kV system is between 525

kV and 540 kV, and the emergency operating voltage range is between 495 kV and 551 kV. Table 7.1 shows the operating voltage ranges of the 500 kV system.

Table 7.1: Operating voltage ranges of the 500 kV system

Nominal voltage	Normal operating voltage range				Emergency operating voltage range			
	Low limit		High limit		Low limit		High limit	
500 kV	525 kV	1.05 pu	540 kV	1.08 pu	495 kV	0.99 pu	551 kV	1.1 pu

The enhanced MMC STATCOM will help regulate the voltage through its reactive capacity to keep the system within the voltage set limits.

During summer peak conditions, approximately 2,000 MW generation is connected to SUB D, power is transferred to the southern region of the grid via the south intertie at SUB M. There are plans to retire the two generation units at SUB D. This will cause a power generation deficiency in the local area and power will need to be imported from the southern region to the northern region, resulting in higher voltages in the local area. During spring off peak conditions, overall load levels are expected to be lower and the high voltage issues will be worse. PSLF studies show that installing a +/- 600 MVAR MMC STATCOM with 8.4 MWh energy storage at SUB G will provide dynamic real and reactive power support in the area and mitigate the voltage issues projected when the generation units are retired. This design will also help stabilize frequency issues experienced during a partly cloudy day if solar generation is lost intermittently.

In a partly cloudy day, when solar generation penetration is reduced, the system experiences a deficiency in generation which may lead to low frequencies in the area. During certain contingencies like loss of critical equipment or transmission lines, the generation output is more than the load demand. This may result in high frequency situations. The desired system frequency is 60 Hz. If the system frequency drops below the

minimum set point of 59.8 Hz for more than 12 cycles, an under-frequency load shedding scheme is activated and blocks of load are dropped in the BUS G area, to balance the generation and load levels.

To avoid the need to drop load, the proposed enhanced STATCOM will include a hybrid energy storage system enough to mitigate frequency deviation issues.

7.3 MMC STATCOM

Matlab has models available for different types of STATCOMS and energy storage systems. In this dissertation, the "power_statcom_22PM" and "parallel_battery_SC_Boost converter" models are used to implement the enhanced STATCOM. The "power_statcom_22PM" is an MMC designed with 22 full bridge modules, each having internal dc link capacitors. This model was modified by replacing the MMC module model with internal capacitors with an MMC full bridge module model with access points for external dc link capacitors. These MMC modules with external capacitors are used to enable connection of the energy storage system in parallel with the dc link capacitor of the MMC submodules. Initially, 11 modules connected in series were used; as a result, the expected converter output voltage and current waveforms exhibited few steps. As a comparison, 22 modules were used; the converter output current and voltage waveforms exhibited more steps as expected. If more modules are utilized, the output waveforms will approach a sinusoidal shape. Each MMC submodule has a dc link capacitor. Since the 22 submodules are connected in series, the output voltage of the MMC STATCOM is approximately the sum of the dc link voltages of the 22 submodules. Figure 7.2 shows a simplified schematic representation of a single-phase, three-submodule MMC STACOM with hybrid energy

storage system connected on the submodule dc link. For simplicity, the hybrid energy storage system is connected only to two submodules of the MMC STATCOM.

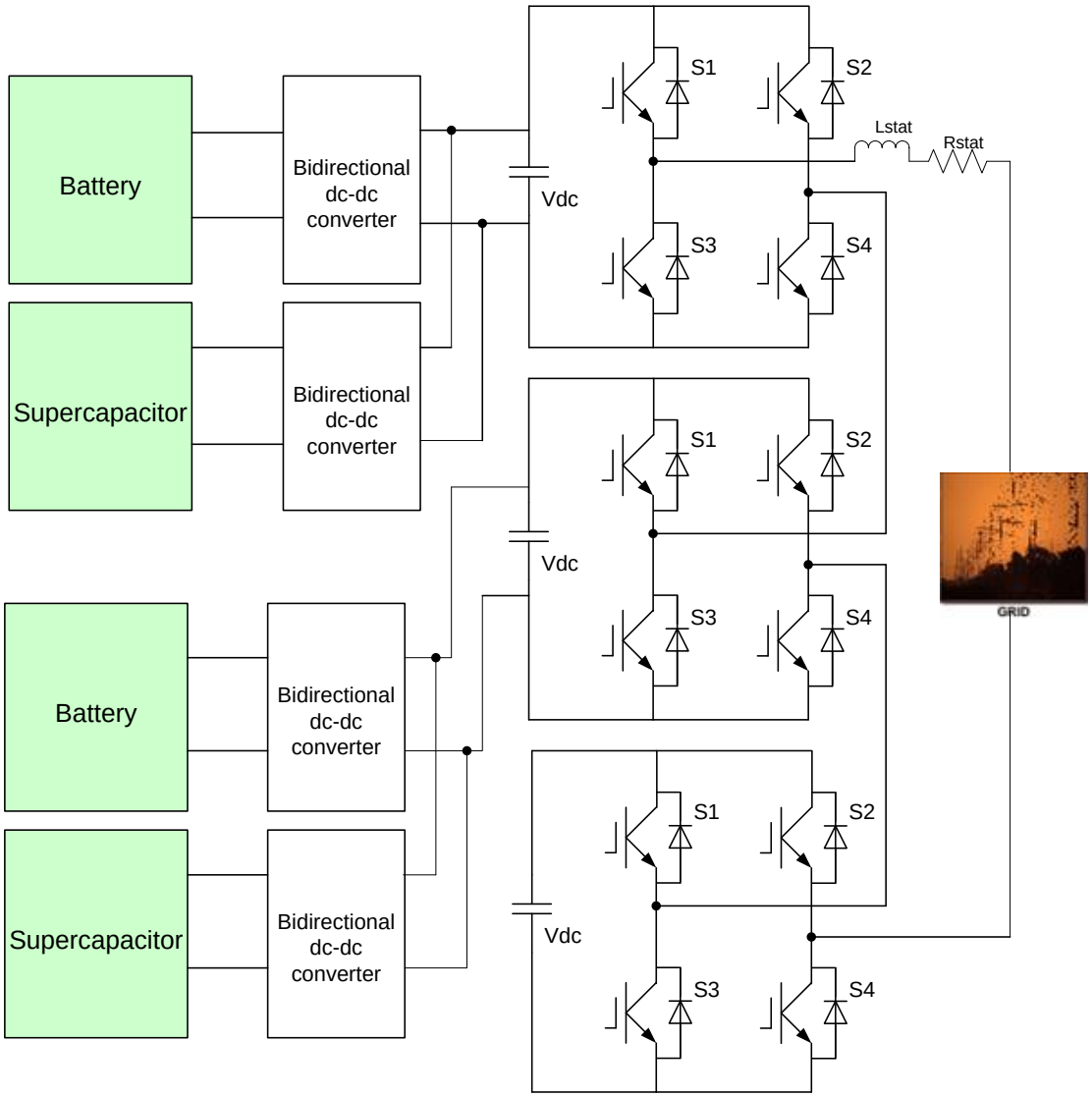

Figure 7.2: Single-phase, three-submodule MMC STATCOM topology with hybrid energy storage connected to two submodules

To improve the waveform quality, a PWM scheme with a switching frequency of 1.2 kHz was used for the MMC STATCOM.

Since the enhanced STATCOM will be regulating the voltage, frequency and power exchange with a 500 kV system without a step-up transformer, the output voltage of the converter is expected to be greater than 500 kV per branch. Figure 7.3 shows a plot of the converter output for each of the phases of the MMC STATCOMs. The impact of the PWM is visible in the waveform.

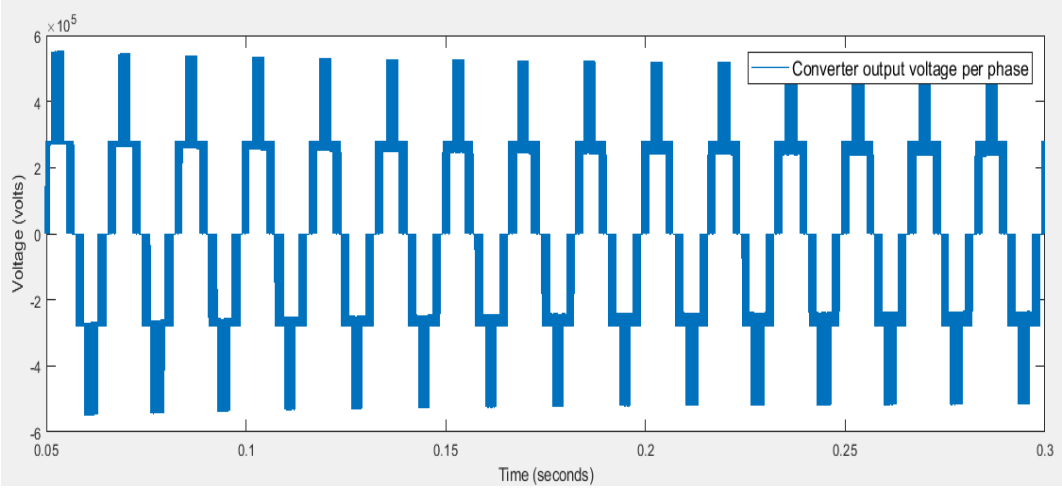

Figure 7.3: Converter output voltage per phase

A hybrid energy storage system is connected to the dc link capacitor of the submodule via a high frequency transformer. The transformer is designed to have a primary to secondary turns ratio of roughly 1/58, to give the desired output voltage. Figure 7.4 shows a schematic representation of the full bridge dc-dc converter, high frequency transformer, inverter and rectifier connected between the HESS and the MMC STATCOM. In Figure 7.4, the ESS is connected to only two submodules based on the total power and energy needs of the system and to avoid impacting harmonic behavior. The converter and transformer each have a switching frequency of 1.2 kHz.

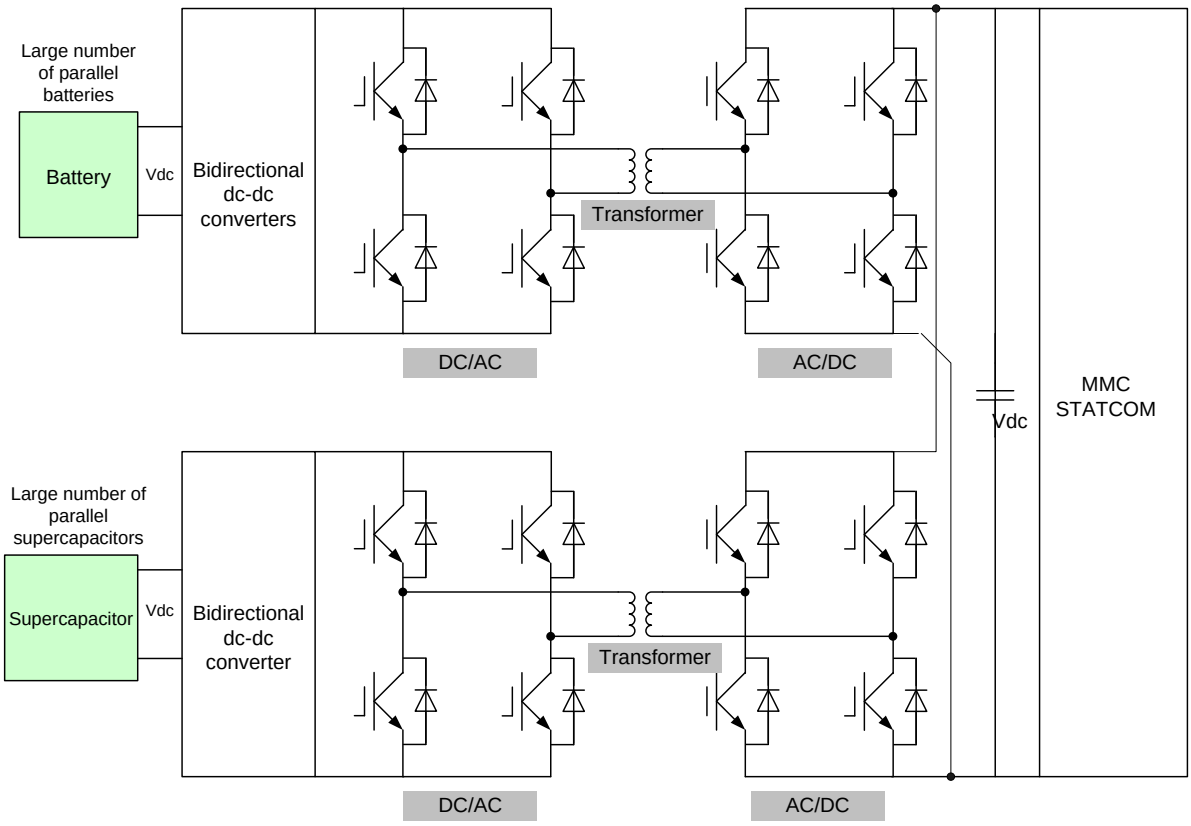

Figure 7.4: Schematic representation of full-bridge dc-dc converter transformer

7.3.1 MMC STATCOM Parameters

As noted earlier, the MMC STATCOM is implemented with 22 submodule per branch. The nominal dc voltage ($V_{nom_{dc}}$) per submodule is set at 28 kV and the nominal power (P_{nom}) is set at 12 MVA per submodule. The base impedance (Z_{base}) is calculated as:

$$Z_{base} = \frac{V_{nom_{grid}}^2}{P_{nom}} \Omega \tag{7.1}$$

Where $V_{nom_{grid}}$ is the nominal grid voltage = 500 kV

The per unit branch reactor is set at 0.12 pu with an X/R ratio of 50. The actual values of branch reactor (L_{stat}) in Henries and branch reactor resistance (R_{stat}) in ohms can be calculated as:

$$L_{stat} = \frac{(L_{stat_{pu}} * Z_{base})}{2*\pi*f} \tag{7.2}$$

$$R_{stat} = R_{stat_{pu}} * Z_{base} \tag{7.3}$$

Where f is the grid frequency.

The dc link stored energy constant $H = 1/(f * \frac{3}{4})$ [90]

The capacitance of the dc link capacitor per module is calculated as:

$$C_{dc} = \left(\frac{P_{nom}}{3*N_m}\right) * H * 2/V_{nom_{dc}}^2 \tag{7.4}$$

Table 7.2 shows the MMC STATCOM parameters used in the simulation.

Table 7.2: MMC STATCOM Parameters

Number of power submodules per branch	22
Nominal capacitor voltage per submodule	28 kV
Apparent power	800 MVA
Base Impedance	313 Ω
Branch reactor	0.12 pu
Branch reactor resistance	0.024 pu
DC link capacitance per module	5.8 µF

7.3.2 STATCOM Gain Parameters

The STATCOM has a closed loop control scheme for I_d and I_q , implemented in the synchronous rotating d-q reference frame. The STATCOM gains K_i and K_p are determined

by tuning with the total branch resistance and inductance values R_s and L_s, respectively, between the converter terminals and the point of interconnect. τ is the desired time constant for the control response.

$$\frac{\mathrm{K_i}}{\mathrm{K_p}} = \frac{\mathrm{R_s}}{\mathrm{L_s}} \tag{7.5}$$

$$\frac{K_p}{L_s} = \frac{1}{\tau} \tag{7.6}$$

From (7.6) $$K_p = \frac{L_s}{\tau} \tag{7.7}$$

From (7.5) $$K_i = K_p \frac{\mathrm{R_s}}{\mathrm{L_s}} \tag{7.8}$$

Example: Using the MMC STATCOM design parameters in from Table 7.2:

$$\mathrm{R_s} = \frac{0.12}{50} = 0.0024\ pu,\ \mathrm{L_s} = 0.12pu,\ \ \tau = 0.01$$

$$V_{rms} = 500\ kV\ , \qquad P_s = 800\ MW$$

$$V_p = \frac{500\ kV}{\sqrt{3}} = 289\ kV\ , \qquad V_{sd} = \sqrt{2}x(V_p)$$

$$Z_{base} = \frac{V_{rms}^2}{P_s}\ , \quad Z_{base} = 313\ \Omega$$

The values of $\mathrm{R_s}$ and $\mathrm{L_s}$ in ohms and Henries are calculated from the per unit values and system base impedance as below:

$$R_s = 0.0024pu\ x\ 313\ \Omega = 0.75\ \Omega$$

$$L_s = \frac{0.12\ pu\ x\ 313\Omega}{2\pi f} = 0.1H$$

From (7.6) $K_p = \frac{L_s}{\tau}$, $K_p = \frac{0.1H}{0.01} = 10$

From (7.5) $K_i = K_p \frac{\mathrm{R_s}}{\mathrm{L_s}}$, $K_i = 10\ x\ \left(\frac{0.75}{0.1}\right) = 75$

7.4 Hybrid Energy Storage system sizing

The hybrid energy storage consists of batteries and supercapacitors each connected through a bidirectional dc-dc converter to enhance flexibility of control of charge and discharge operations. To avoid shedding load during outage of 1.26 GW solar generation in a partly cloudy day, the HESS is sized with a sufficient power rating and sufficient energy capacity to mitigate frequency deviation issues that may result on load shedding.

In Chapter 5, we covered calculations for sizing the HESS. Tables 7.3 and 7.4 show specifications of the battery and supercapacitor used in the implementation of the simulation. The initial SOC is set at 50% to ensure the HESS is ready for the next charge/discharge activity.

Table 7.3: Battery specifications

Nominal DC voltage	480 V
Battery capacity per phase	2,500 Ah
Energy storage capacity per phase	1.2 MWh
Initial SOC	50%
Internal resistance	1.92 mΩ
Nominal maximum discharge current	1.1 kA
Cut-off voltage	360 V
Type	Lithium-ion

Table 7.4: Supercapacitor specifications

Nominal DC voltage	480 V
Rated capacitance per phase	10,000 F
Number of parallel capacitors	5
Energy storage capacity per phase	1.6 MWh
Initial SOC	50%
Equivalent DC series resistance	1 mΩ

7.5 Bidirectional dc-dc Step-up Converter

The bidirectional dc-dc converters consist of self-commutated power electronic switches connected in H-bridges, an inductor L to smooth current ripple, capacitors for filtering voltage ripple and smoothing output waveforms, and a high frequency transformer for stepping up HESS output voltage via a DC/AC converter. Table 7.5 shows the converter parameters used in simulation.

Table 7.5: Bidirectional dc-dc converter specifications

Inductance L	1 mH
Output capacitance C	1,000 μF
Switch FET Resistance	0.1 Ω
Switch internal diode resistance	0.01 Ω

To get the required dc link capacitor voltage roughly 28 kV per submodule (that is 22 x 28 kV = 616 kV for a 22-submodule MMC), a high frequency transformer is used to step up the voltage. Since the transformer cannot be connected to a dc system, VSC is used to convert dc to ac before connecting the transformer. The inverter consists of IGBTs configured in an H-bridge. After transforming the ac voltage to the desired level, a second H-bridge is used to convert the ac voltage back to dc. The arrangement is bidirectional as covered in Chapter 6; the transformer turns ratio is set to obtain the desired output voltage:

$$V_{out} = \frac{N_s}{N_p} . V_{in} \tag{7.9}$$

Tables 7.6 shows the specifications of the high frequency transformer used in the simulation.

Table 7.6: High frequency transformer specifications

Nominal power	1 kVA
Frequency	1.2 kHz
Primary winding nominal voltage	480 V
Secondary winding nominal voltage	28 kV
Primary winding resistances	0.005 pu
Secondary leakage inductances	0.02 pu

7.6 Summary

In this chapter, implementation of the enhanced STATCOM model in Matlab/Simulink and PSLF is discussed. The model is implemented by building a modular multilevel converter model in combination with battery and supercapacitor energy storage models. A typical 500 kV system in the WECC that has experienced high and low voltage issues is modelled and connected with the enhanced STATCOM via bidirectional dc-dc converters.

The model consists of a 500 kV transmission grid with sources and loads, a 22-submodule MMC STATCOM, a HESS consisting of batteries and supercapacitors, and a bidirectional dc-dc step-up converter.

The enhanced STATCOM is rated adequately and the parameters of the components are set appropriately to control system stability and mitigate frequency variation issues during transmission line or generation outages. The design also helps mitigate load shedding due to reduced solar generation during a cloudy day.

Chapter 8 will test the performance of the system over a range of simulations scenarios and evaluate the simulation results.

Chapter 8: Evaluation and Analysis of Simulation Results

This chapter demonstrates performance of the proposed E-STATCOM/BE3SC on a set of cases requiring the capabilities of both real and reactive power control. As described in Chapter 7, the 22-submodule MMC STATCOM model in Matlab is modified to both connect an external dc capacitor across the entire bridge to provide a connection point for the hybrid energy storage system. This model is a compromise to demonstrate connection of the energy storage system with a reasonable initial simulation effort. As discussed earlier, the preferred solution is to use standard sized modular hybrid energy storage systems connected to each submodule of the MMC STATCOM.

This chapter will analyze the simulation results of the response of the electric transmission system with the following cases:

1) Dynamic response of the STATCOM controls to varying Q_{ref} setpoints
2) Case comparing the converter dc capacitor voltages with the MMC STATCOM alone and with the E-STATCOM/BE3SC.
3) Compare ac converter output voltage with 22 MMC submodules and with 11 MMC submodules
4) Verification of converter output current against measured reactive power (Q_{mea})
5) Comparison of dynamic response to three-phase fault conditions without compensation, with a STATCOM alone and with the enhanced STATCOM with hybrid energy storage system.
6) Response of E-STATCOM/BE3SC to variations in the $P_{command}$ and the response of the charge and discharge controls of the battery and supercapacitor

7) Voltage magnitude response at select buses with reduced solar generation output

The Matlab Simpower Systems block set simulations were validated with PSLF for the following cases

8) E-STATCOM/BE3SC connected to mitigate overvoltages
9) Power system frequency response of system with variation in solar generation without compensation and with the E-STATCOM/BE3SC.

In order to speed-up simulation while keeping simulation fidelity, a switching function MMC model in the Simpower Systems blockset is selected for the MMC STATCOM. The switching function emulates the responses to the firing pulses produced by PWM generator as voltage and current steps without representing the details of the switching behavior. This is a quasi-switching model for the MMC-VSC, but a switching model is used in the dc-dc converter stages.

8.1 Dynamic response to Moderate Step Change in Reactive Power Command

Dynamic reactive response for a moderate step change in the reactive power command is tested by varying $\mathrm{Q_{ref}}$ from -5 MVARs to 10 MVARs. While this is a small step relative to the rating of the MMC STATCOM, it demonstrates the response. The MMC STATCOM initially operates in inductive mode following its set-point Q_{ref} of -5 MVARs. At 0.5 seconds, the set-point is changed from -5 MVARs to 10 MVARs. The MMC STATCOM controls modify the converter output voltage and current to vary reactive power. Figure 8.1 shows the dynamic response of the MMC STATCOM. The average value of the measured

reactive power tracks the step change in the reference. It takes roughly 1 millisecond for the MMC STATCOM to respond.

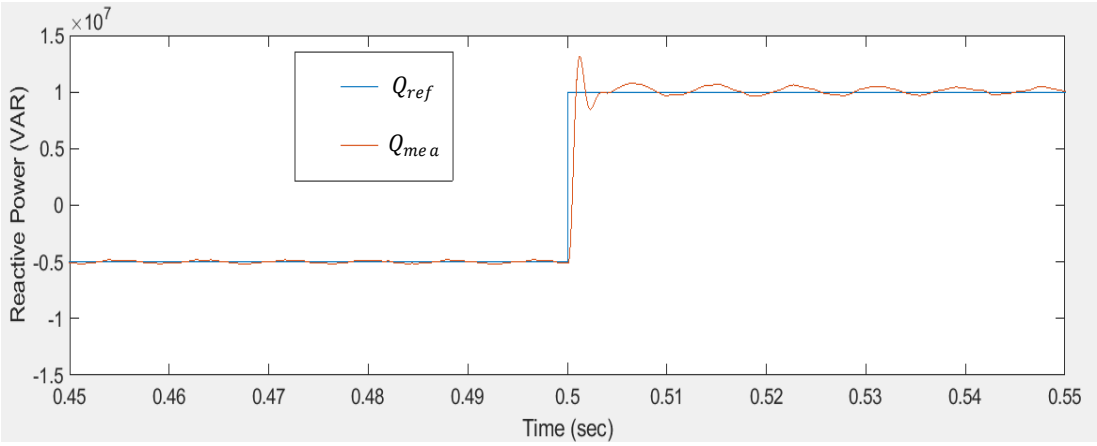

Figure 8.1: Dynamic response for moderate step change in Q_{ref} in MMC STATCOM operation

8.2 Submodule Capacitor Voltage Comparison

The low-level capacitor voltage was measured for a case with three submodules with the E-STATCOM/BE3SC and with the MMC-STATCOM alone. Figures 8.2 and 8.3 show the steady-state capacitor voltage behavior of the E-STATCOM/BE3SC and the MMC STATCOM, respectively. The low-level capacitor voltage is higher in Figure 8.2 than in Figure 8.3 due to the additional real power injected by the hybrid energy storage system onto the STATCOM dc link. These results are expected.

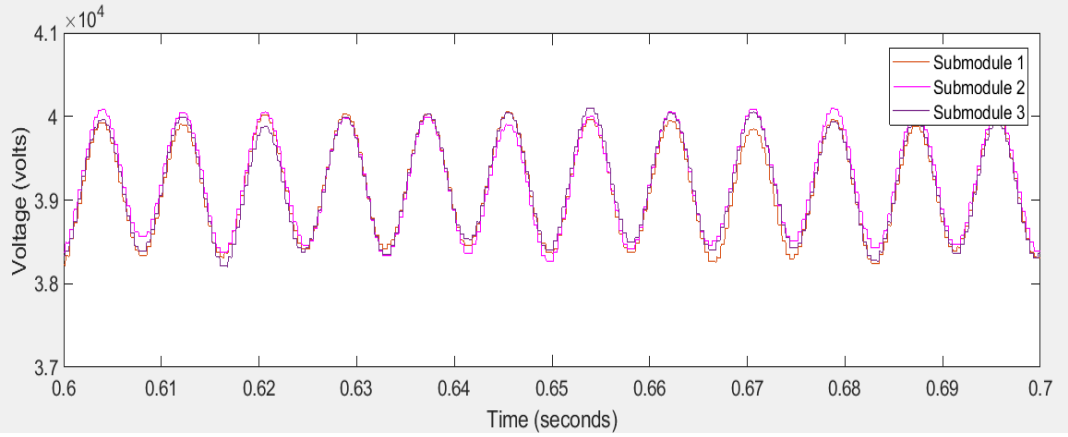

Figure 8.2: Capacitor voltage of three submodules with E-STATCOM/BE3SC (at 40kV)

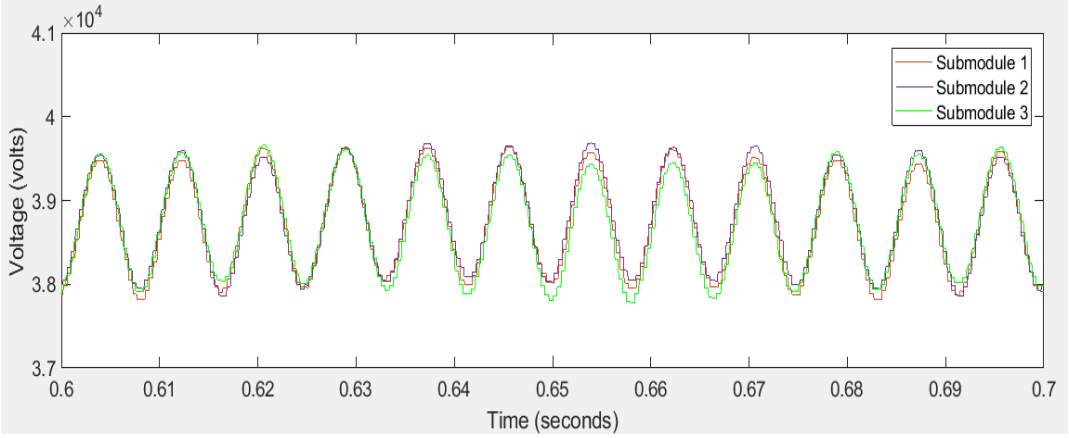

Figure 8.3: Capacitor voltage of three submodules with MMC STATCOM alone (at 39.5kV)

8.3 Impact of Increasing Number of Submodules on AC Voltage Waveform

Figures 8.4 and 8.5 show the phase converter output voltage waveforms for a 22-submodule and an 11-submodule MMC STATCOM, respectively. Both cases use a PWM switching frequency of 1.2 kHz. The 22-submodule case will have an effective switching frequency twice as high as that of the 11-submodule system. The size of the voltage steps in the waveforms are proportional to the number of submodules in the MMC STATCOM design. The larger the number of submodules, the more the steps in the waveform and the more the waveform approaches a sinusoidal shape. Notice that the 22-submodule waveform in Figure 8.4 has more steps and visually shows a better approximation of a sinusoidal

waveform, compared to the 11-submodule waveform in Figure 8.5. Based on these results, later simulations will use the 22-submodule design.

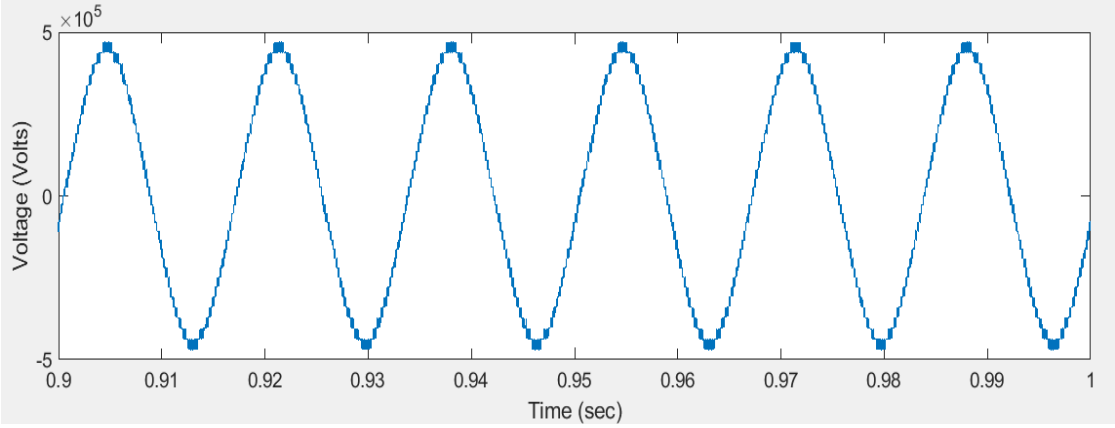

Figure 8.4: Converter output voltage per phase with 22-submodules E-STATCOM/BE3SC

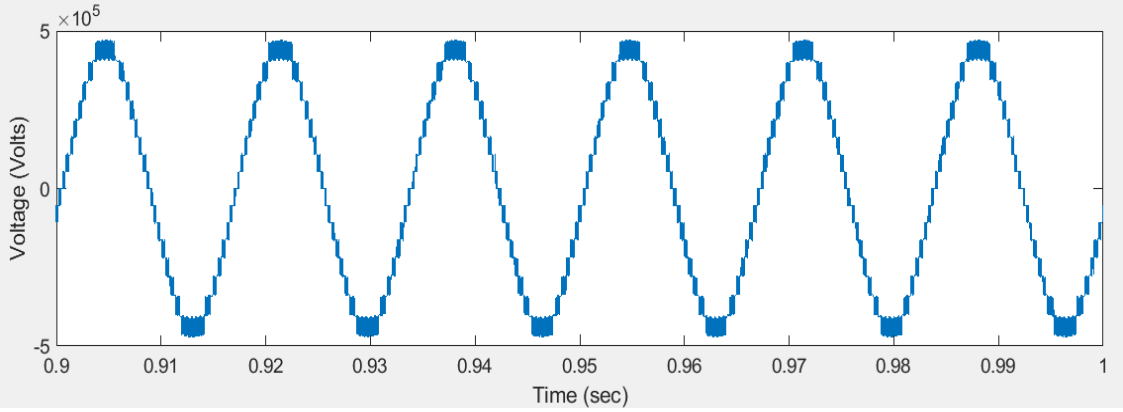

Figure 8.5: Converter output voltage per phase with 11-submodules E-STATCOM/BE3SC

8.4 Verification of Converter Ouput Current Against Reactive Power Command

The converter output current per phase can be calculated from Q_{ref} and the converter terminal line to neutral ac output voltage, V_{conv}. For $Q_{ref} = 100\ MVAR$ capacitive and $V_{conv} = 465\ kV$:

$$I_{conv} = \frac{Q_{ref}}{V_{conv} * \sqrt{3}} \tag{8.1}$$

$$I_{conv} = \frac{100MVAR}{465kV*\sqrt{3}} = 124\ Amps$$

Figure 8.6 shows the ac current for the 22-submodule E-STATCOM with a reactive power setpoint of 100 MVAR capacitive. The calculated converter output current per phase is 124 Amps. This is the RMS current at the converter output per phase. The waveforms of Figure 8.6 show the peak current of the converter output per phase. Assume the waveform is sufficiently close to a single frequency sinusoidal due to the action of the 22 level PWM MMC.

$$I_{peak} = \sqrt{2} * I_{rms} \tag{8.2}$$

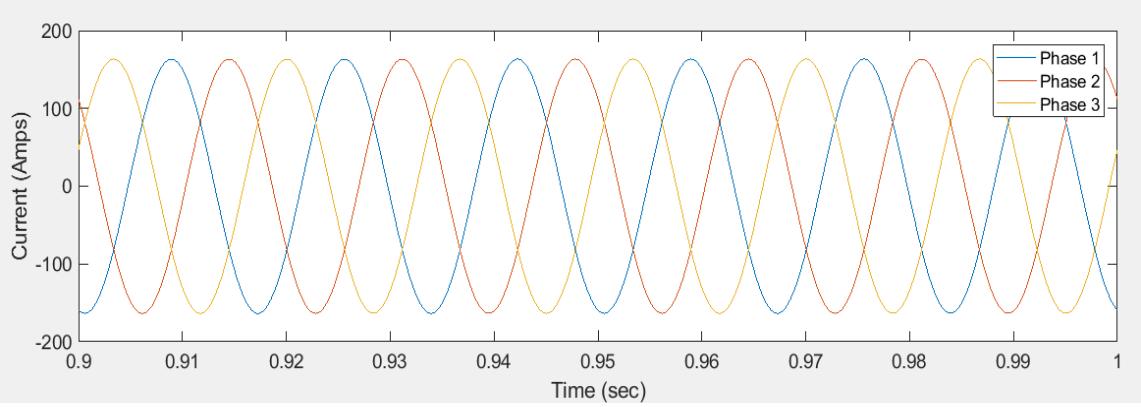

Figure 8.6: Converter output peak current with 22-submodule E-STATCOM/BE3SC for Q_{ref} = 100 MVAR

8.5 Response During Recovery From a Close-In Three-Phase Fault

In this section, three cases are studied to examine the system response following a fault on the 500 kV system: (1) with no compensation, (2) with MMC STATCOM alone and (3) with enhanced MMC STATCOM.

Case 1: System without compensation

In Case 1, the 500 kV system in Figure 7.1 is subjected to a three-phase fault for 5 cycles (between 20 cycles and 25 cycles), 72 miles from SUB L, on the line between SUB L and SUB M, without compensation. Figures 8.7 and 8.8 show waveforms of the voltage and current measured at SUB L, respectively. Notice the initial current imbalance during the fault due to the decaying dc offsets from the transient response.

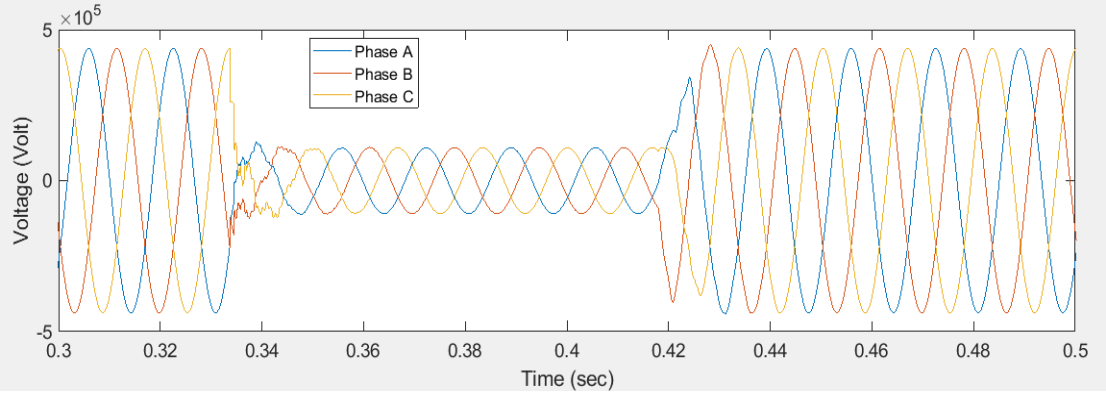

Figure 8.7: Voltage measured at SUB L for a three-phase fault on the 500 kV line between SUB L and SUB M, without compensation

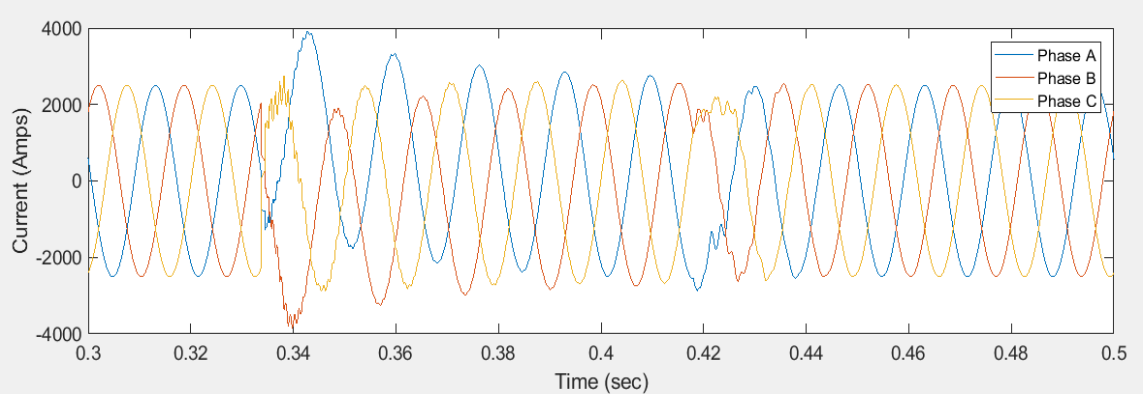

Figure 8.8: Fault current measured at SUB L for a three-phase fault on the 500 kV line between SUB L and SUB M, without compensation

Case 2: System Recovery from Fault with MMC STATCOM

In Case 2, an MMC STATCOM is connected at SUB G and a three-phase fault is applied on the line between SUB L and SUB M as mentioned in Case 1. Figure 8.9 shows waveforms of voltage and current, measured at SUB L.

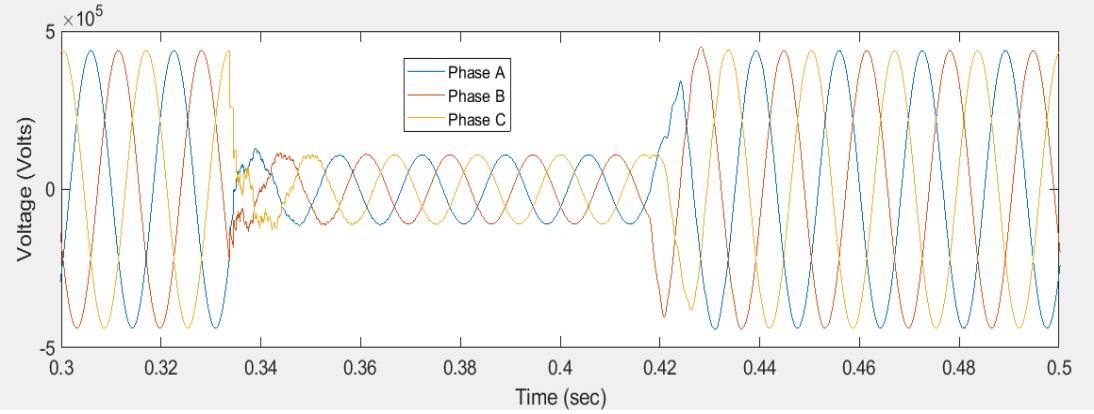

(a) Voltage waveform with MMC STATCOM

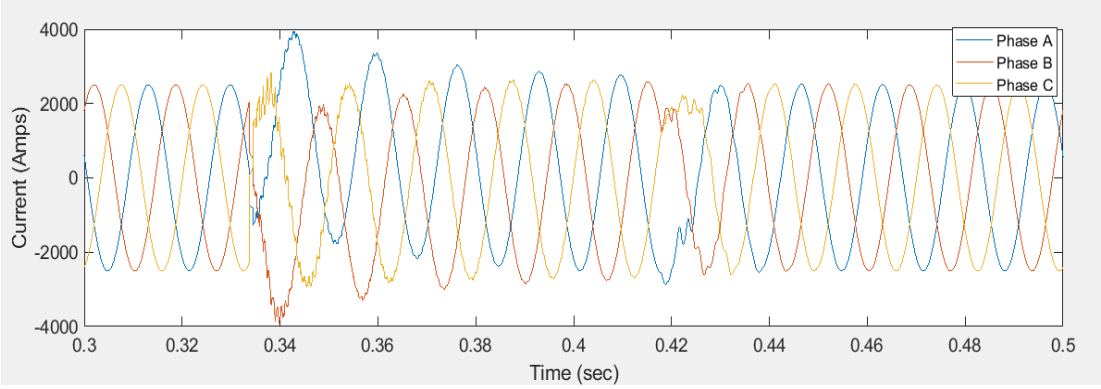

(b) Current waveform with MMC STATCOM

Figure 8.9: Voltage and current measured at SUB L for a three-phase fault on the 500 kV line between SUB L and SUB M, with MMC STATCOM

Figure 8.10 shows real and reactive power waveforms of the high-level control, with a three-phase fault applied from 20 cycles to 25 cycles, between SUB L and SUB M, with the MMC STATCOM. Notice that during the fault, the STATCOM does exchance real power with the system through the dc link capacitor, but the power goes to zero after the fault is cleared other than supplying losses to the STATCOM. Also notice the reactive power behavior at the onset of the fault and at the time the fault is removed. The STATCOM is controlled to supply a fixed reactive power, so it does not try to increase reactive power to support voltage during the fault.

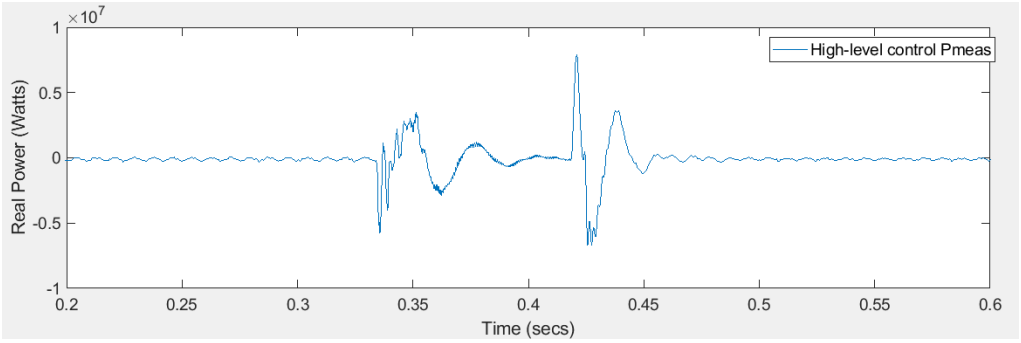

(a) Real power waveform with MMC STATCOM

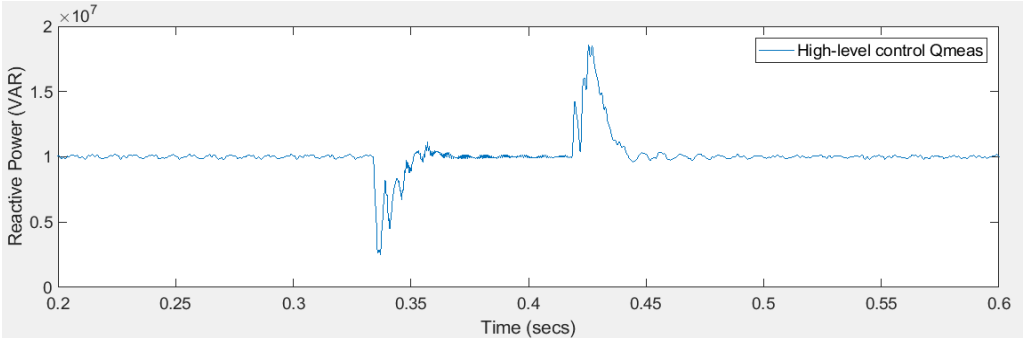

(b) Reactive power waveform with MMC STATCOM

Figure 8.10: High-level control real and reactive power with three-phase fault, with MMC STATCOM

Case 3: System with E-STATCOM/BE3SC

In Case 3, the enhanced STATCOM with hybrid energy storage system is connected to the 500 kV system at SUB G. Recovery from the three-phase fault is similar to Cases 1 and 2 as seen in Figure 8.11, because the enhanced STATCOM is controlled to maintain constant reactive power in Matlab/Simulink.

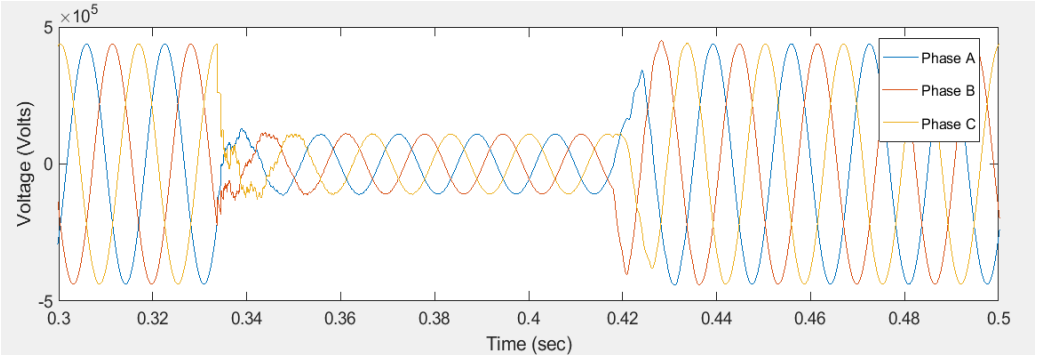

(a) Voltage waveform with E-STATCOM/BE3SC

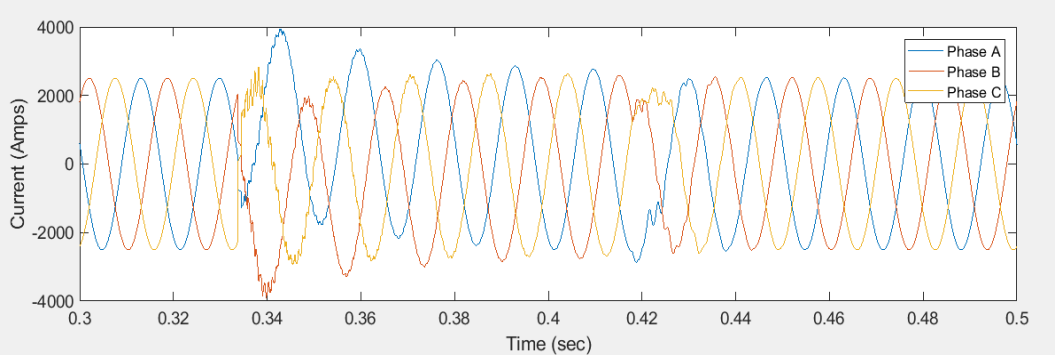

(b) Current waveform with E-STATCOM/BE3SC

Figure 8.11: Voltage and current measured at SUB L for a three-phase fault on the 500 kV line between SUB L and SUB M, with E-STATCOM/BES3SC

Figure 8.12 shows real and reactive power waveforms of the high-level control, with a three-phase fault applied from 20 cycles to 25 cycles, between SUB L and SUB M, with E-STATCOM/BE3SC. The real and reactive power is the same as in Case 2 due to the control settings used.

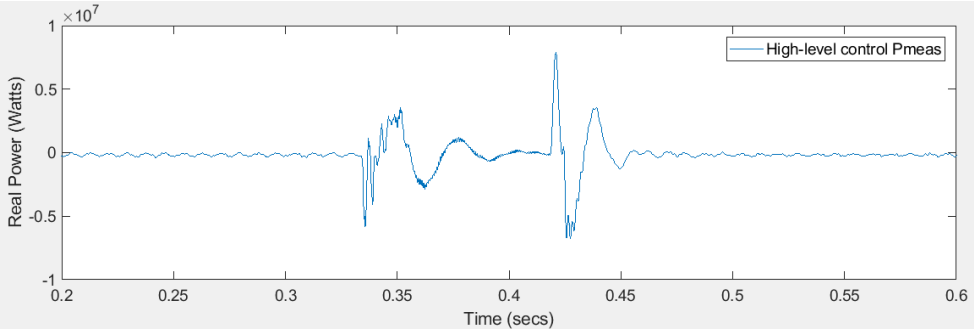

(a) Real power waveform with E-STATCOM/BE3SC

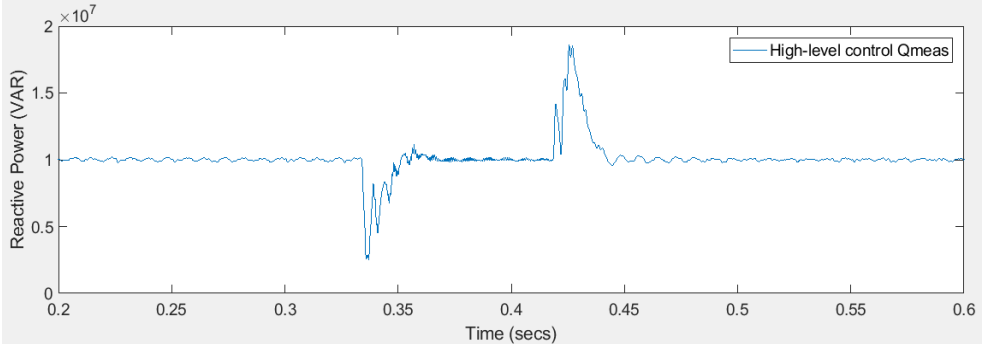

(b) Reactive power waveform with E-STATCOM/BE3SC

Figure 8.12: High-level control real and reactive power with three-phase fault, with E-STATCOM/BE3SC

8.6 Control of Hybrid Energy Storage System Charge/Discharge Operations

As discussed in Chapters 6 and 7, bidirectional dc-dc converters are utilized to allow both directional power flow to charge and discharge the energy storage system. During certain abnormal conditions, total power generation less than the load demand will result in low system frequency. Similarly, total generation more than load demand will result in high system frequency. A frequency that is not within the acceptable range between 59.8 Hz and 60.2 Hz may result in system instability and possible outages. System operations would normally respond with generator runback if the frequency is too high or load shedding when the frequency is too low.

To avoid the need for load shedding or generation tripping and reduce the potential for system instability, the bidirectional dc-dc converters are controlled to facilitate power exchange between the ESS and the grid. The following subsections cover the power controls for the charge and discharge operations.

8.6.1 Control of charge/discharge operations when no power transfer is required

During steady state conditions, when power generation and load demand balance each other, power exchange between the grid and ESS is not required. In this case, $P_{command}$= 0 (P_{zero}). However, the battery and supercapacitor can exchange power to ensure that the initial SOC on each is at a level appropriate to respond to the next disturbance. Figures 8.13, 8.14, and 8.15 show the SOC, current, and voltage waveforms, respectively, in a case where the battery SOC is too high and it is discharging to charge the supercapacitor. The battery SOC decreases from 50% to roughly 49.8% in 1 second as seen in Figure 8.13. During this time, the discharge current for the equivalent battery representing all of the submodule

banks increases from 0 A to roughly 20 kA as seen in Figure 8.14 and the battery voltage decreases from roughly 520 kV to 420 kV in 1 second as seen in Figure 8.10c. The battery is rated at 2500 Ah and the supercapacitor is rated at 10,000 F, per phase Figure 8.11 shows a plot of the supercapacitor SOC in charge mode and Figure 8.12 shows a plot of $P_{command}$= 0.

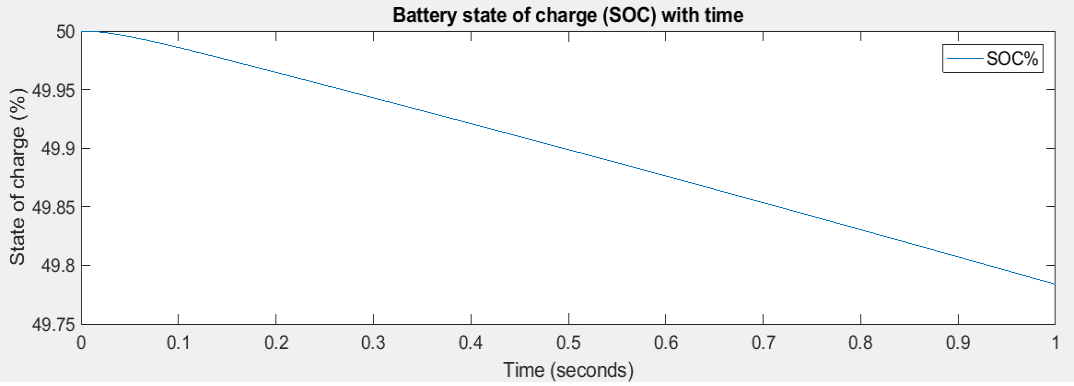

Figure 8.13: Battery state of charge providing charge balance between battery and supercapacitor

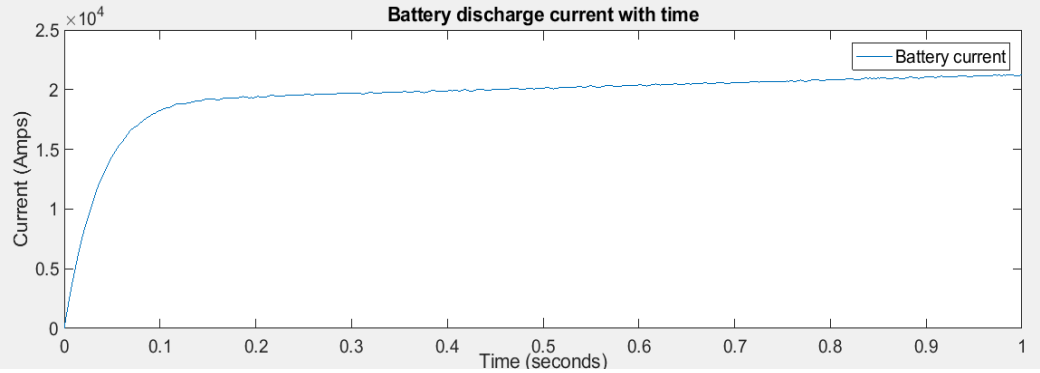

Figure 8.14: Battery discharge current providing charge balance between battery and supercapacitor

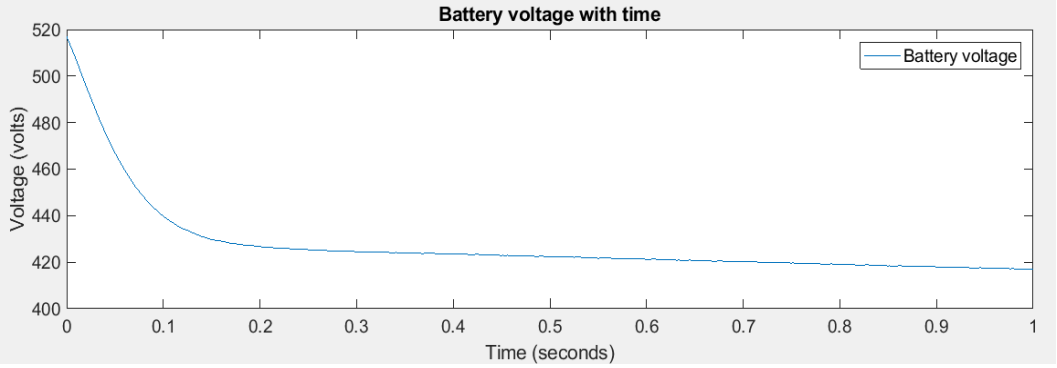

Figure 8.15: Battery voltage providing charge balance between battery and supercapacitor

As the battery initially discharges from SOC of 50%, the energy is used to charge the supercapacitor. Figure 8.16 shows the corresponding supercapacitor SOC increasing from 0%.

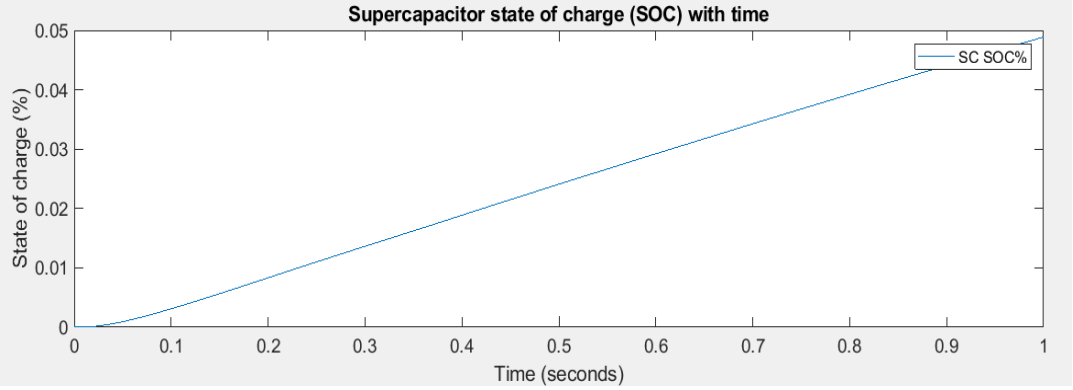

Figure 8.16: Supercapacitor state of charge providing charge balance between battery and supercapacitor

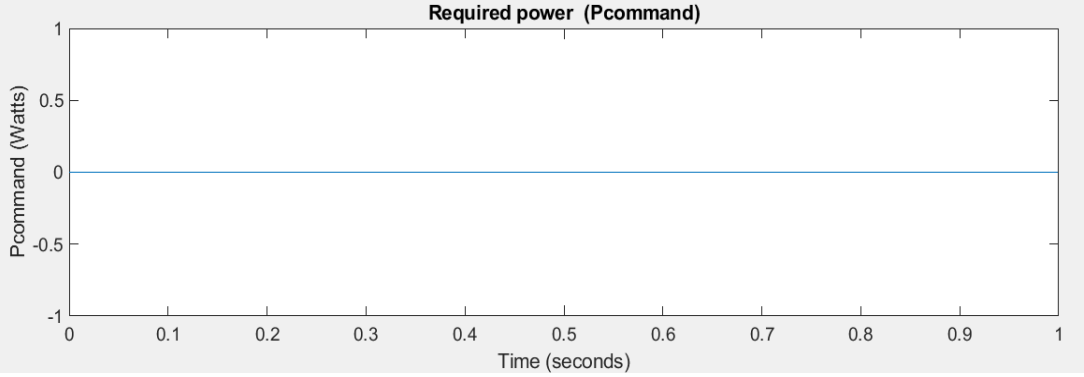

Figure 8.17: AC power command = 0

8.6.2 Control of charge/discharge operations at $P_{command} \neq 0$

During an abnormal condition on the grid, when the measured system frequency is less than the minimum acceptable frequency, the bidirectional dc-dc converter controls the hybrid energy storage system to transfer power to the grid to keep the restore the system frequency. To achieve this, the $P_{command}$ generates a current command, $I_{command}$, which is processed via a PI controller as discussed in Chapter 6. In this simulation, the $P_{command}$ is set at a maximum value of 900 kW for both the battery and the supercapacitor so both discharge power into the grid to mitigate the low frequency issue. While the battery is discharging, as shown in the state of charge in Figure 8.13, the supercapacitor is also discharging as shown in Figure 8.18. Note that the supercapacitor discharge current is initially high, and then decreases as the battery current increases as shown in Figure 8.19. This initial peak of the current waveform is due to initial transients.

In this simulation, notice that the discharge current of the battery is roughly 8 times more than the discharge current of the supercapacitor. Figure 8.14 shows that the discharge current of the battery is roughly 20 kA while Figure 8.19 shows that the discharge current of the supercapacitor is roughly 2.5 kA and Figure 8.20 shows the supercapacitor voltage is roughly 237 kV when discharging to the grid.

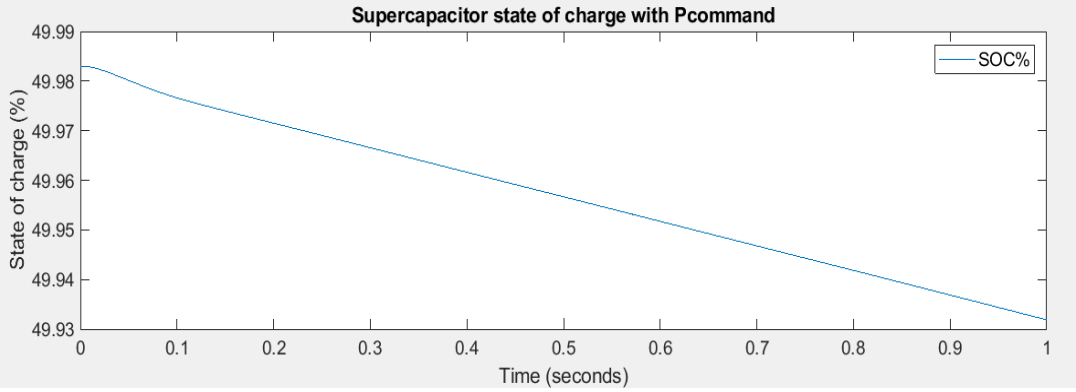

Figure 8.18: Supercapacitor state of charge discharging to the grid

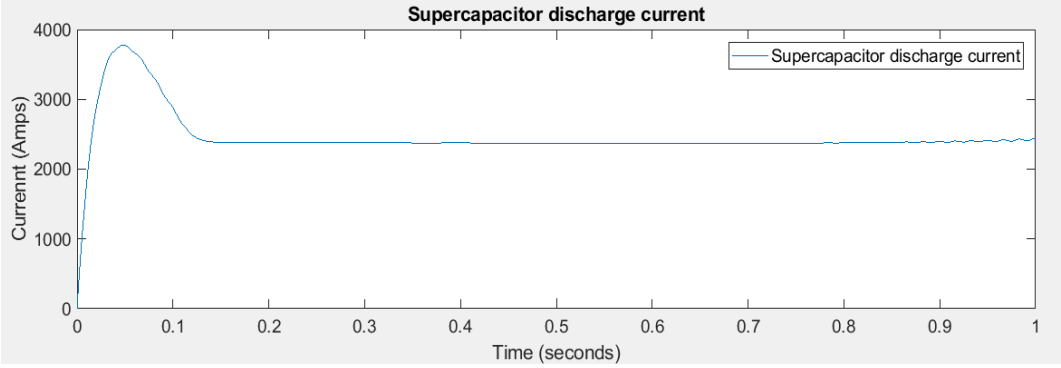

Figure 8.19: Supercapacitor current when discharging to the grid

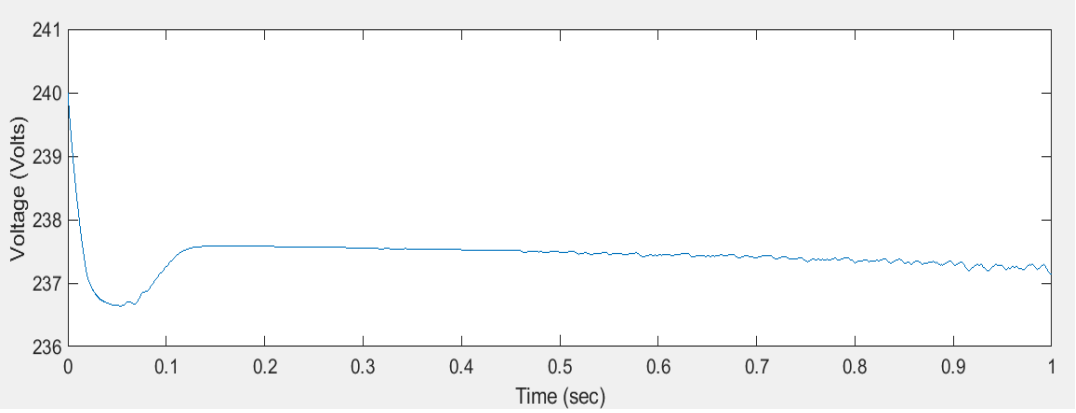

Figure 8.20: Supercapacitor voltage when discharging to the grid

8.7 System Voltage Magnitude Response to Changes in Solar Generation Output

The response of the grid system is analyzed with total generation of 3,170 MW installed and with reduced system generation; predominantly 1,259 MW solar generation dropped at

SUB G of the system shown in Figure 7.1, Figure 8.21 shows waveforms with all generation installed in the system. Notice that the initial RMS voltage at the 500 kV bus is roughly 532 kV (1.06 pu). This is the required scheduled voltage of the bus.

Also, voltage drops are experienced due to reduced generation. This causes a voltage drop as low as13% (from 532 kV to 463 kV as will be discussed in Section 8.9, and it is a voltage violation based on the North American Electric Reliability Cooperation (NERC) reliability standards. If this reduced generation occurs during routine system maintenance when some equipment is out of service, the system frequency may drop below the minimum setpoint of 59.8 Hz, resulting in stability issues.

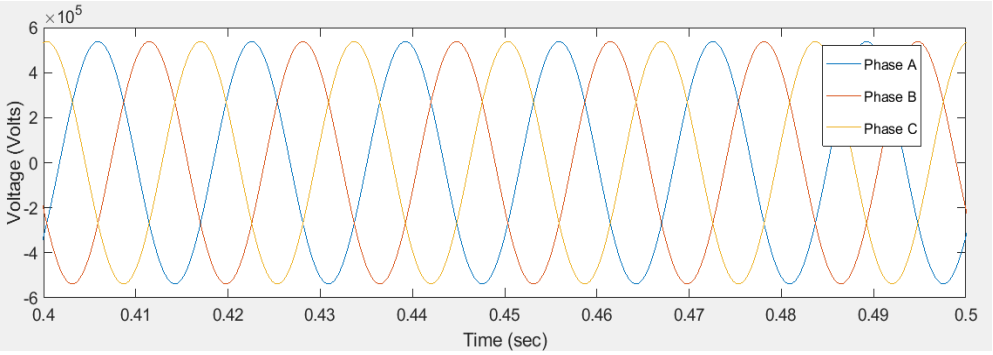

Figure 8.21: RMS voltage response for all generation (3,170MW) with E-STATCOM/BE3SC

8.8 System Frequency Response to Changes in Solar Generation Output

Figure 8.22 shows system frequency drops with reduced generation at SUB G during outage of the line between SUB L and SUB M. Notice that the frequency at SUB G initially drops from 60 Hz to 59.845 Hz and the synchronous generators try to regain stability by increasing speed to increase the system frequency to 59.965 Hz. Figure 8.23 shows frequency fluctuations at SUBS L, G, M and D. Notice that the lowest frequency of 59.800 Hz is experienced at SUB L due to the highest load-generation imbalance experienced at the substation. If additional PV was reduced from the system or an outage of a critical

equipment were to occur during this time, this could result in system instability and system operators may need to shed load to avoid local blackout.

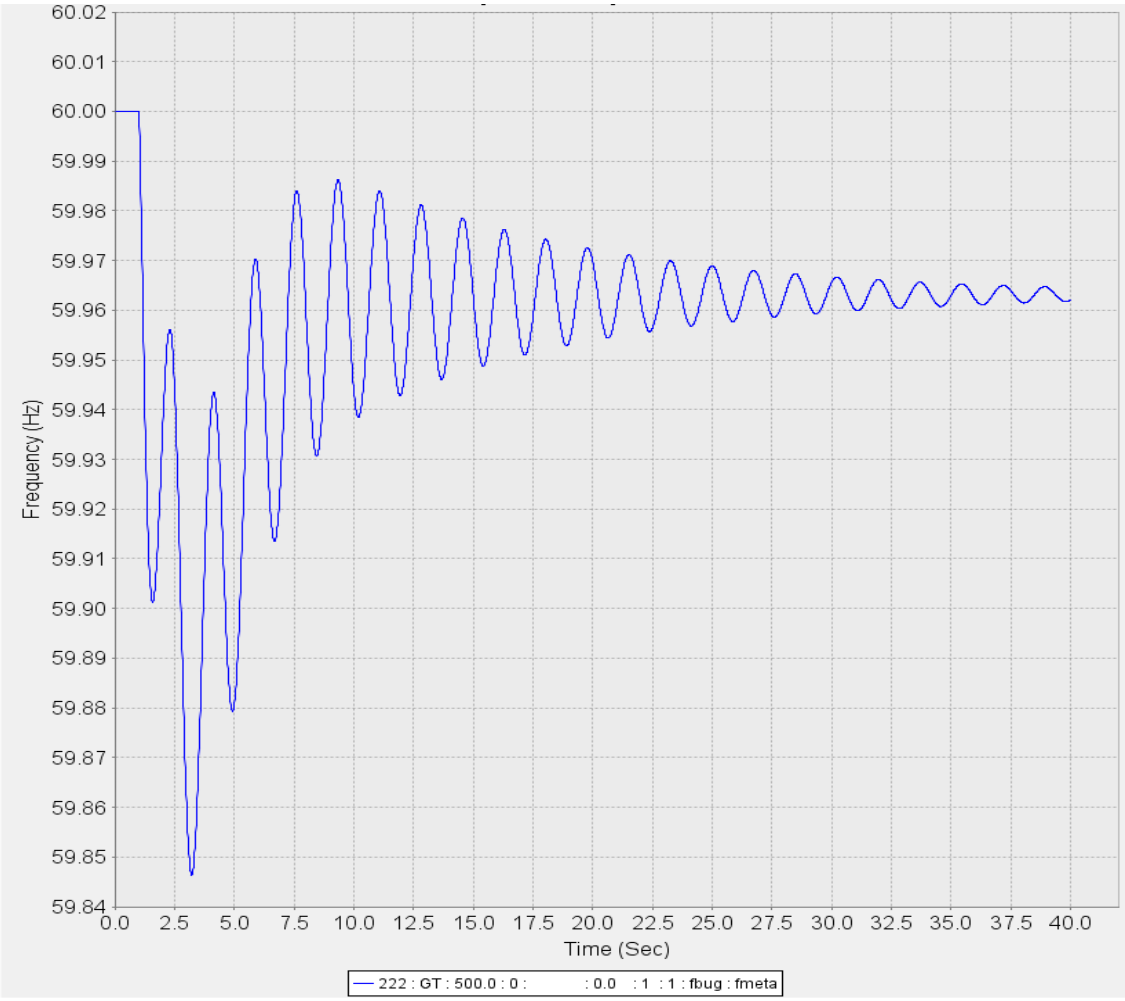

Figure 8.22: Low frequency variations at SUB G, for reduced PV at SUB G, without compensation

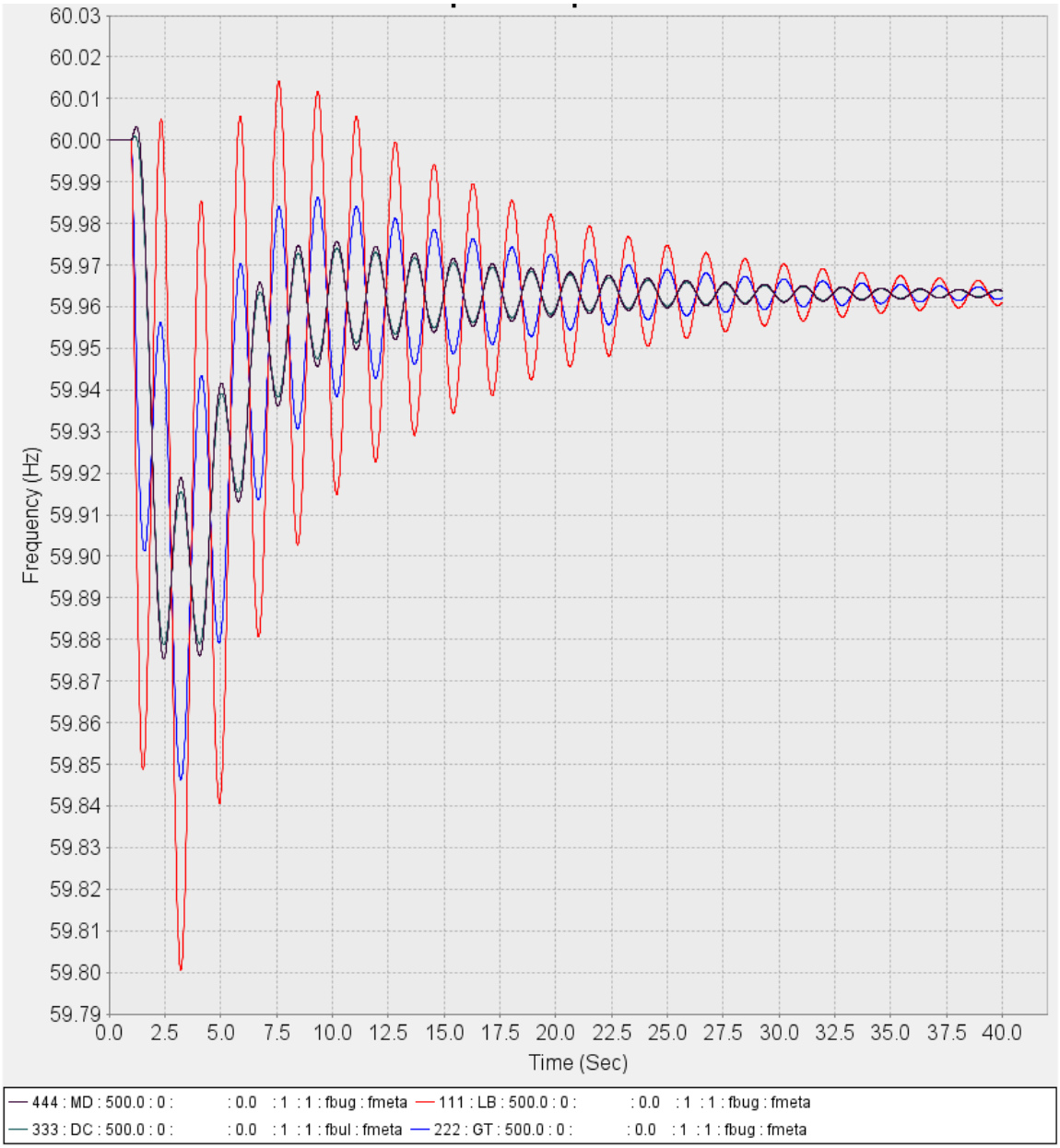

Figure 8.23: Low frequency variations at SUBS L, G, D, and M
for reduced PV at SUB G, without compensation

To increase the system frequency, the E-STATCOM is connected at SUB G. Figure 8.24 shows that the frequency measured at SUB G for reduced PV barely drops below 60 Hz with the enhanced STATCOM connected at SUB G, with a minimum frequency of 59.9917 Hz. This mitigates the risk of possible load shedding due to the next outage. The E-STATCOM injects roughly 340 MVAR, 8 MW power into the system to improve the

system stability. Figure 8.25 shows the waveform of the frequency at SUB G when all the generation and the system is restored in its normal configuration. Notice that the frequency is at 60 Hz and this is the desired frequency.

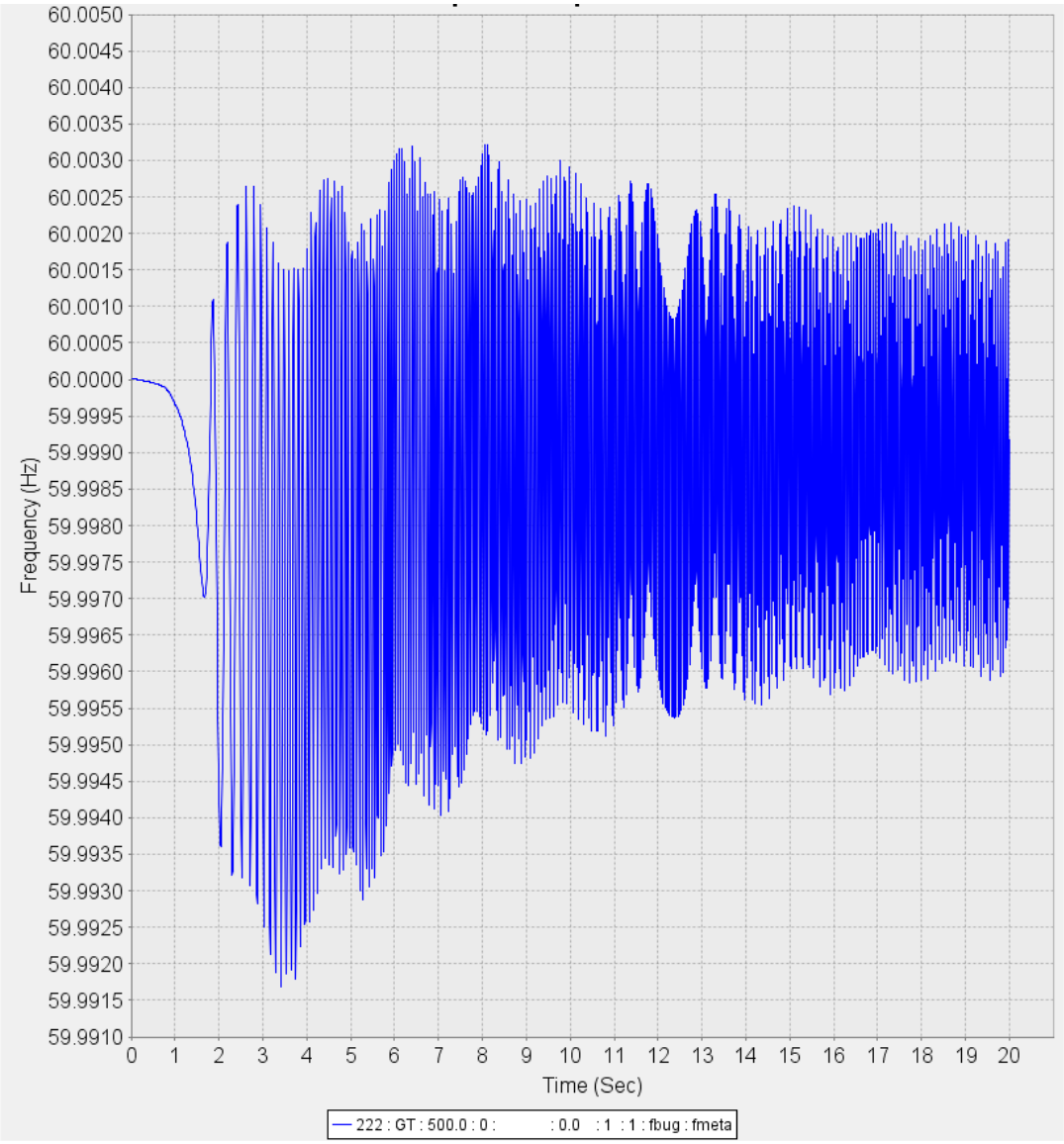

Figure 8.24: Frequency increase at SUB G with reduced PV,
when E-STATCOM/BE3SC is connected

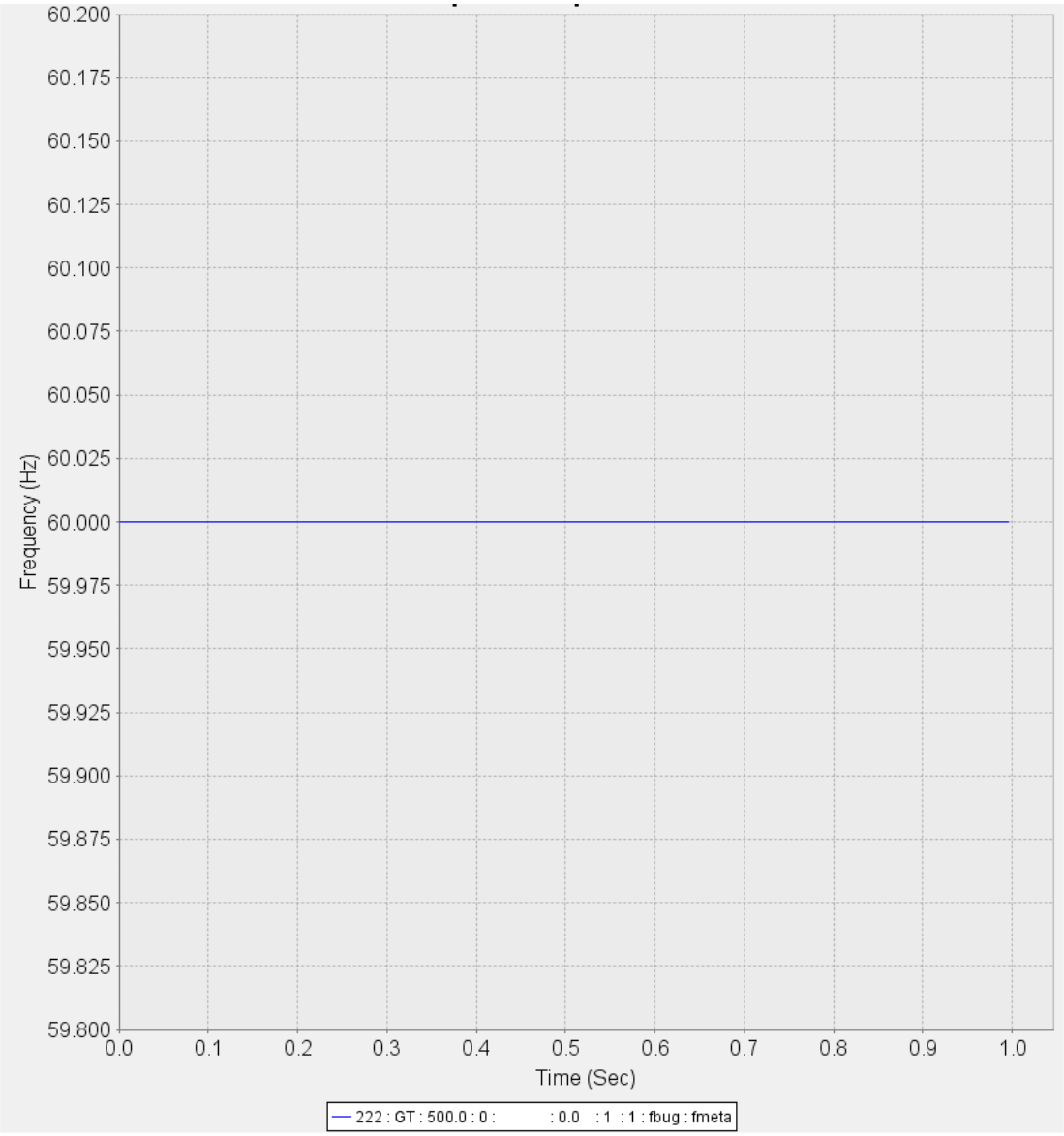

Figure 8.25: System frequency response for full generation restored at SUB G

8.9 E-STATCOM/BE3SC connected to mitigate high voltages

As mentioned in Chapter 7, the 500 kV system under studies experiences both high and low voltage issues under certain operating conditions. The high voltages are due to high solar penetration in the area at buses G and L and the low voltages are due to certain outages. The PSLF schematic in Figure 8.26 show high steady-state voltages on the system without the enhanced STATCOM, and Figure 8.27 shows the regulated case. The orange

color at the buses signifies high voltages above 500 kV and the red color signifies low voltages below 500 kV. For this 500 kV system, nominal voltages between 525 kV and 540 kV are acceptable to ensure that the underlying 230 kV system has adequate voltage levels. Notice that the high voltage on BUS G is of greatest concern due to high PV generation and as a result, this is where the enhanced STATCOM is installed.

The power flow results in Figure 8.26 show that the highest voltage in the system is at SUB G (roughly 554 kV and angle 6.86 leading). This voltage is above the acceptable limit under normal operating conditions. This location is chosen to install the enhanced STATCOM because it has the highest voltage issues due to high PV generation; it is around the midpoint of the area of interest, and it has space to accommodate the enhanced STATCOM device.

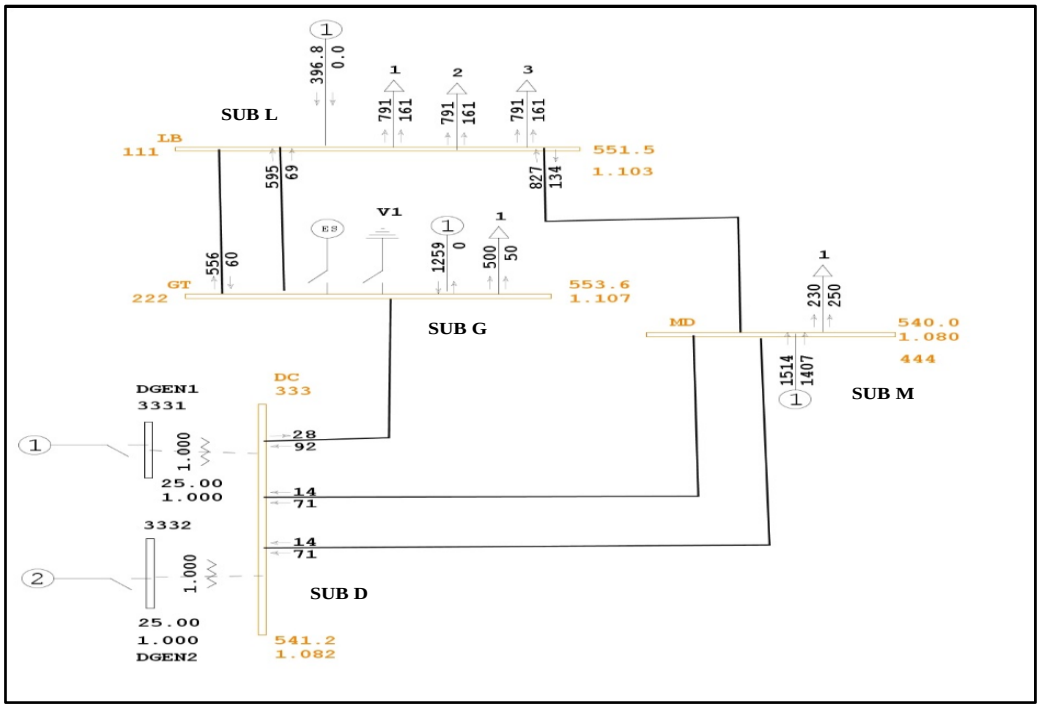

Figure 8.26: High voltages without E-STATCOM/BE3SC

Figure 8.27 shows power flow results with the enhanced STATCOM connected at SUB G. The rating of the device is +/- 600 MVAR, 8.4 MWh. As seen in the plot, the E-STATCOM/BE3SC designated (V1) is absorbing roughly 531 MVAR , 8 MW from the system to reduce the bus voltage from 554 kV to 526 kV; a 5% voltage reduction. The voltage levels in the rest of the system are within an acceptable normal operating range of between 525 kV and 540 kV.

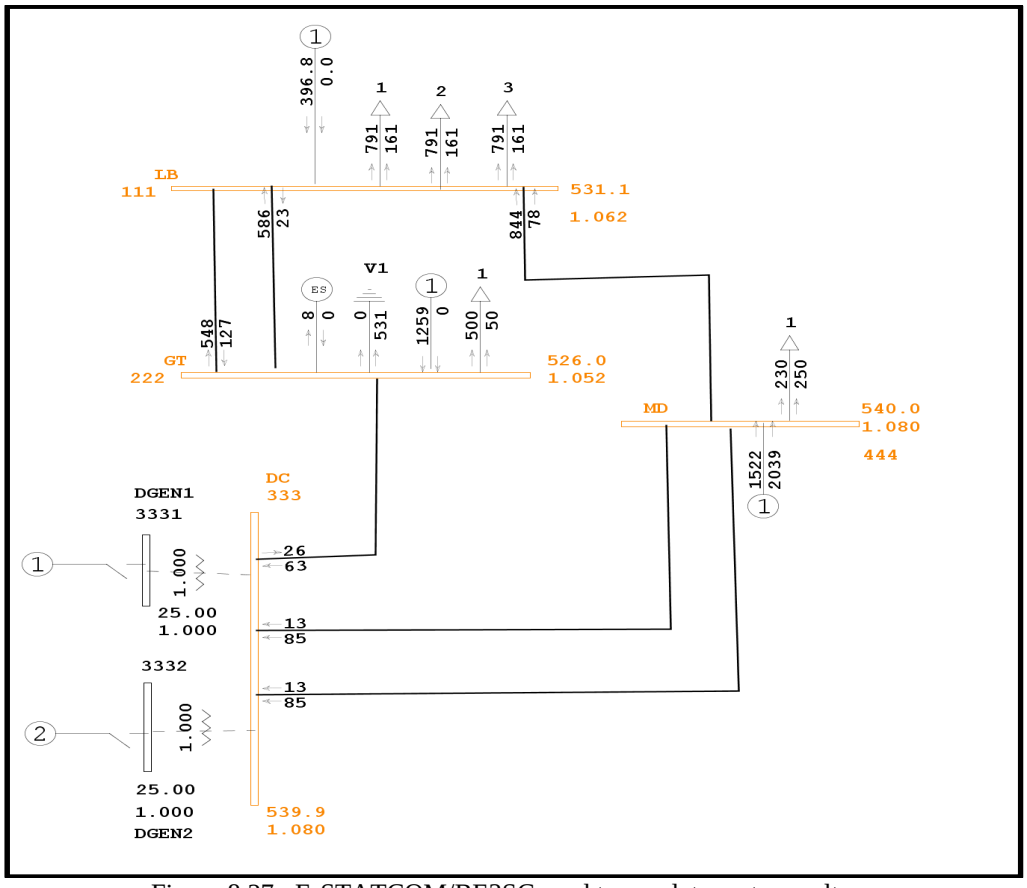

Figure 8.27: E-STATCOM/BE3SC used to regulate system voltage

8.10 E-STATCOM/BE3SC used to mitigate low frequency issues due to Loss of PV

In a partly cloudy day, if solar generation is suddenly reduced in the area (by roughly 1.26 GW) while the transmission line between SUB L and SUB M is out of service for maintenance, this will result in low voltages at SUB L (462 kV or 0.93 pu) and SUB G (479

kV or 0.96 pu), and a low frequency on the system. The enhanced STATCOM connected at SUB G injects real and reactive power into the grid to increase the system frequency and increase the system voltage respectively.

As described in Section 6.4.1, the $P_{command}$ is the required power command to keep the grid within an acceptable frequency range, between 59.8 Hz and 60.2 Hz. To generate the $P_{command}$, the controller senses the grid voltage, V_{grid} and grid current, I_{grid} and multiplies the components. The resulting grid power, P_{grid} which is equivalent to the grid power or generation capability, is compared with the grid load, Ld_{grid}. In this case, P_{grid} is less than Ld_{grid}. The $P_{command}$ of 8 MW is generated to discharge the ESS into the grid to increase grid frequency. The enhanced STATCOM will also need to inject 365 MVAR into the system to raise the voltage. This will eliminate the need to shed customer load. Figure 8.28 shows power flow results for the system without the enhanced STATCOM, and Figure 8.29 shows power flow results for the system with the enhanced STATCOM connected at SUB G.

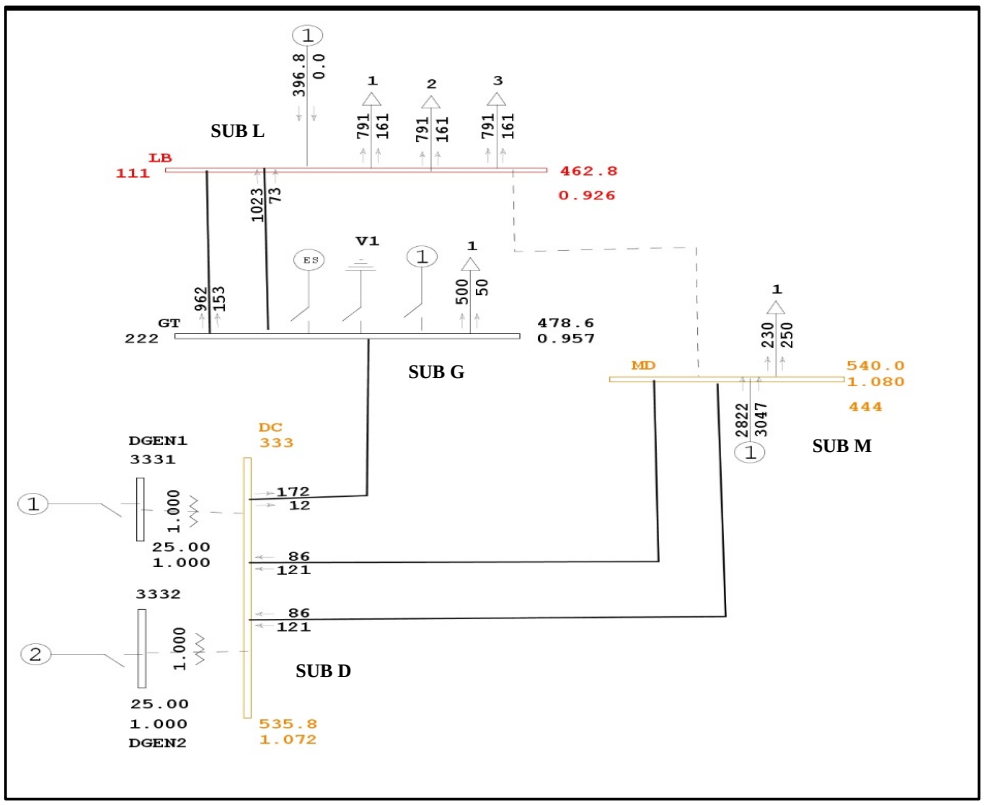

Figure 8.28: Low voltages at SUB G and SUB L due to reduced PV generation at SUB G without compensation

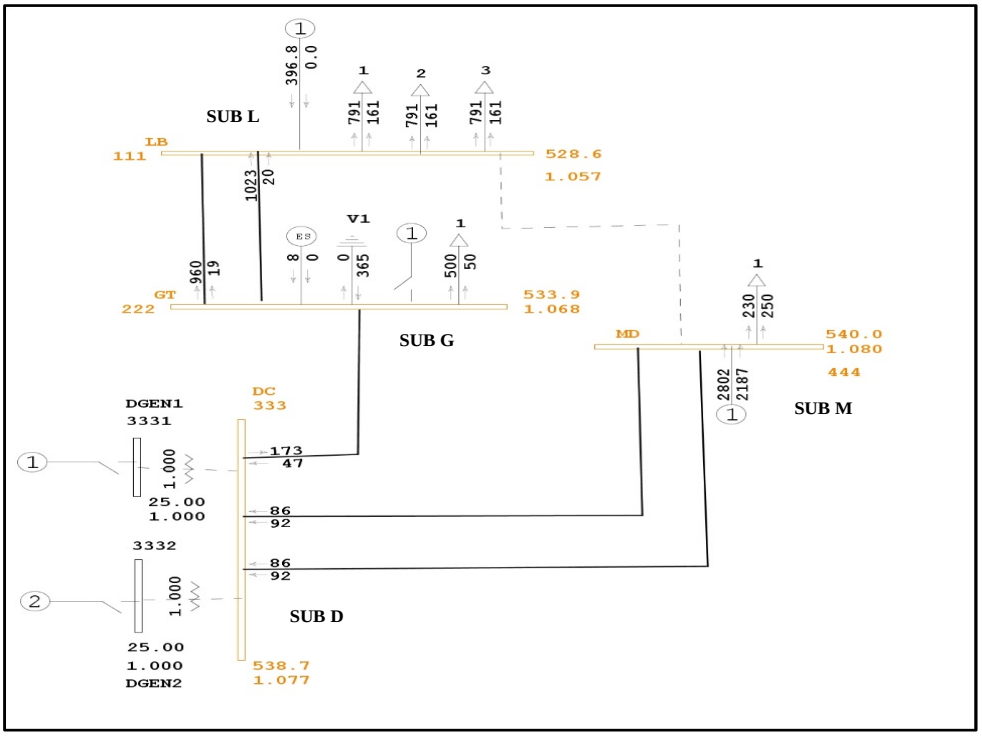

Figure 8.29: E-STATCOM/BE3SC installed at SUB G to mitigate low voltages

8.11 Summary of Simulation Results

Table 8.1 summarizes the PSLF voltages of the 500 kV system without compensation, with MMC STATCOM and with E-STATCOM/BE3SC connected to the system. Notice that the enhanced STATCOM shows better results during both low voltage and high voltage than either the case with the MMC STATCOM or for the system without compensation. Due to the small size of ESS used in this simulation, the frequency performance for the enhanced STATCOM and MMC STATCOM do not show a significant difference. If the energy capacity of the ESS were to be increased to a magnitude of hundreds of megawatts-hours, there would be significant difference in frequency performance between the two STATCOMs.

Table 8.1: Bus voltages comparison without compensation, with MMC STATCOM and with E-STATCOM/BE3SC

Contingency	Without Compensation				With MMC STATCOM				With E-STATCOM/BE3SC			
	BUS L	BUS G	BUS M	BUS D	BUS L	BUS G	BUS M	BUS D	BUS L	BUS G	BUS M	BUS D
No contingency (High voltage issue)	552 KV 1.10 pu	554 KV 1.11 pu	540 KV 1.08 pu	541 KV 1.08 pu	532 KV 1.06 pu	527 KV 1.05 pu	541 KV 1.08 pu	540 KV 1.08 pu	531 KV 1.06 pu	526 KV 1.05 pu	540 KV 1.08 pu	540 KV 1.08 pu
Outage of PV at SUB G with outage of 500 kV Line between SUB L and SUB M (low voltage issue)	462 KV 0.93 pu	479 KV 0.96 pu	540 KV 1.08 pu	536 KV 1.07 pu	528 KV 1.06 pu	533 KV 1.07 pu	540 KV 1.08 pu	538 KV 1.08 pu	529 KV 1.06 pu	534 KV 1.07 pu	540 KV 1.08 pu	539 KV 1.08 pu

Based on Table 8.1, the following can be concluded:

I) The E-STATCOM/BE3SC improves both high voltage and low voltage performances during normal system operations and during contingencies

II) The E-STATCOM/BE3SC and MMC STATCOM provide dynamic voltage compensation nearly equally well. The E-STATCOM/E3SC has the capability for both real and reactive power exchange based on the system needs.

III) A major advantage of the E-STATCOM/BE3SC over the MMC STATCOM is in frequency control.

Table 8.2 summarizes the frequency response of the system with reduced PV generation:

Table 8.2: Frequency response without compensation and with E-STATCOM/BE3SC

	Without Compensation	**E-STATCOM/BE3SC**
PV reduced and line outage	59.861 Hz - 59.750 Hz	59.991 Hz – 60.001 Hz
Risk of load shedding	High	Low
Maintenance flexibility	Low	High

Based on Table 8.2, the following can be concluded:

I) The E-STATCOM/BE3SC increases the frequency of a system to reduce the risk of load shedding during low frequency conditions.

II) The risk of load shedding is higher in a system without power compensation and lower in a system with the enhanced STATCOM connected.

III) Flexibility for performing routine maintenance is higher in a system with the enhanced STATCOM connected because the device provides capability of the system to control and regulate frequencies for the next contingency.

Table 8.3 compares the attributes of the number of the 11-submodule MMC STATCOM and the 22-submodule MMC STATCOM.

Table 8.3: Comparison of 11-submodule MMC STATCOM and 22-submodule MMC STATCOM

	11 submodules MMC	**22 submodules MMC**
Number of submodules	11	22
Voltage waveform	few steps	more steps, close to sinusoidal

From Table 8.3, the higher the number of submodules, the higher the number of steps and closer the voltage waveforms are to sinusoidal shape, reducing filtering needs or the need for pulse width modulation. This represents a trade off in capital cost versus operational costs.

Table 8.4 shows that the low-level capacitor output voltage for the enhanced STATCOM is pretty much same as that for the MMC STATCOM.

Table 8.4: Low level capacitor out voltage level for the MMC STATCOM and E-STATCOM/BE3SC

	MMC STATCOM	**E-STATCOM/BE3SC**
Low level capacitor voltage	39.5 kV	40 kV

This chapter presented simulation results when a hybrid energy storage system with MMC STATCOM provided real and reactive power compensation when connected to a 500 kV system. The enhanced STATCOM has bidirectional dc-dc converters that controlled the exchange of power between the hybrid energy storage system and the grid to control power exchange to maintain frequency stability of the grid. The simulation results show that the enhanced STATCOM has better frequency control than the system with STATCOM alone and better dynamic voltage performance and frequency control than the system without compensation.

8.12 Assumptions, Challenges and Validation

The assumptions made in the research are that the model is correct, and the actual devices operate correctly. Also, it is assumed that the devices are installed in a fenced substation, protected from external access or attack. The communication system has redundancy and has reduced failure risk.

The challenges running this system are to determine the number of submodules to connect the HESS to, in order not to cause unacceptable levels of harmonic distortion. This is a good topic for future research. Another challenge is balancing voltages when sharing series connection of batteries and supercapacitors. In this research, perfect sharing among the series connected batteries and supercapacitors is assumed.

The E-STATCOM/BE3SC can be validated in the field by using regular STATCOM response first and comparing with the E-STATCOM/BE3SC response. To validate regular STATCOM response, the HESS is removed by disconnecting the terminals of the bidirectional dc-dc converters from the dc-link capacitors of the STATCOM submodules. As discussed in the cases in Chapter 8, one approach is to reduce PV generation by disconnecting solar generation at SUB G. The system frequency and voltages are measured at various substations. To validate the E-STATCOM/BE3SC response, HESS is added by connecting the terminals of the bidirectional dc-dc converters to the dc-link capacitors of the STATCOM submodules. With the same amount of generation reduced, measure the system frequency and voltages at the substations. Notice that the system frequency and voltages are higher with the E-STATCOM/BE3SC connected. The assumption is that the frequency and voltage measurements are made under identical load demand levels and system conditions.

Chapter 9: Summary, Conclusions and Future Work

9.1 Summary

There is an increasing need for sources of dynamically controllable real and reactive power to maintain stability of electric power systems. FACTS devices such as SVCs and STATCOMs are presently used improve the stability of electric power systems by dynamically controlling reactive power supplied to the system. However, they cannot provide dynamic real power control. In this dissertation, a device capable of both dynamic real power control and reactive power control was discussed. The device consists of a modular multilevel converter-based STATCOM combined with a hybrid energy storage system that integrates a battery energy storage system with a supercapacitor energy storage system.

The STATCOM generates or absorbs reactive power by regulating ac voltage and current waveforms using a VSC. Modular multilevel converter - based VSC applications have attracted a lot of interest for high-voltage and high-power applications with reduced switching losses.

However, the STATCOM alone cannot provide dynamic real power control. In the proposed approach, battery and supercapacitor energy storage devices are utilized with the STATCOM to add dynamic real power control. The devices in the hybrid storage system are sized in order to get the acceptable quantity of output power and controlled to increase the lifetime of the battery.

Supercapacitors have benefits of large capacitance, quick charge and discharge capabilities in bursts, and high-power density. Supercapacitors can accept and deliver charge

much faster than batteries and tolerate many more charge and discharge cycles than rechargeable batteries. However, supercapacitors have poor energy density compared to batteries and are not as cost effective for bulk energy storage applications.

Batteries have benefits of high energy density and the ability to supply bulk energy over a long period of time. However, in many cases, battery life and performance is degrading with frequent fast charging and discharging operations, conditions that also tend to lower turn-around efficiency. Although batteries and supercapacitors have limitations, the hybrid energy storage system combined benefits cited in a complementary fashion for energy storage and active power injection in electric grid applications.

Matlab/Simulink was utilized to simulate the response of an electric transmission system under fault conditions and with a line outage, without compensation, with a STATCOM alone and with the enhanced STATCOM with energy storage. Simulation plots show that the system voltage magnitudes improved significantly when the hybrid energy storage system was combined with the STATCOM for power compensation. A few results for bidirectional dc-dc converter control for charging and discharging of the hybrid energy storage system were also presented. This control allowed the exchange of power between the hybrid energy storage system and the grid, thereby mitigating system stability issues during abnormal conditions. PSLF was used to perform some of the simulations that could not be performed with Matlab due to limitations of Matlab. PSLF results were consistent with Matlab outcomes.

9.2 Conclusions

This dissertation discussed the enhancement of the MMC STATCOM to improve low and high voltage issues, system stability during reduced PV generation, frequency imbalance and three-fault conditions. The dynamic performance of the power system was analyzed based on the following attributes:

- System recovery following a three-phase fault
- Charge/discharge controls of the bidirectional dc-dc converters
- Dynamic response of the system with varying Q_{ref} values
- System response with reduced solar generation output

These attributes were simulated, and the following conclusions can be drawn:

1) The steady-state waveforms improved when the enhanced STATCOM (hybrid energy storage system was combined with the STATCOM for power compensation).
2) The low-level capacitor voltage is pretty much the same for the enhanced MMC STATCOM with hybrid energy storage as with the MMC STATCOM alone.
3) These charge/discharge operations help maintain steady-state stability of the system
4) The enhanced MMC STATCOM might be a promising technique for electric utility applications. The ability to connect real power sources (such as batteries with supercapacitors) in modular multilevel submodules makes the devices versatile and suitable for many applications. The batteries and supercapacitors share benefits of high energy density and high-power density. The battery life can be significantly increased by combining them with supercapacitors and controlling the

supercapacitors to provide fast, frequent charge and discharge operations since they have higher tolerance for charge/discharge operations than batteries.

5) Incorporating real and reactive capabilities into one device provides operational flexibility, reduces possible unstable control interactions when operating multiple devices from different manufacturers at different locations
6) This design also supports incorporation of renewables and clean energy into the grid and helps meet state mandates for clean energy emission and storage.

9.3 Future Work

For researchers who will be interested in working further on this topic, the following areas could be further studied:

i) Additional research is needed to compare the performance and relative costs of connecting energy storage system across the dc link capacitor for each MMC submodule versus connecting energy storage system across the dc link capacitor of the entire series combination of MMC submodules.
ii) Future studies should look at advanced control of real and reactive power balancing during charge and discharge operations of the ESS. Controls should be designed to determine the best combination of real or reactive power needed, based on the system needs.
iii) Future studies should look at what connecting the HESS to a subset of the MMC submodules does to harmonic distortion. The studies should determine if the needed energy storage should be lumped and connected to one submodule or if it should be

spread out to each submodule of the MMC STATCOM. Determine how the harmonic distortion of the waveforms be impacted in either case.

iv) Further study is needed to evaluate the trade-off on cost/performance having more supercapacitors versus more batteries. Supercapacitors are not cheaper than batteries for an equivalent power rating or energy storage rating. Having more supercapacitors than batteries will increase cost of the design but will also improve performance of the system and improve battery life. The study should look at the benefit-to-cost ratio of the design.

v) When connecting batteries or supercapacitors in series, it can be a challenge to balance voltages when sharing them. Perfect sharing among the series connected supercapacitors or batteries in strings was assumed in this dissertation. Future work should look at the voltage balancing mechanism.

References

[1] Sajna Soman, “Facts Devices to Enhance Power System Performance,” Electrical Engineering Portal, September 28th, 2015

[2] ABB STATCOM. [Online]. Available ABB website: http://www.new.abb.com/facts/statcom

[3] M. Davies, M. Dommaschk, J. Dorn, J. Lang, D. Retzmann, D. Soerangr, “HVDC PLUS – Basics and Principle of Operation,” Technical article [online]. Available: http://www.siemens.com/energy.hvdcplus

[4] Phinit Srithorn, Control of A STATCOM with Supercapacitor Energy Storage. Ph.D, thesis, University of Nottingham, June 2009.

[5] Chang Qian, “Study on Multilevel Converters for Static Synchronous Compensators with Energy Storage,” University of Missouri-Rolla Proquest Dissertations Publishing, 2003.

[6] Arindam Chakraborty, Shravana Musunuri, Anurag Srivastava, Anil Kondabathini, “Intergrating STATCOM and Battery Energy Storage System for Power System Transient Stability: A Review and Application,” *Advances in Power Electroni*cs, vol. 2012, Article ID 676010, 12 pages, 2012.

[7] P.F. Ribiero, B.K. Johnson, M.L. Crow, A. Arsoy, and Y. Liu, “Energy Storage Systems for Advanced Power Applications,” *Proceedings of the IEEE*, Vol 89, No. 12, December 2001

[8] Zuhair Alaas, “Cascaded Converters for Integration and Management of Grid Level Energy Storage,” Dissertation submitted to the Graduate School of Wayne State University, Detroit, Michigan, 2017.

[9] Ying Cheng “StatCom /BESS using a diode-clamped multilevel Inverter,” University of Missouri - Rolla, ProQuest Dissertations Publishing, 2004. 3115160.

[10] Lirong Zhang, Yi Wang, Heming Li, Pin Sun, “Hybrid Power Control of Cascaded STATCOM/BESS for Wind Farm Integration,” IECON 2013 - 39th Annual Conference of the IEEE Industrial Electronics Society. Nov. 10-13, 2013, Vienna, Austria.

[11] Tanneeru Renuka, Gattu Kesavarao, “STATCOM with Battery and Super Capacitor Hybrid Energy Storage System for Enhancement of Voltage Stability,” Indonesian Journal of Electrical Engineering and Computer Science, Vol. 5, No. 2, February 2017, pp 250-259.

[12] Umesh Kumar, Bharat Modi, "Simulation and Analysis of Various Configurations of MMC for New Generation STATCOM," 8th ICCCNT 2017, July 3-5, 2017, Delhi, India.

[13] M. Pereira, D. Retzmann, J. Lottes, M. Wiessinger, G. Wong, "SVC PLUS: A MMC STATCOM for Network and Grid Access Applications," 2011 IEEE Trondheim PowerTech.

[14] M. Noroozian, N Petersson, B. Thorvaldson, Bo A. Nilsson, C.W Taylor, "Benefits of SVC and STATCOM for Electric Utility Application," ABB Utilities, FACTS Division S-721 64 Västerås, Sweden, Carson Taylor Seminars Portland, Oregon USA

[15] A. E. Hammad, "Comparing the Voltage Control Capabilities of Present and Future Var Compensating Techniques in Transmission Systems," IEEE Transaction on Power Delivery, Vol. 11, No. 1, January 1996.

[16] E. Larsen, et al., "Benefits of GTO-Based Compensation Systems for Electric Utility Applications," IEEE Transaction on Power Delivery, Vol. 7, No. 4, pages 2056–2064, Oct. 1992.

[17] Anjan K. Deb, " Power Line Ampacity System," CRC Press. pp. 169–171. ISBN 978-0-8493-1306-6.

[18] N. Mithulananthan, C. A. Cañizares and J. Reeve, "Comparison of PSS, SVC and STATCOM controllers for damping power system oscillation," IEEE Trans. Power Syst., 18 (2003), 786–792.

[19] Sode-Yome, A & Nadarajah, Mithulananthan, "Comparison of shunt capacitor, SVC and STATCOM in static voltage stability margin enhancement," International Journal of Electrical Engineering Education. 41. 10.7227/IJEEE.41.2.7, 2004

[20] Siemens AG, Energy Sector, Power Transmission Division, Power Transmission Solutions, Freyeslebenstrasse 1 91058 Erlangen, Germany Siemens, Order No. E50001-G610-A108-V2-4A00, Published by and copyright © 2011. https://www.energy.siemens.com/mx/en/power-transmission/facts/static-var-compensator-plus/#content=Benefits

[21] Siemens AG 2016, Energy Management Division, Freyeslebenstrasse 1 91058 Erlangen, Article No. EMTS-B10018-00-7600, Printed in Germany, Dispo 30003 TH 263-160391 BR 1116

[22] Flexible AC Transmission Systems - EE6004, Electrical Engineering, Copyright © 2018-2020 BrainKart.com; All Rights Reserved. Developed by Therithal info, Chennai.
https://www.brainkart.com/article/V-I-Characteristics-of-STATCOM_11681/
https://www.brainkart.com/subject/Flexible-AC-Transmission-Systems_183/

[23] N. G. Hingoranl and L. Gyugyi, “Understanding FACTS: Concepts and Technology of Flexible AC Transmission Systems,” IEEE Press and Wiley Interscience, 2000.

[24] Abosalah El Mehdi, “Dynamic Reactive Compensation Requirements at the Rectifier End of An LCC HVDC Link Connected to a Weak AC System,” A Ph.D Dissertation Presented to the University of Idaho, Department of Electrical Engineering, August 2013.

[25] The Authoritative Dictionary of IEEE Standards Terms, Seventh Edition, IEEE Press, 2000,ISBN 0-7381-2601-2, page 588

[26] Jim Doucet, Dan Eggleston, Jeremy Shaw, Stephen J. Bitar, “DC/AC Pure Sine Wave Inverter,” NECAMSID, MQP Terms A-B-C 2006-2007

[27] Jos Arrillaga,”High Voltage Direct Current Transmission,” second edition, Institution of Electrical Engineers, ISBN 0852969414, 1998, Chapter 1, pp 1-9.

[28] O. Peake, “ The History of High Voltage Direct Current Transmission,” 3rd Australasian Engineering Heritage Conference 2009

[29] G., Asplund, K. Svensson, H. Jiang, J. Lindberg, R. Pålsson, “ DC transmission based on voltage source converters,” CIGRÉ session, Paris, 1998, paper reference 14-302.

[30] A. Lesnicar, R. Marquardt, “ An innovative modular multi-level converter topology for a wide power range,” IEEE Power Tech Conference, Bologna, Italy, June 2003.

[31] Amirnaser Yazdani, Reza Iravani, “Voltage-Sourced Converters in Power Systems” Modeling, Control and Applications, IEEE Press.

[32] Ching Han, “Power System Dynamic Voltage Management with Advanced STATCOM and Energy Storage System,” North Carolina State University, ProQuest Dissertations Publishing, 2006. 3293624.

[33] Stephane Chapman, “Electric machinery Fundamentals, ” Electrical Engineering Supersite, www.mhhe.com/engcs/electrical/chapman/fundamentals/PWM.pdf

[34] L. Angquist and L. Lindberg, “Inner Phase Angle Control of Voltage Source Converter in High Power Applications,” IEEE Power Electronics Specialists Conference PESC 91, pp. 293–298, June 1991.

[35] L. Xu, V. G. Agelidis, and E. Acha, “Development Considerations of DSP Controlled PWM VSC-Based STATCOM,” IEE Proceedings: Electric Power Application, vol. 148, no. 5, pp. 449–455, September 2001.

[36] M. C. Chandorkar, D. M. Divan, and R. Adapa, “Control of Parallel Connected Inverters in Standalone AC Supply Systems,” IEEE Transactions on Industry Applications, vol. 29, no. 1, pp. 136–143, January/February 1993.

[37] A. R. Bergen, Power System Analysis, Prentice-Hall, 1986.

[38] Shukla A., Nami A. (2015) Multilevel Converter Topologies for STATCOMs. In: Shahnia F., Rajakaruna S., Ghosh A. (eds) Static Compensators (STATCOMs) in Power Systems. Power Systems. Springer, Singapore

[39] J. Rodriguez, FZ. Peng, JS. Lai, “Multilevel inverters: a survey of topologies, controls, and applications”, IEEE Trans Ind Electron 49(4):724–738 (2002)

[40] J. Rodriguez, LG. Franquelo, JI Leon, RC Portillo, MAM Prats, MA Perez, “Multilevel inverters: an enabling technology for high-power applications. Proc IEEE 97 (11):1786–1817, (2009)

[41] H. Abu-Rub et al, “Medium-voltage multilevel converters—state of the art, challenges, and requirements in industrial applications”, IEEE Trans Indust Electron 57(8):2581–2596, (2010)

[42] S. Kouro et al,”Recent advances and industrial applications of multilevel converters”, IEEE Trans Indust Electron 57(8):2553–2580, (2010)

[43] Yang Liu “Cascaded Multilevel Inverters and its FACTS Applications”, Michigan State University, ProQuest Dissertations Publishing, 2016. 10109121

[44] Jin Wang, “Multilevel Inverters and their Application in Power System” A Dissertation Submitted to Michigan State University in partial fulfilment of the requirements for the degree of Doctor of Philosophy, 2005. Page ii.

[45] Shodhganga “Shodhganga.inflibnet.ac.in/bitstream”, Modelling and Simulation of Cascaded Multilevel Inverters – Chapter 3.

[46] www.engineering.electrical-equioment.org, “Cascaded H-bridge Multilevel Inverters” Electrical Installation and Energy Efficiency December 5th, 2013

[47] Mariaraja P., Brindha Sakthi B., Saranya A.V., Prabha Rani S.J., Sathyapriya M., “Reduction of Harmonics using Seven Level Cascaded Multilevel Inverter,” International Journal of Engineering Research & Technology (IJERT), ISSN: 2278-0181, Vol. 3 Issue 3, March - 2014

[48] Carlet Enang, Brian Johnson, “Enhanced Modular Multilevel Converter-Based STATCOM with Hybrid Energy Storage,” proceedings of the 2019 IEEE PES General Meeting. Atlanta, Georgia, August 2019.

[49] P Rao, ML Crow, Z Yang, "STATCOM control for power system voltage control applications", IEEE Transactions on power delivery. 2000; 15 (4): 1311-1317.

[50] C. Schander, H. Metha, "Vector analysis and control of the advanced static VAR compensators", Proc. Inst. Elect. Eng. Gen. Transm. Distribution. 1993; 140(4): 299-306.

[51] B Wu, F Zhuo, F Long, W Gu, Y Qing, Y Liu, " A management strategy for solar panel-battery- super capacitor hybrid energy system in solar car," Proc. IEEE 8th Int. conf. power Electron. ECCE Asia. 2011: 1682-1687.

[52] David Williams, "Understanding, Calculating, and Measuering Total Harmonic Distortion (THD)," All about circuits, February 20, 2017, https://www.allaboutcircuits.com/technical-articles/the-importance-of-total-harmonic-distortion/

[53] H. Babazadeh, W. Gao, J. Lin,L. Cheng, "Sizing of Battery and Supercapacitor in a Hybrid Energy Storage System for Wind Turbines," 2012 IEEE Transmission and Distribution Conference and Exposition. May 7-12, 2012, Orlando, FL.

[54] Huilong Yu, Federico Cheli, Francesco Castelli-Dezza, Dongpu Cao, Fei-Yue Wang,'Multi-Objective Optimal Sizing and Energy Management of hybrid Energy Storage System for Electric Vehicles," IEEE 2018

[55] M. R Moharaj, R. Gunasekaran,C. Kanmani, R. Santhiya, D. Kubendhiran, " Battery and Super Capacitor for Photovoltaic Energy Storage: a Fuzzy Logic Management," College of Technology Komarapalayam.

[56] Ming Pang, Yikai Shi,Wendong Wang, Shun Pang," Optimal Sizing amd Control of Hybrid Energy Strrage System for Wind Power Using hybrid Parallel PSO-GA Algorithm," Northwestern Polytechnical University, Thermal Power Research Institute Co., Ltd China, Energy Exploration Exploitation, 2018.

[57] https://mpoweruk.com/performance.htm, "Battery and Energy technology," Electropaedia

[58] Dorin PETREUS, Daniel MOGA, Ramona GALATUS, Radu A. MUNTEANU," Modeling and Sizing of Supercapacitors," Technical University of Cluj Napoca str. C. Daicoviciu nr. 15, RO-400020 Cluj-Napoca

[59] Conway B. E., Electrochemical Supercapacitors: Scientific Fundamentals and Technological Applications (Kluwer Academic/Plenum, New York, 1999).

[60] A Power-Cap press release, 2006 http://www.apowercap.com, Accessed Aug 2011.

[61] T.R. Crompton," Battery Reference Book," ISBN 978-0-08-049995-6, third edition, Glossary 3, Retrieved 18 March 2016.

[62] J. McDowall, "Conventional battery technologies—Present and future," in Proc. 2000 IEEE Power Engineering Society Summer Meeting, vol. 3, July 2000, pp. 1538–1540.

[63] Immanuel N. Jiya, Nicoloy Gurusinghe, Rupert Gouws, "Electrical Circuit Modelling of Double Layer Capacitors for Power Electronics and Energy Storage Applications: A Review," School of Electrical, Electronic and Computer Engineering, North-West University South Africa, Faculty of Engineering and Physical Sciences, Queen's University Belfast, Electronics MDPI 2018

[64] C. Enang, "Energy Storage Hybridization for Enhanced Battery Life Span," submitted to the 2020 IEEE PES General Meeting, Montreal, Canada

[65] R.A. Dougal, L. Gao, S. Liu, "Ultracapacitor model with automatic order selection and capacity scaling for dynamic system simulation," Journal of Power Sources; 126 (2004) p. 250–257.

[66] J.R. Pillai, B. Bak-Jensen; "Integration of Vehicle-to-Grid in the Western Danish Power system," IEEE Transactions on Sustainable Energy Conversion, Vol. 2, NO. 1, January 2011, p. 12-19.

[67] Pierre Clement Blaud, L.-A. Dessaint, " Supercapacitor Model," MATLAB Example parallel_battery_SC_boost_Converter, Ecole de technologie superieure, Montreal

[68] Xconomy, Technology in Exponential Economy; http://www.xconomy.com/boston/2007/08/10/a123-inks-deal-todevelop-battery-cells-for-gm-electric-car/, Accessed Aug 2011.

[69] S. K. Kim and E. S. Kim, "PSCAD/EMTDC-Based Modeling and Analysis of a Gearless Variable Speed Wind Turbine," IEEE Transactions on Energy Conversion, Vol. 22, NO. 2, June 2007, p. 421-430.

[70] https://electricalfundablog.com/supercapacitor-ultracapacitor-characteristics-working, "Electrical Fundablog-Electrial & Electronics Engineering group for Engineers."

[71] Ilovegm in Technology, "How to Calculate Charging Time & Energy of Your Supercapacitor," Electronics, Instructables. https://www.instructables.com

[72] P. A. Topan, M. N. Ramadan, G. Fathoni, A. I. Cahyadi and O. Wahyunggoro, "State of Charge (SOC) and State of Health (SOH) estimation on lithium polymer battery via Kalman filter," 2016 2nd International Conference on Science and Technology-Computer (ICST), Yogyakarta, 2016, pp. 93-96.doi: 10.1109/ICSTC.2016.7877354

[73] X. Hu, S. Li, and H. Peng, “A comparative study of equivalent circuit models for Li-ion batteries,” Journal of Power Sources, vol. 198, pp. 359–367, 2012.

[74] O. Tremblay, L.-A. Dessaint, A.-I. Dekkiche, “A Generic Battery Model for the Dynamic Simulation of Hybrid Electric Vehicles,” 2007 IEEE® Vehicle Power and Propulsion Conference, September 9-13, 2007, Arlington/Texas, USA.

[75] N. Omar, M. A. Monem, Y. Firouz, J. Salminen, J. Smekens, O. Hegazy, H. Gaulous, G. Mulder, P Van den Bossche, T. Coosemans, J. Van Mierlo, “Lithium iron phosphate based battery - Assessment of the aging parameters and development of cycle life model,” Applied Energy, Volume 113, January 2014, Pages 1575-1585.

[76] J. Remmlinger, M. Buchholz, M. Meiler, P. Bernreuter, and K. Dietmayer, “State-of-health monitoring of lithium-ion batteries in electric vehicles by on-board internal resistance estimation,” Journal of Power Sources, vol. 196, no. 12, pp. 5357–5363, Jun. 2011.

[77] C. Enang, B. Johnson, “Bidirectional dc-dc Converter Control in Battery-Supercapacitor Hybrid Energy Storage System,” accepted to the 2020 IEEE PES General Meeting, Washington, DC, February 2020.

[78] A. Yu, Z. Chen, R. Maric, L. Zhang, J. Zhang, J. Yan, "Electrochemical Supercapacitors for Energy Storage and Delivery: Advanced Materials, Technologies and Applications," Applied Energy, Vol 153, 2015.

[79] B. Maher, “Ultracapacitors and the Hybrid Electric Vehicle,” Maxwell Technologies, 2001.

[80] E. Cegnar, H. Hess, B. Johnson, “A Purely Ultracapacitor Energy Storage System for Hybrid Electric Vehicles Utilizing a Microcontroller-based DC-DC Boost Converter,” 19th Annual IEEE Applied Power Electronics Conference and Exposition (APEC ’04). Volume 2, February 2004, pp 1160-1164.

[81] C. Enang, B. Johnson, “Enhanced Modular Multilevel Converter Based STATCOM with Hybrid Energy Storage,” Proceedings of the 2019 IEEE PES General Meeting. Atlanta, Georgia, August 2019.

[82] M. Ashar, “Integration of Ultra Capacitor with Battery using DC-DC Bidirectional Buck Boost Converter in an Electric Vehicle,” International Research Journal of Engineering and Technology, Volume:03, Issue: 02, Feb 2016, pp. 1513-1517.

[83] L. Xu, X. Ruan, C. Mao, B. Zhang, Y. Luo, “An Improved Optimal Sizing Method for Wind-Solar-Battery Hybrid Power System,” IEEE Transactions on Sustainable Energy. Vol. 4, No. 3, July 2013, pp. 774-785.

[84] A. Burke, “Batteries and Ultracapacitors for Electric, Hybrid and Fuel Cell Vehicles”, Proceedings of the IEEE, Vol 95, No. 4, pp.806-820, April 2007

[85] C. Alan, S. Ali, H. Alaa and B. Eric, "Optimal Sizing of an Energy Storage System for a Hybrid Vehicle applied to an Off-road Application," 2014 IEEE/ASME International Conference on Advanced Intelligent Mechatronics, Besacon, 2014, pp. 775-780.

[86] J. Shen, S. Dusmez, A. Khaligh, "Optimization of Sizing and Battery Cycle Life in Battery/Ultracapacitor Hybrid Energy Storage Systems for Electric Vehicle Applications,"*IEEE Transactions on Industrial Informatics*, Vol. 10, no. 4, pp. 2112-2121, Nov. 2014.

[87] https://www.zekalabs.com, “ RedPrime DC/DC Converter, 200kW, 1,200V,” Via Web.

[88] H. Babazadeh, W. Gao, J. Lin, L. Cheng “Sizing of Battery and Supercapacitor in a Hybrid Energy Storage System for Wind Turbines”, 2012 IEEE Transmission and Distribution Conference and Exposition. May 7-12, 2012, Orlando, FL.

[89] L. Luckose, H. Hess and B. Johnson, "Power Conditioning System for Fuel Cells for Integration to Ships," *2009 IEEE Vehicle Power and Propulsion Conference*, Dearborn, MI, 2009, pp. 973-979.

[90] Pierre Giroux, “STATCOM (Detailed MMC Model with 22 Power Modules per phase,” (Hydro-Quebec), a MATLAB example

Appendix A

Major components of STATCOM Power Module [From Siemens]

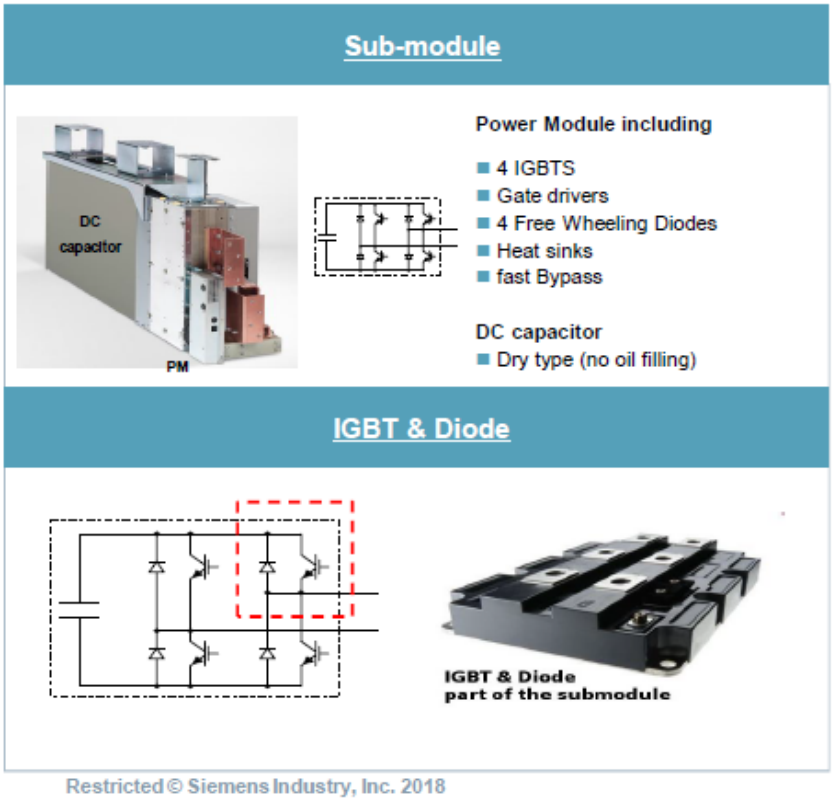

Appendix B

Typical STATCOM System [Siemens]